



Use of Biomatrices to Improve Axon Regeneration after Chronic Spinal Cord Injury in the Rat

Inaugural-Dissertation

zur Erlangung des Doktorgrades der
Mathematisch-Naturwissenschaftlichen Fakultät
der Heinrich-Heine-Universität Düsseldorf

vorgelegt von
Veronica Estrada
aus Neuss

Düsseldorf 2010

Gedruckt mit Genehmigung der Mathematisch-Naturwissenschaftlichen Fakultät der
Heinrich-Heine-Universität Düsseldorf

Referent: Prof. Dr. H.W. Müller

Koreferent: Prof. Dr. D. Willbold

Tag der mündlichen Prüfung: 16.06.2010

“[SCIENCE IS] AN
IMAGINATIVE ADVENTURE
OF THE MIND SEEKING
TRUTH IN A WORLD OF
MYSTERY.”

Sir Cyril Herman Hinshelwood (1897-1967)

ABBREVIATIONS6

1 INTRODUCTION11

1.1 PATHOPHYSIOLOGY OF SPINAL CORD INJURY 11

1.1.1 Spinal Cord Anatomy 11

1.1.2 The Injured Spinal Cord 12

1.1.2.1 Outcome of Spinal Cord Injury 12

1.1.2.2 Chronic Spinal Cord Injury 13

1.1.2.3 Axonal Regeneration after Nerve Injury 14

1.2 THE LESION SCAR - A BARRIER TO AXON REGENERATION 15

1.2.1 The Glial Scar Component 17

1.2.2 The Fibrous Scar Component 17

1.3 CURRENT APPROACHES IN THE TREATMENT OF SPINAL CORD INJURY 20

1.4 BRIDGING THE INJURED SPINAL CORD 21

1.4.1 Cellular Bridges 21

1.4.2 Acellular Scaffolds 22

1.4.2.1 Alginate Hydrogel 22

1.4.2.2 Collagen 24

1.4.2.3 Matrigel 24

1.4.2.4 Polyethylene Glycol 25

1.4.2.5 NeuroGel® 26

1.4.2.6 Matrix Materials Applied in the Present Study 26

1.5 THE ADULT RAT AS A MODEL SYSTEM FOR SPINAL CORD INJURY 26

1.6 AIM OF THIS THESIS 28

2 MATERIALS AND METHODS29

2.1 EXPERIMENTAL ANIMALS 29

2.2 BUFFERS AND ANTIBODIES 29

2.2.1 Buffers and Solutions 29

2.2.2 Antibodies 30

2.2.2.1 Primary Antibodies 30

2.2.2.2 Secondary Antibodies, Reagents and Tracer Substances 33

2.3 EXPERIMENTAL SETUP 34

2.3.1 Experimental Animal Groups 34

2.3.2 Surgical Procedures 35

2.3.2.1 Dorsal Transection Lesion 35

2.3.2.2 Scar Removal and Cavity Filling 37

2.3.2.3 Matrix Preparation and Implantation 39

2.3.2.4 Anterograde Labeling of Axons in the Thoracic Spinal Cord 40

2.3.2.5 Anterograde Labeling of Corticospinal Tract Neurons 41

2.3.3 Post-Operative Care 43

2.3.4 Animal Sacrifice 43

2.4 TISSUE PROCESSING 43

2.4.1 Paraffin Sections 43

2.4.2 Cryo Sections 44

2.4.3 Freezing-Microtome Sections 44

2.5 STAINING PROTOCOLS 45

2.5.1 Histological Stainings 45

2.5.1.1 Nissl Staining 45

2.5.1.2 Masson Trichrome Staining 45

2.5.2	Immunohistochemical Staining.....	47
2.5.2.1	DAB-Staining of Paraffin Sections.....	47
2.5.2.2	DAB-Staining of Cryo Sections.....	48
2.5.2.3	Immunofluorescent Staining of Paraffin Sections.....	49
2.5.2.4	Immunofluorescent Staining of Cryo Sections.....	50
2.5.2.5	Immunofluorescent Staining of Freezing-Microtome Sections.....	51
2.6	ANALYSIS AND DOCUMENTATION.....	51
2.6.1	Documentation of Immunohistological Stainings.....	51
2.6.2	Axon Quantification.....	51
2.6.2.1	Quantification of PAM-positive Axon Profiles via Pixel-Threshold in Image J.....	52
2.6.2.2	Quantification of PAM-positive Axon Profiles with Neuron J.....	52
2.6.2.3	Quantification of PAM-positive Axon Profile Density with Image J.....	53
2.6.2.4	Quantification of BDA-positive Axon Profiles.....	55
2.7	FUNCTIONAL TESTING.....	56
2.7.1	Open Field Observation of Locomotor Behavior.....	56
2.8	STATISTICS.....	57
3	RESULTS.....	58
3.1	CHRONIC SPINAL CORD INJURY MODEL IN THE ADULT RAT.....	58
3.1.1	Scar Removal.....	58
3.2	GENERAL APPLICABILITY AND SUITABILITY OF THE MATRICES.....	60
3.2.1	Matrigel™.....	60
3.2.2	Alginate.....	62
3.2.3	Polyethylene Glycol.....	63
3.3	TISSUE AND MATRIX PRESERVATION.....	65
3.4	AXONAL IN-GROWTH INTO THE LESION AREA.....	67
3.4.1	PAM-Positive Axons.....	67
3.4.1.1	Axon Regeneration into Matrix at 1 wpr.....	67
3.4.2	Axon Quantification.....	69
3.4.2.1	Quantitative Analysis with Neuron J.....	72
3.4.2.2	Quantitative Analysis with Feature J.....	75
3.4.3	General Anterograde Labeling of Descending Axons.....	76
3.4.3.1	Quantitative Analysis of Regenerated Axons in the Lesion Area via Manual Counting of BDA-Labeled Axons.....	78
3.5	CHARACTERIZATION OF THE LESION AREA AT AN EARLY TIME POINT.....	81
3.5.1	Extracellular Matrix Composition.....	82
3.5.2	Vascularization.....	83
3.5.3	Cell Invasion of the Lesion Area.....	86
3.5.3.1	Astrocytes.....	86
3.5.3.2	Fibroblasts.....	89
3.5.3.3	Oligodendrocytes.....	90
3.5.3.4	Schwann Cells.....	91
3.5.4	Inflammatory Response.....	94
3.5.4.1	Activated microglia, monocytes and macrophages.....	94
3.5.4.2	T- and B-Lymphocytes.....	95
3.5.5	Association of Regenerated Axons with Growth-Supporting Schwann Cells.....	97
3.5.6	Regeneration of Axons from Different Neuronal Populations into PEG Matrix.....	99
3.6	BEHAVIORAL ANALYSIS.....	101
3.6.1	Basso, Beattie & Bresnahan Open Field Locomotor Analysis.....	101
4	DISCUSSION.....	103
4.1	DEFINING THE TIME POINT FOR CHRONIC SCI.....	103

4.2	REMOVAL OF THE SPINAL CORD INJURY LESION SCAR AS A SUITABLE LESION MODEL	103
4.3	EVALUATION OF AXONAL REGENERATION AFTER CHRONIC SCI SCAR RESECTION	104
4.3.1	Realistic axon quantification requires detailed analyses	105
4.3.2	Matrigel™ alone is not sufficient to promote spontaneous axonal regeneration when used as a bridging material in chronic SCI.....	109
4.3.3	Alginate hydrogel promotes little spontaneous axonal regeneration and reveals poor integration into host tissue when applied as a matrix into the chronically injured spinal cord	109
4.3.4	Significantly increased axon regeneration into the stable matrix which forms in the PEG-treated resection area	112
4.4	CHARACTERIZATION OF ACUTE AND CHRONIC LESION AREA	113
4.4.1	Increased amounts of collagen type IV in ALG matrix.....	114
4.4.2	Decreased extracellular matrix deposition in PEG matrix.....	115
4.4.3	Regenerating axons are attracted to grow into well-revascularized PEG-treated chronic SCI scar resection site	116
4.4.4	Cellular invasion of the lesion area	117
4.4.4.1	Astrocytes frequently invade PEG-, but not ALG matrix.....	117
4.4.4.2	Increased Col4-immunoreactivity is accompanied by the presence of many fibroblasts in ALG matrix	119
4.4.4.3	No invasion, but accumulation of oligodendrocytes in lesion border regions of matrix-treated animals	120
4.4.4.4	Many invading Schwann cells are present in PEG-, but not ALG matrix.....	122
4.4.5	Decreased invasion of inflammatory cells after matrix implantation.....	124
4.5	REGENERATION OF AXONS FROM DIFFERENT NEURONAL POPULATIONS INTO PEG MATRIX AFTER CHRONIC SCAR RESECTION	125
4.6	CHRONIC SCAR RESECTION DOES NOT NOTABLY IMPAIR OPEN FIELD LOCOMOTIVE BEHAVIOR	126
4.7	ADDITIONAL CONSIDERATIONS	129
4.7.1	Chemical/Physical Aspects	129
4.7.1.1	Possible influence of matrix viscosity on regenerative events	129
5	SUMMARY AND PERSPECTIVES.....	133
	ZUSAMMENFASSUNG.....	135
6	REFERENCES	137
	DANKSAGUNG.....	168

ABBREVIATIONS

5-HT	serotonin (5-hydroxytryptamine)
ABC	avidin-biotin-complex
ALG	alginate
A/P	anterior/posterior
APC	<i>Adenomatous polyposis coli</i> Clone CC-1
<i>aq. bideest</i>	<i>aqua bidestillata</i>
AST	anti-scarring treatment
BBB	locomotor test/scale (developed by Basso, Beattie and Bresnahan)
BDA	biotinylated dextran amine
BDNF, NT-3	neurotrophic factors
BM	basement membrane
BPY-DCA	2,2'-bipyridine-5,5'-dicarboxylic acid (iron chelator)
BV	blood vessel
ca.	<i>circa</i>
Ca ²⁺	calcium
CaCl ₂	calcium chloride
cAMP	cyclic adenoside monophosphate
cc	central canal
CD 4,5,8	T- and B-cell markers
CGRP	Calcitonin gene-related peptide
CNS	central nervous system
Col4	collagen type IV
CSF	cerebrospinal fluid
CSPG	chondroitin sulfate proteoglycan
CST	corticospinal tract
d	dorsal
DAB	3,3' diaminobenzidine
DAPI	4',6-Diamidino-2-phenylindole
dh	dorsal horn
dk	donkey
DPX	xylo- containing mounting fluid
ECM	extracellular matrix

ED1	ED1 protein of lysosomes (CD68), marker of activated microglia and macrophages
e.g.	for example (<i>exempli gratia</i>)
Elvax	ethylene vinyl acetate-copolymer
etc.	<i>et cetera</i>
EtOH	ethanol
FC	<i>fasciculus cunneatus</i>
FG	<i>fasciculus gracilis</i>
Fe ²⁺	divalent iron cation
fig.	figure
FL	forelimb
G	guluronate
HL	hindlimb
GAG	glycosaminoglycan
GFAP	glial fibrillary acidic protein, astrocyte marker
gm	gray matter
gt	goat
H ₂ O ₂	hydrogen peroxide
HCl	hydrochloric acid
hs	horse
i.e.	that is (<i>id est</i>)
IR	immunoreactivity
LANUV	state office of environmental and consumer protection
L/I	lateral
M	mannuronate
MAG, NOGO, OMgp	myelin-associated inhibitors
MBP	myelin basic protein
MeOH	methanol
MG	Matrigel™
MR	magnetic resonance
ms	mouse
n	number
Na ⁺	sodium
NaBH ₄	sodium borohydrate

Na ₂ HPO ₄	di-sodium hydrogen phosphate anhydrous
Na ₂ HPO ₄ x 2H ₂ O	sodium di-hydrogen phosphate
NaBH ₄	sodium borohydride
NaCl	sodium chloride
NaH ₂ PO ₄ x H ₂ O	sodium di-hydrogen phosphate monohydrate
NaOH	sodium hydroxide solution
NgR	NOGO receptor
NO ₂	nitrous oxide
NRW	North-Rhine Westfalia
O ₂	oxygen
ON	over night
OPC	oligodendrocyte precursor cell
P4H	prolyl-4-hydroxylase
PAM	pan-axonal marker
PB	phosphate buffer
PBS	phosphate buffered saline
PEG	polyethylene glycol
PFA	paraformaldehyde
pHPMA	poly[N-(2-hydroxypropyl)methacrylamide]
PNS	peripheral nervous system
rb	rabbit
ReST	reticulospinal tract
rPH	rat prolyl-4-hydroxylase
ROTI	Roti-Histol
RST	rubrospinal tract
RT	room temperature
RX	chronic scar resection
S100/S100β	S100 calcium binding protein, Schwann cell marker
SC	Schwann cell
SCI	spinal cord Injury
SCT	spinocerebellar tract
STT	spinothalamic tract
SWK	Scouten wire knife
TGFβ	transforming growth factor <i>beta</i>

Th	thoracic level
TH	tyrosine hydroxylase
TIF	tagged image file
TRIS/Tris	tris(hydroxymethyl)-aminomethane
v	ventral
vh	ventral horn
vs.	<i>versus</i>
VST	vestibulospinal tract
vWF	von Willebrand factor, endothelial marker
v/v	volume per volume
wm	white matter
wpl	weeks post lesion
wpr	weeks post chronic scar resection
w/v	weight per volume

UNITS

°C	degree Celsius
cm	centimeter
g	gram
G	gauge
h	hour
m	meter
M	molar
min (')	minute
μl	microliter
μm	micrometer
mg	milligram
ml	milliliter
mm	millimeter
mM	millimolar
s (")	second
W	watt

1 Introduction

1.1 Pathophysiology of Spinal Cord Injury

1.1.1 Spinal Cord Anatomy

The central nervous system (CNS) comprises brain and spinal cord. The spinal cord descends from the brain and is protected by the vertebral column. It is surrounded by cerebrospinal fluid (CSF), which acts as a cushion to protect the delicate nerve tissues against damage from banging against the inside of the vertebrae. The spinal cord itself consists of millions of nerve fibers which are grouped together in different bundles of ascending and descending tracts. Ascending tracts carry information such as touch and pain from the body to the brain, whereas descending tracts carry information to initiate movement and control body functions from the brain downwards. Additionally, interneurons which allow establishment of local circuits and signal modulation in the different spinal segments, as well as motoneurons are located in the spinal cord. A magnetic resonance (MR) image overlaid with a histologic rat spinal cord cross section is depicted in Fig. 1.1. Different ascending and descending spinal tracts are marked.

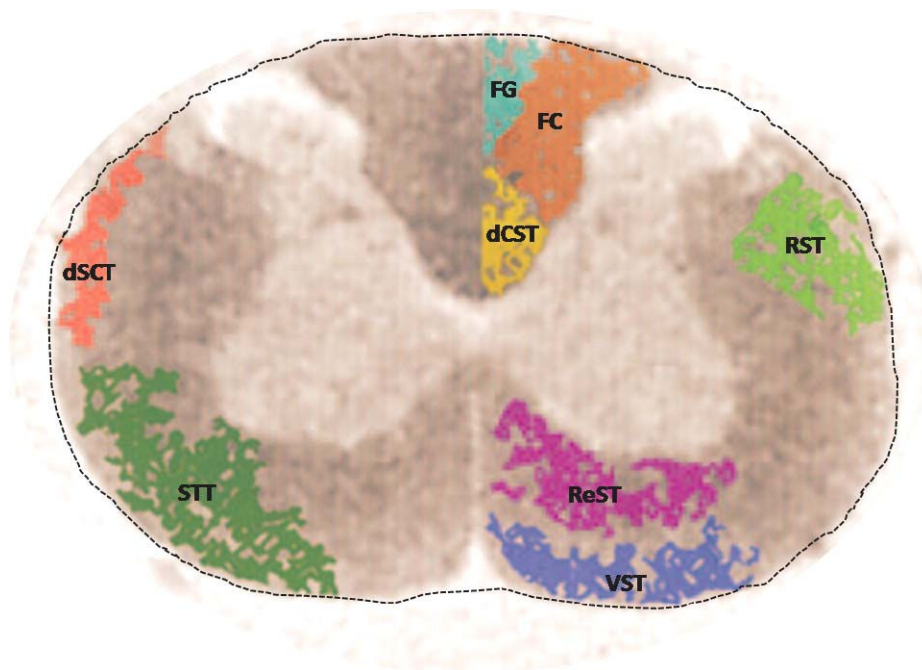


Fig. 1.1: Schematic illustration of a spinal cord cross cut. In the MR image overlaid with a histologic spinal cord cross section (modified from Schwartz et al., 2005b) spinal fiber tracts are depicted; STT: spinothalamic tract, dSCT: dorsal spinocerebellar tract, dCST: dorsal corticospinal tract (CST, descending), RST: rubrospinal tract, ReST: reticulospinal tract, VST: vestibulospinal tract, FG: *fasciculus gracilis*, FC: *fasciculus cuneatus*.

The spinal gray matter is characterized by many optically dense neuronal cell bodies of mainly motoneurons. The posterior *funiculus* in the dorsal spinal cord contains the sensory tracts of cuneate (FC) and gracile (FG) *fasciculi*. Underlying these tracts in the rat (differing from human and primate anatomy) is the dorsal corticospinal tract (dCST).

The CST is part of the pyramidal system. The neurons of origin, which are located in layer V of the motor cortex, project to the spinal cord via the pyramidal tracts. In the majority of higher mammals, large parts of the CST cross the spinal cord midline at the decussation of pyramids at the level of the *medulla oblongata* and run in the lateral columns (lateral CST, ICST), whereas in the rat, the major part of the decussated CST runs in the dorsal spinal cord in between the dorsal horns. Only few CST-fibers are located in the lateral columns. Furthermore, both, human and rat exhibit an un-decussated ventral part of the CST (vCST). A pyramidal neuron forms synapses with another neuron in the ventral horn. While the cells of destination are mainly gray matter α -motoneurons in lamina 9 in the ventral horn in humans, apes and some monkey species, rodent CST axons project mainly to dorsal horn neurons in laminae 3-6 and premotor spinal circuits (The Spinal Cord, 2009). From these cells the information is transmitted to the periphery.

The rubrospinal tract (RST) originates from the *nucleus ruber* in the *mesencephalon*. Its decussated projections run in the far lateral regions of the dorsal spinal cord. The RST projects to gray matter interneurons which innervate α -motoneurons.

The spinocerebellar tract is a set of axonal fibers originating in the spinal cord. It terminates in the ipsilateral cerebellum. This tract conveys proprioceptive information about limb and joint position to the cerebellum (Afifi and Bergman, 2005).

1.1.2 The Injured Spinal Cord

1.1.2.1 Outcome of Spinal Cord Injury

Spinal cord injury (SCI) often results in a devastating condition causing long-lasting impairments for both, directly affected patients and their affiliated. Worldwide, SCI affects over two million people (Afshari et al., 2009). Traumatic SCI often results in a direct mechanical trauma. Following such traumatic SCI, electrophysiological signal transduction is interrupted, resulting in a dramatic impairment of locomotion and aesthesia, and sometimes even the death of the person concerned. Damage

caused by SCI will spread further and affect areas, which were initially not affected by the primary insult, in the process of secondary degeneration. This term comprises biochemical events eventually leading to apoptotic, necrotic and excitotoxic cell death in wider areas in consequence of damage of neurons, glial cells and blood vessels (BV) in the lesion core. It has been demonstrated in experimental rat SCI that such events prolongate over longer periods of several weeks (Liu et al., 1997). When the normal blood flow is disrupted, ischemia (deprivation of oxygen) and necrosis (instantaneous cell death) are the consequence. Apoptotic events are in part correlated with the Wallerian degeneration of severed axonal fragments distal to the site of injury. Although necrotic cell death initially only occurs in directly affected cells, it can further be initiated in other cells due to secretion of cytokines by invading and proliferating immune cells (lymphocytes, macrophages and microglia) leading to long-lasting necrosis in the affected area. Additionally, excitotoxic neurotransmitters (glutamate and aspartate) are released into the extracellular space due to the destruction of cells and cell membranes (Beattie et al., 2000; Buss and Schwab, 2003; Stichel and Müller, 1998). Extracellular matrix (ECM) molecules are produced mainly by invading meningeal fibroblasts, endothelial cells and activated astrocytes. The presence of Semaphorin 3A in the lesion scar (Pasterkamp and Verhaagen, 2006) leads to growth cone collapse, secretion of TGF β results in an increase in the proliferation of collagen-producing fibroblasts. The consequence of these events is a restructuring of the ECM at the site of injury. In subacute and chronic stages of SCI, scarring and cord tethering, demyelination and development of syringomyelia present the main complications. In addition, chronic pain syndromes might develop due to permanent hyperexcitability of some cells types (Ramer et al., 2000; Sandvig et al., 2004; Stoll and Muller, 1999).

1.1.2.2 Chronic Spinal Cord Injury

Today, the majority of on-going research in the field of SCI still focuses on the acute injury situation, where much progress has been achieved in understanding the involved mechanisms. The increased knowledge has allowed the development of improved therapies and treatment options and still continues to do so. However, the majority of spinal cord injured patients are those with chronic SCI who benefit only insufficiently from available treatments. Although axonal regeneration is most extensive following a short delay between injury and treatment, and although

regeneration of chronically injured axons is impaired compared to acutely injured ones (Dolbeare and Houle, 2003), regenerative response is still possible after several months (Akesson et al., 2001;Cai et al., 2007;Fraidakis et al., 2004;Grill et al., 1997;Hejcl et al., 2010;Woerly et al., 2001a;Ye and Houle, 1997) or even a year (Kadoya et al., 2009;Kwon et al., 2002b).

However, repair of the injured human spinal cord requires not only neuronal survival, axonal outgrowth and remyelination, but further the reconnection across the area affected by the trauma by means of bridging grafts (Novikova et al., 2003). Known reasons for observed regeneration failure after SCI include scar formation (Camand et al., 2004;Fernandez and Pallini, 1985;Hagg and Oudega, 2006;Hermanns et al., 2001a;Kawano et al., 2005;Klapka et al., 2005;Zhang et al., 2007), degeneration of axons (Kerschensteiner et al., 2005), myelin components (Kastin and Pan, 2005;Ruff et al., 2008;Schweigreiter and Bandtlow, 2006;Xie and Zheng, 2008) and a prolonged post-injury period before an intervention (Fehlings and Perrin, 2006;Ibarra et al., 2004;Koob et al., 2008;Rosenberg and Wrathall, 2001). Some further factors influencing the outcome of SCI are activity dependent plasticity (Dunlop, 2008), neuro-immune responses (Popovich and Longbrake, 2008;Schwartz and Hauben, 2002), changes in ECM composition (Brazda and Muller, 2009;Buss et al., 2007;Jones et al., 2002;Schiwy et al., 2009), and changes in gene expression (Ahn et al., 2006;De Biase et al., 2005;Di Giovanni et al., 2004;Urso et al., 2007;Wu et al., 2005).

1.1.2.3 Axonal Regeneration after Nerve Injury

Axotomy following traumatic injury evokes different responses in peripheral (PNS) and central nervous system (CNS). After PNS injury, the distal axon part separated from its cell body undergoes Wallerian degeneration. Invading macrophages clear up cell and myelin debris to make way for regeneration by provision of a favorable environment. In addition to proteases, the macrophages further secrete a number of growth-promoting factors and stimulants for the proliferation of Schwann cells (SC). The SC de-differentiate and longitudinally align to form the bands of Bünger, which serve as guidance structures for regrowing axon fibers (Lee and Wolfe, 2000). Within one day after injury, axons begin to form bulbous swellings at their proximal ending as a sign of accumulation of newly arrived axoplasm. These structures give rise to growth cones which guide the axon's

regeneration at a rate of 1-2 mm/day, following guidance cues. After PNS transection injury, regeneration and target innervation occurs only after re-anastomosis of the cut ends in injuries which result in a gap of 1 cm maximum. After PNS crush lesions, even longer distances can be overcome.

For a long time, damage to the mature central nervous system (CNS) was considered permanent in contrast to PNS injuries (Fu and Gordon, 1997), until transplants of peripheral nerve grafts illustrated the potential for axonal regrowth (Aguayo et al., 1981;Fu and Gordon, 1997). The distal nerve stump degenerates at the same rate in PNS and CNS. However, the response of CNS-neurons to the degradation is very different to that of PNS-neurons: Microglia are activated and some blood-born macrophages invade the lesion site around the third day after injury, but the number of phagocytizing cells remains lower than that after PNS injury, resulting in a much slower removal of debris in CNS (George and Griffin, 1994). After initial retraction, the proximal stump shows some sprouting for several millimeters to eventually stop its growth at the lesion site (Stichel and Müller, 1998), as has initially been described by Ramon y Cajal in 1928. Such observations reveal the intrinsic capability of central nervous system neurons to regenerate, which was eventually proven by the group of Aguayo in 1981 (David and Aguayo, 1981). Since then, further repair strategies with the aim of achieving, improving, and directing axonal growth after SCI have included changing the inhibitory environment, application of fetal grafts or cellular grafts, artificial bridges, matrix changes, and addition of neurotransmitters or growth factors (Hulsebosch, 2002).

However, although much progress has been made in spinal cord research in the past years, the final reason for the growth arrest at the site of lesion remains unknown. Several hypotheses have been developed on the basis of the results of experimental SCI research trying to explain the nature of this insurmountable barrier to CNS regeneration.

1.2 The Lesion Scar - a Barrier to Axon Regeneration

After SCI, formation of a lesion scar occurs as was first described by Ramon y Cajal in the beginning of the 20th century. Such a response is comparable to general tissue injury events: Local intercellular and extracellular modifications occur to restrict the initial damage. The integrity of the CNS is re-established by sealing it off from the

external environment. The blood-brain-barrier is re-sealed in order to prevent infections, and the wound margins converge due to contractile properties of the scar tissue. Nutrition is provided by the invasion of epithelial cells leading to initial neovascularization (Stichel and Müller, 1998). In the 1970s, the development of a basement membrane (BM) at the site of SCI was described by Russian scientists. The connective tissue-containing scar was soon suggested as the more important impediment for axonal regeneration than the glial scar-component. Early experiments aimed at removing the fibrous BM-scar via enzymatic digestion did not prove successful since the BM which also surrounds BV was simultaneously destroyed, leading to increased further bleedings (Guth et al., 1980). Due to the respective observations, the fibrous lesion scar was for a long time not considered as a potential inhibitor of CNS axon regeneration. Finally, in the late 1990s it could be shown that the regenerating axons abruptly stop at the area of Collagen type IV (Col4) deposition (Stichel et al., 1999b; Stichel et al., 1999a; Stichel and Müller, 1998). It was eventually demonstrated that the lesion scar which forms after CNS injury is composed of two major constituents: The fibrous component in the lesion center and the surrounding glial part in peri-lesion areas, characterized by strong expression of the glial fibrillary acidic protein (GFAP) (Fawcett and Asher, 1999; Klapka et al., 2002). A schematic illustration of the SCI lesion scar is presented in Fig. 1.2.

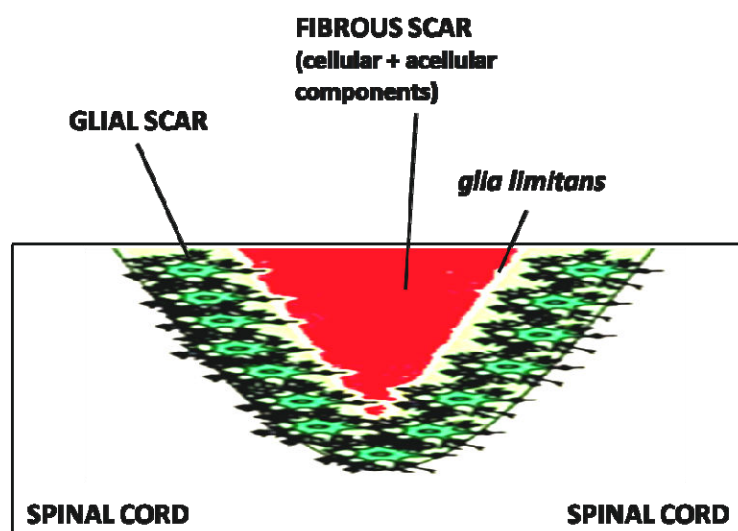


Fig. 1.2: Schematic illustration of the SCI lesion scar in a sagittal spinal cord section (modified from Stroncek and Reichert, 2007). The fibrous scar is comprised of ECM (acellular components) and invading cells, e.g., meningeal cells, blood cells, etc. The glial scar contains reactive astrocytes. *Glia limitans* is formed in marginal regions between fibrous and glial scar.

1.2.1 The Glial Scar Component

Glial cells are important functional components of the CNS. Oligodendrocytes are essential for myelination (Fitch and Silver, 1999). Astrocytes hold important functions in maintenance of the blood-brain-barrier (Pekny and Nilsson, 2005) and of ion homeostasis (Fitch and Silver, 1999). Microglia present the resident phagocytic cells of the CNS. Following SCI, astroglia undergo structural changes. In the course of reactive astrogliosis, they proliferate, establishing a dense network of their processes (Pekny and Nilsson, 2005). The astrocytes are connected with cells of other cell types (oligodendrocytes, microglia, macrophages, endothelial cells and meningeal cells) via tight junctions and gap junctions (Fawcett and Asher, 1999;Klapka et al., 2002). Involved astrocytes become hypertrophic, hyperplastic and reveal an increase in the production of intermediate filaments. GFAP, the marker of reactive astrocytes, presents the main intermediate filament protein in the unlesioned spinal cord (Pekny and Nilsson, 2005). Occurrence of astrogliosis appears to be important in the acute post-injury phase in the restoring of function, where it might contribute to beneficial events. Such a positive role is attributed to reactive astrocytes in the reconstitution of the blood-brain-barrier due to antioxidative and neurotransmissive effects (Reier et al., 1983). In the subacute phase of SCI, however, astrogliosis has been implicated with the regenerative failure (Fawcett and Asher, 1999;Pekny and Nilsson, 2005;Silver and Miller, 2004). Such hypotheses originally arose from histological observations of transected axon fibers stopping (often within the glial matrix) at the site of injury. However, the presence of collagenous connective tissue was found to frequently coincide with the gliosis (Reier et al., 1983) and it has been indicated by the results of different experimental studies that inhibitory proteins attach to the BM of the fibrous lesion scar (Klapka et al., 2002;Klapka et al., 2005;Reier et al., 1983;Stichel et al., 1999b;Stichel et al., 1999a), thus leading to the failure in regeneration.

1.2.2 The Fibrous Scar Component

In the lesion core, acellular ECM is intermingled with cellular components, e.g., blood cells, macrophages, meningeal cells, Schwann cells and microglia. A major component of this fibrous scar is Col4. Col4 is one of 29 known types of collagen. It is generally present in BM-structures where it assembles in sheet-like

networks (Aumailley and Gayraud, 1998). Other molecules, such as laminin and entactin, are further associated with the fibrous scar. The observation of the respective molecules in the SCI lesion core have led to the conclusion that it is mainly composed of BM structures which are apparent at five days post lesion (Hermanns et al., 2005). Col4 is a collagen which is primarily found in the basal lamina, a layer of ECM on which epithelium sits, and which is secreted by the epithelial cells. Col4 is synthesized by different cells of the CNS, e.g., meningeal fibroblasts (Berry et al., 1983), astrocytes (Liesi and Kauppila, 2002) and endothelial cells (Schwab et al., 2001). By means of immunohistological staining of sections from spinal cord-injured animals with an antibody against Col4, BM structures can be visualized.

Being comprised of the aforementioned Col4-network linked to a network of laminin via nidogen/entactin (see Fig. 1.3), the BM serves as a supporting structure during development and in tissue repair, as well as a scaffold for the anchorage of different constituents via integrins (Yurchenco and Schittny, 1990).

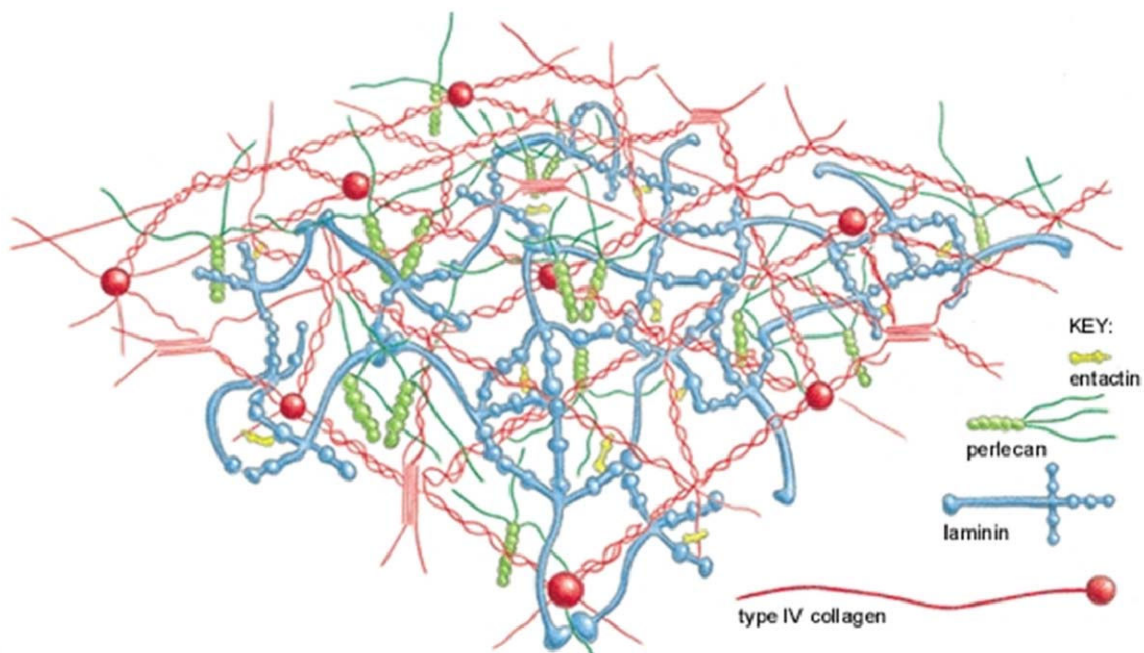


Fig. 1.3: Schematic representation of a basal membrane. The BM is comprised of a network of Col4 and laminin as the major constituents, interconnected via entactin (Alberts et al., 2007).

Molecules which are associated with the BM are mainly secreted by reactive astrocytes, oligodendrocytes and fibroblasts (Davies et al., 1997; Fawcett and Asher, 1999). Some of these molecules, e.g., Ephrins, Semaphorin 3A or chondroitin sulfate

proteoglycans (CSPG) have been implicated with the inhibition of axonal regeneration (Klapka et al., 2002; Miranda et al., 1999; Silver and Miller, 2004). Following SCI, an up-regulation of these molecules occurs. The correlation between the up-regulation of CSPG in the area of SCI and axonal growth arrest in corresponding areas has previously been demonstrated by Davies and his colleagues (Davies et al., 1997). The application of an enzyme (Chondroitinase ABC) which digests the GAG-chains of CSPG molecules results in a decrease of the inhibitory effects and has even been shown to restore post-synaptic activity (Bradbury, 2002).

Prolyl 4-hydroxylase (P4H) is a key enzyme in collagen synthesis. It mediates the formation of stable triple helices, thus allowing the spontaneous network formation. In order to work properly, the enzyme requires iron (Fe^{2+}) as a co-factor. Based on this known interaction, a pharmacological treatment (anti-scarring treatment, AST) has previously been developed in the Molecular Neurobiology Laboratory of the University of Düsseldorf. The treatment comprises the local application of an iron chelator solution, amongst other substances, in order to deprive P4H of its co-factor. Such iron-deprivation has been assumed to result in a decreased rate of hydroxylation of proline residues. As a consequence, the formation of stable collagen network structures would be transiently inhibited. It has previously been demonstrated that this treatment indeed leads to a diminished fibrous scar formation in the first week after experimental rat SCI and results in axonal regeneration, neuroprotection and functional recovery (Hermanns et al., 2001b; Klapka et al., 2005). AST was established and proved successful as a treatment after acute SCI. However, in its originally developed form, AST cannot be applied after chronic SCI for obvious reasons: The lesion scar in chronically injured animals is fully developed; therefore scar removal with subsequent matrix application into the resulting cavity is required. Different matrix materials were therefore tested in a model of chronic SCI in regard to their ability to promote the spontaneous axon regeneration capacity after chronic SCI. Promising materials could serve as a basis for therapeutic treatments in future studies concerning chronic SCI.

1.3 Current Approaches in the Treatment of Spinal Cord Injury

Many research groups are working on the development of therapeutical strategies to achieve regeneration after SCI. The regeneration of only few axons can lead to a return of some respectable function and thus enable an improved quality of life (Fawcett, 1998). On the other hand, stated recovery is not necessarily indicative of axonal regeneration. Plasticity of the nervous system, as well as compensational mechanisms and collateral sprouting can further play an important role in functional improvement. However, to achieve long-distance regeneration in the original pathways affected by SCI, several demands need to be met: Initial events of regrowth (regenerative sprouting) must be followed by elongation of respective axon fibers, which may consequently grow through the site of injury into the distal spinal cord where, after finding of appropriate target cells, a re-formation of synapses as well as remyelination must occur to result in actual functional recovery mediated by successful regeneration (Stichel and Muller, 1998). Although today it is clear that CNS neurons hold an intrinsic capacity to regenerate (David and Aguayo, 1981), the actual reason for the general regenerative failure of nerve regeneration in the CNS remains unclear.

Various factors and mechanisms have been identified which might synergistically act to result in insufficient axonal regeneration. Repair strategies with the aim of achieving, improving, and directing axonal growth after SCI have included changing the inhibitory environment, application of fetal nerve grafts or cellular grafts, artificial bridges, matrix changes, and addition of neurotransmitters or growth factors (Hulsebosch, 2002). Axonal regeneration after injury in the CNS has been achieved by blocking the inhibitory effects of myelin (Buchli and Schwab, 2005;Kastin and Pan, 2005;McKerracher, 2001;Rowland et al., 2008), by changing the composition of the hostile lesion scar environment, e.g., through application of an iron chelator (Klapka et al., 2005;Schiwy et al., 2009), or through enzymatic digestion of inhibitory proteoglycan molecules via treatment with chondroitinase ABC (Barritt et al., 2006;Bradbury, 2002;Garcia-Alias et al., 2008;Tester and Howland, 2008), by application of trophic factors (Burdick et al., 2006;Houle and Ziegler, 1994;Jones et al., 2001;Lu and Tuszynski, 2008;Plunet et al., 2002;Tuszynski et al., 2003;Yang et al., 2005;Ye and Houle, 1997), by introduction of matrices for axonal growth through

a lesion site (Bunge, 2001;Hejcl et al., 2008) and by combined interventions (Bregman, 1998;Fouad et al., 2005;Houle and Tessler, 2003;Kalderon et al., 2007;Lu and Tuszynski, 2008;Luo et al., 2009;Nomura et al., 2006;Pearse and Bunge, 2006). However, not only is the efficacy of treatment variable with time after injury, but do different neuronal subpopulations also respond differentially to treatment (Houle and Tessler, 2003).

1.4 Bridging the Injured Spinal Cord

Since in most cases of human SCI there is no significant loss of spinal cord tissue, the formation of cavities presents an important obstacle which impedes axonal regeneration. Therefore, in addition to neuronal survival and axonal growth and remyelination, the reconnection across the trauma cavity (or across the resection cavity as in the case of the lesion model presented here) by means of bridging grafts may be required.

1.4.1 Cellular Bridges

Cellular grafting presents a promising strategy for the treatment of SCI. Main objectives are facilitation of growth due to the graft serving as a bridge for regenerating axons, administration of neuronal cells, and neurotrophic factor secretion. Different sources have been considered for transplantation: Peripheral nerve grafts (David and Aguayo, 1981;Tom et al., 2009;Tom and Houle, 2008), Schwann cells (Bunge, 2002), olfactory ensheathing glia (Ramon-Cueto et al., 1998), fetal CNS tissue (Coumans et al., 2001), neural stem cells (Cao et al., 2002), bone marrow stromal cells (Ankeny et al., 2004), umbilical cord blood stem cells (Dasari et al., 2007), blood-born autologous macrophages (Franzen et al., 1998), astrocytes (Davies et al., 2006), or genetically modified fibroblasts (Grill et al., 1997) have widely been used in the course of SCI. However, the above-listed therapies have so far proven no or only little successful regeneration when applied alone. The combination of various strategies is therefore indispensable (Blakemore, 2000;Christie and Mendez, 2001;Dobkin and Havton, 2004;Hulsebosch, 2002;Jones et al., 2001;Kwon et al., 2002a;Lakatos et al., 2003;Murray et al., 2002;Murray, 2004;Reier, 2004;Ribotta et al., 2002;Sandvig et al., 2004;Stichel and Muller, 1998).

1.4.2 Acellular Scaffolds

Although many studies have proven the beneficial effects of autologous or heterologous cellular grafts in acute and chronic SCI models in animals (Jones et al., 2001; Oudega and Xu, 2006; Reier, 2004; Samadikuchaksaraei, 2007), the use of cell transplantation in human patients often remains a controversial issue (Markakis and Redmond, Jr., 2005). The search for artificial biomaterials for implantation into the injured spinal cord has been prompted due to the limited access to autologous donor material and immunological problems associated with allograft rejection. Respective materials should ideally be easily modifiable, serve as a scaffold for matrix molecules and/or cellular implants, and further be immunologically inert and absorbable (Novikova et al., 2003). Using alternative materials for bridging a spinal cord lesion site is advantageous. Positive results with acellular matrices have been obtained in several recent studies (Bakshi et al., 2004; Cai et al., 2007; Friedman et al., 2002; Horn et al., 2007; Houle and Ziegler, 1994; Novikov et al., 2002; Novikova et al., 2003; Prang et al., 2006; Samadikuchaksaraei, 2007). A promising therapy using acellular materials after acute SCI has been developed by Tysseling-Mattiace et al. (Tysseling-Mattiace et al., 2008) in a mouse SCI model. The treatment described by the authors comprised the application of bioactive three-dimensional nanofiber structures which display high densities of neuroactive epitopes on their surfaces. Treatment reduced astrogliosis and cell death, while it increased the number of oligodendroglia at the site of injury, and achieved significant functional recovery due to regeneration of ascending sensory and descending motor axons.

Important advances have recently been reported in the development of biosynthetic conduits for spinal cord repair. Biosynthetic conduits equipped with ECM molecules and different cell lines, and supplemented with neurotrophic growth factors have been shown to yield encouraging results in the treatment of experimental SCI (Novikova et al., 2003). The following paragraphs will provide an introduction to some of the applied materials.

1.4.2.1 Alginate Hydrogel

Alginate (ALG) is an example of a natural polymer. It is an anionic polysaccharide distributed widely in the cell walls of brown algae, where it forms a viscous gum through binding water. ALG is a linear copolymer with homopolymeric

blocks of (1-4)-linked β -D-mannuronate (M) and its C-5 epimer α -L-guluronate (G) residues, respectively, covalently linked together in different sequences or blocks (Fig. 1.4).

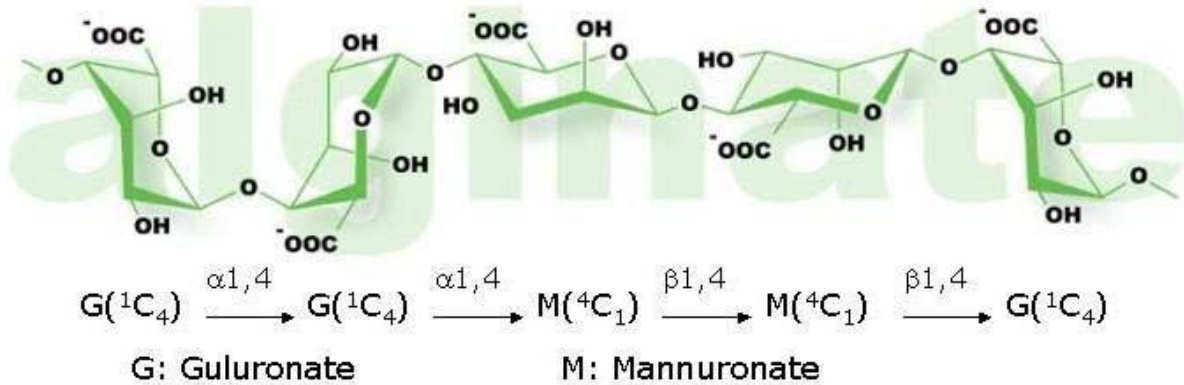


Fig. 1.4: Example of the chemical structure of an ALG-copolymer (NovaMatrix Product Information Bulletin).

The monomers can appear in homopolymeric blocks of consecutive G-residues (G-blocks), consecutive M-residues (M-blocks), alternating M- and G-residues (MG-blocks), or randomly organized blocks. Its mannuronic and glucuronic acid blocks can be cross-linked ionically by Ca^{2+} ions (Gacesa, 1988). Cross-linking can be carried out at room temperature and physiological pH. ALG is immunologically inert and is not digested by mammalian cells. As the Ca^{2+} ions gradually diffuse out from the gel, it slowly degrades and is excreted in urine (Novikova et al., 2003). ALG gels are frequently used as matrices for encapsulation of living cells (Goosen et al., 1985) and for the release of proteins (Wee and Gombotz, 1998). Due to its capacity to absorb water quickly, to its simple gelation with divalent cations, and to its biocompatibility, ALG is widely used in industrial applications, e.g., as a gelling or thickening agent in food, cosmetic and pharmaceutical industry, and for cell immobilization and encapsulation (Klock et al., 1997; Nunamaker et al., 2007; Remminghorst and Rehm, 2006; Wee and Gombotz, 1998; Yen et al., 2008). In SCI research, ALG gels – often applied as cell carrier substances - have been used successfully to promote axonal regeneration and elongation, both, *in vitro* and *in vivo* (Dhoot et al., 2004; Kataoka et al., 2001; Kataoka et al., 2004; Novikov et al., 2002; Novikova et al., 2003; Novikova et al., 2006; Prang et al., 2006; Suzuki et al., 1999; Tobias et al., 2001; Tobias et al., 2005). Positive effects of ALG on axonal regeneration have in part been attributed to be supported by the

invasion of SC into the graft, and to the young age of animals which were used in the respective studies (Novikova et al., 2003).

1.4.2.2 Collagen

Collagen type I is another natural polymer which has been used as a scaffold material in experimental spinal cord injury repair. It does not promote axonal regeneration of injured spinal axons across the trauma zone. However, when collagen tubes were used to reconnect the spinal cord with disconnected ventral roots, this material yielded some encouraging results (Liu et al., 2001).

1.4.2.3 Matrigel™

Matrigel™ (MG) is the trade name for a gelatinous protein mixture obtained from the Engelbreth-Holm-Swarm sarcoma, a mouse sarcoma containing laminin and additional ECM components. MG, a synthetic biodegradable implant, resembles the complex extracellular environment found in many tissues and is widely used as a substrate for cell culture. MG comprises a mixture of Col4 (about 20%), laminin (about 70%) and heparan sulfate proteoglycan (about 10%) admixed with other minor amounts of extracellular components, as well as growth factors (e.g., insulin-like growth factor-1 and transforming growth factor- β). MG is liquefied at low temperatures (manufacturer recommended temperature of $-20\text{ }^{\circ}\text{C}$ for storage, subsequent thawing overnight on ice at $4\text{ }^{\circ}\text{C}$), but it will gel rapidly at $22\text{ }^{\circ}\text{C}$ – $35\text{ }^{\circ}\text{C}$ to form a nonporous hydrogel. It has been described as a suitable matrix for tissue generation (Cassell et al., 2001) and has been tested as a control substance in axon regeneration studies, where its application promoted axonal growth to varying degrees from only limited growth (Iannotti et al., 2003; Novikova et al., 2006) to extensive axonal sprouting (Novikova et al., 2006). MG is widely used as a matrix in combination with cellular transplants, where it has been shown to obtain positive results regarding axonal regeneration after SCI (Novikova et al., 2006; Rodriguez et al., 2000; Someya et al., 2008; Xu et al., 1995; Xu et al., 1997).

1.4.2.4 Polyethylene Glycol

Another synthetic biodegradable implant which is used in experimental spinal cord repair is polyethylene glycol (PEG), an oligomer or polymer of ethylene oxide (Fig. 1.5).

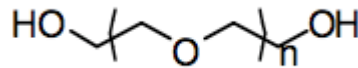


Fig. 1.5: Chemical structure of PEG.

Depending on the respective molecular weight, PEG is a liquid or a low-melting solid, which is chemically inert, water-soluble and generally non-toxic. Because of these features, PEG is widely used not only for industrial purposes, but also in medical applications, as a carrier substance in pharmaceutical applications and cosmetics and in cell biological research. The fusogen copolymer is often used for production of hybridomas in the development of immortal cell lines. PEG with different molecular weights find use in different applications and are known to have different physical properties due to their chain length effects, but their chemical properties remain nearly identical. Their melting points vary depending on the formula weight of the polymer.

In recent experimental SCI studies, application of PEG has been demonstrated to successfully repair crushed as well as transected spinal cord axons, leading to immediate recovery of axonal conduction (Shi and Borgens, 1999; Shi and Borgens, 2000). The fusogenic activity of PEG in the respective investigations was not dependent on its molecular weight (Shi and Borgens, 1999). Here, too, PEG acts in the capacity of a fusogen to reconnect the injured axons. PEG has proven a potent neuroprotector (Baptiste et al., 2009; Liu-Snyder et al., 2007; Marks et al., 2001), since it inhibits excitotoxic neuronal cell death via direct intercalation within neural membranes (Baptiste and Fehlings, 2006). Furthermore, PEG treatment of SCI has been shown to directly repair injured neuronal mitochondria (by suppression of the rate of oxygen consumption due to H₂O₂ and/or calcium and reduction of axonal swelling (Chen et al., 2009)) and to scavenge reactive oxygen species to prevent lipid peroxidation (Luo and Shi, 2004) resulting in functional recovery (Baptiste et al., 2009; Borgens et al., 2002).

Other examples of synthetic biodegradable implant materials used for treatment of SCI, applied either alone or in combination with neurotrophic growth factors or beneficial cells present fibronectin, fibrin glue/fibrin clot, and poly(α -hydroxy acids) (Novikova et al., 2003).

1.4.2.5 NeuroGel®

NeuroGel® shall here be described as a representative of the material class of synthetic nonbiodegradable polymers. Other representatives of this group are several acrylic polymers. NeuroGel® is a biocompatible porous hydrogel made from cross-linked poly[N-(2-hydroxypropyl)methacrylamide] (pHPMA). Implantation of pHPMA or pHPMA combined with a cell-adhesive peptide sequence into completely transected spinal cord yielded promising results regarding bridge stability, vascularization and axon regeneration. The hydrogel further reduced necrosis and cavitation in the area of insult. Positive results, i.e., regeneration and functional improvement, were even described after NeuroGel® transplantation in chronic SCI (Woerly et al., 2001b;Woerly et al., 2001a;Woerly et al., 2001c).

1.4.2.6 Matrix Materials Applied in the Present Study

In the present study, three matrix materials – Matrigel™ (MG), alginate (ALG) and polyethylene glycol 600 (PEG) – were chosen for the comparison of spontaneous axonal in-growth and accountable features. This is the first time that the application of these materials in their pure form as a matrix in chronic SCI has been investigated.

1.5 The Adult Rat as a Model System for Spinal Cord Injury

Several demands need to be met by animal models of SCI: They should be reliable, consistent and reproducible. They should further reflect aspects of human SCI and allow assessment of structural features of the injured area and of functional recovery after injury. The major experimental SCI models which have been developed in the rat in this context are models of contusion, compression and transection injury (Kwon et al., 2002c;Rosenzweig and McDonald, 2004;Talach et al., 2004). While lesion models of contusion and compression injury quite realistically reflect aspects of human SCI, their major disadvantage is the occurrence of axon-

containing tissue bridges even after dramatic injuries. Thereby reliable assessment of axonal regeneration is problematic in the injury models due to the possibility of axon sparing. Partial or total transection injuries allow the detailed investigation of specific tract systems or areas, since they enable the induction of reproducible local insult.

For the present study, a transection injury (dorsal hemisection) was chosen as the initial type of rat chronic SCI. In a second SCI surgery, the inhibitory lesion scar was removed via a combination of partial transection and tissue aspiration (see Materials & Methods for details). In chronic human SCI, there is usually a lesion cavity or a gap of certain distance which needs to be bridged. Resection surgery presents an approved method as it is widely used in the course of the removal of fibrous tissue, tumors, metastases or syringomyelia. In Fig. 1.6, a schematic overview of the chronic SCI model is illustrated.

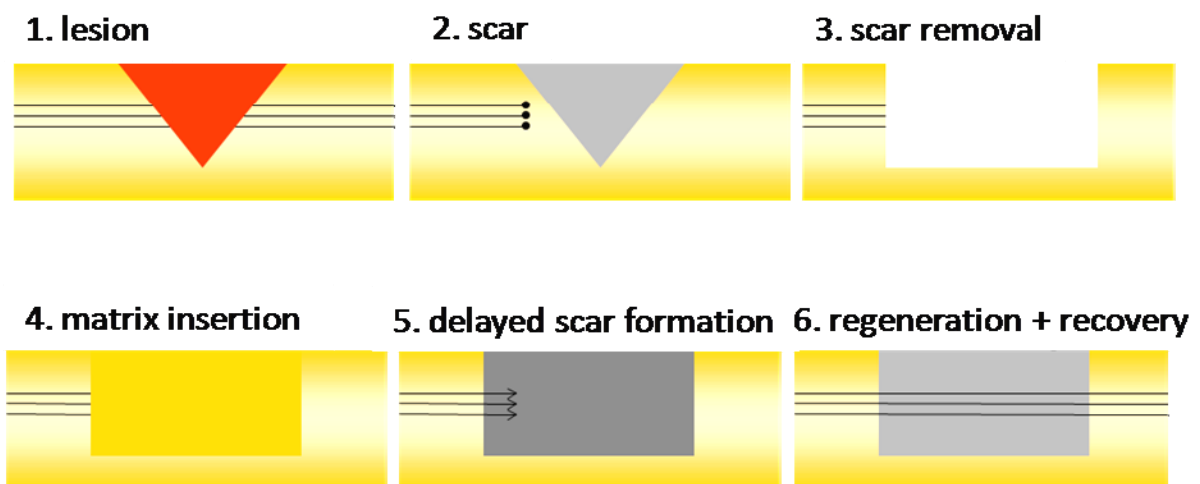


Fig. 1.6: Schematic illustration of the different steps and aims of the applied experimental chronic SCI model.

1.6 Aim of this Thesis

Spinal cord injuries predispose patients to numerous complications. It has been indicated by various studies that a chronically injured neuron generally is not dead. However, the vast majority of previous SCI studies have attempted to stimulate regeneration when treatment is begun almost immediately after injury – because, in part, it has been considered very difficult to achieve regeneration at long time points after injury. Regeneration in later chronic stages of injury has only rarely been reported. Several mechanisms create barriers to regeneration of chronically injured axons, all contributing to an unfavorable environment for axonal re-growth: A partial deficiency in the intrinsic growth capacity of adult neurons, scar formation at the site of injury and the presence of growth inhibitors. Further, a progressive degeneration of spinal cord white matter may have occurred in the time period after injury. In addition to scar formation, gaps may form in the spinal cord due to tissue necrosis or cyst formation in the subacute and chronic stage of injury. In order to provide a favorable environment for regenerating axons and growth-promoting cells and structures, approved therapeutic interventions are likely needed to be modified.

The purpose of the present study was

- the establishment of a chronic SCI model in the rat which comprises the removal of the inhibitory lesion scar,
- the application of the different matrix materials MatrigelTM, alginate hydrogel and polyethylene glycol 600 after chronic SCI scar resection and the analysis of their suitability as a matrix in the applied lesion model in regard to tissue integration and axon growth-promoting features at five weeks post SCI scar resection,
- immunohistological characterization of the area of matrix material implantation at an early time point of one week post scar resection in regard to ECM composition, vascularization, inflammation, and cellular invasion.

Materials which achieve promising results can further be used as a basis for combinatory therapeutical interventions, as they may be combined with, e.g., iron chelators, neurotrophic growth factors, or various cell types.

2 Materials and Methods

2.1 Experimental Animals

Adult female Wistar rats (outbred; HanTac:WH; Taconic, Denmark) weighing 200-230 g were operated. The animals were housed in a specifically pathogen-free environment (21 °C, 50 % ± 5 % air humidity). They were kept in groups in standard cages, provided that individual caging was not required due to altered circumstances (e.g., injuries). Animals were housed with pelletized dry food and germ-free water (pH 3) *ad libitum*.

Institutional guidelines for animal safety and comfort were adhered to and all surgical interventions and pre- and post-surgical animal care were provided in compliance with the German Animal Protection law (State Office of Environmental and Consumer Protection of North-Rhine Westfalia, LANUV NRW).

Experimental groups are listed in Fig. 2.1 and Table 2.4.

2.2 Buffers and Antibodies

2.2.1 Buffers and Solutions

Buffers and solutions which were used in the course of the experiments are listed in Table 2.1.

Table 2.1: Buffers and solutions.

0.2 M PB (phosphate buffer) pH 7.4	28.8 g Na ₂ HPO ₄ 5.2 g NaH ₂ PO ₄ <i>ad</i> 1000 ml <i>aq. bideest</i>
0.1 M PBS (phosphate-buffered saline) pH 7.4	50 ml 0.2 M PB 9 mg NaCl <i>ad</i> 1000 ml <i>aq. bideest</i>
TRIS buffer 20 mM pH 8.1	2.1 g C ₄ H ₁₁ NO ₃ <i>ad</i> 1000 ml <i>aq. bideest</i> pH titration to 7.9 via addition of HCl
BPY-DCA (2,2'-bipyridine-5,5'-dicarboxylic acid) 40 mM pH 7.4	1: 20.1 mg BPY-DCA powder (Sigma) + 2.06 ml TRIS buffer (pH 5.5) 2: 1.9 ml of solution 1 + 20 µl 5 M NaOH (pH 6.1) 3: 1.7 ml of solution 2 + 5 µl 5 M NaOH (pH 8.4) final titration with HCl
NHS (Normal Horse Serum) 3 %	300 µl NHS <i>ad</i> 10 ml PBS
NGS (Normal Goat Serum) 3 %	300 µl NGS <i>ad</i> 10 ml PBS
DS (Donkey Serum) 5 %	500 µl DS <i>ad</i> 10 ml PBS

Sodium-Citrate-Puffer pH 4.5	A: 21.01 g citric acid monohydrate (0.1 M) <i>ad</i> 1000 ml <i>aq. bidest</i> B: 29.41 g sodium citrate (0.1 M) <i>ad</i> 1000 ml <i>aq. bidest</i> for 10 mM buffer solution: 9 ml A + 41 ml B <i>ad</i> 450 ml <i>aq. bidest.</i>
Protease XXIV (Sigma)	2.5 mg Protease XXIV <i>ad</i> 5 ml TRIS buffer
Diaminobenzidin (DAB, Sigma)	140 mg DAB <i>ad</i> 200 ml PB
PFA (Paraformaldehyde) 4 % pH 7.4	40 g PFA powder <i>ad</i> 1000 ml 0.1 M PB pH-titration with NaOH
Nissl-Solution	1.6 g Na acetate anhydrous 2.88 ml acetic acid (glaciously) <i>ad</i> 300 <i>aq. bidest</i> + 100 mg Cresyl Violet, mix 15'/ 60 °C filtration
DPX (mounting fluid, Fluka)	
Rotihistol (Roth, Karlsruhe)	
Alginate	Pronova UP LVM Batch-N° FP-106-02 (preparation protocol see Materials and Methods)
Matrigel™	Basement Membrane Matrix (BD Bioscience N° 356324)
Polyethylene glycol 600 (Merck)	
Paraffin for tissue embedding	100 g paraffin 5 g <i>Cera Alba</i> (wax) 57 °C
Sucrose for cryoprotection 10 % or 30 %	10 g sucrose or 30 g sucrose <i>ad</i> 100 ml PBS
Elvax copolymer	0.1g Ethylen-Vinyl-Acetate copolymer beads (Elvax, DuPont) 1ml Dichlormethane use test tube shaker (Heidolph Reaxtop) for mixing after 20': addition of 10 µl Fast Green TRIS (200 mM) use test tube shaker for additional 40'
Triton-X100	0.1 % in PBS

2.2.2 Antibodies

2.2.2.1 Primary Antibodies

In Table 2.2, primary antibodies used in the course of the present experiments are listed.

Table 2.2: Primary antibodies.

Antibody	Class	Antigen	Antigen Localization	Manufacture	Dilution	Treatment
Col4	gt IgG	collagen type IV	BM, ECM	Biodesign	1:1000	Protease (0.05 %)
PAM SMI-312 (panaxonal neurofilament marker)	ms IgG ₁	phosphorylated neurofilament	axons	Covance	1:1000	-
GFAP (glial fibrillary acidic protein)	ms IgG ₁	glial fibrillary acidic protein (astrocyte intermediate filament)	astrocytes, ependymal cells, Schwann cells	Chemicon	1:350	-
GFAP (glial fibrillary acidic protein)	rb IgG	glial fibrillary acidic protein (astrocyte intermediate filament)	astrocytes, ependymal cells, Schwann cells	Dako	1:1000	-
ED1 (rat CD68 equivalent)	ms IgG ₁	ED1 protein of lysosomes (CD68)	phagocytizing macrophages and microglia	Serotec	1:1000	Triton X-100 (0.1 %)
S100 β	rb IgG	S100 calcium binding protein	Schwann cells, glial and ependymal cells	Sigma	1:200	-
vWF (von Willebrand factor)	rb IgG	von Willebrand factor (factor VIII related antigen)	endothelial cells, megakaryocytes, platelets (blood vessel marker)	Dako	1:1000	Protease (0.05 %)
APC (<i>Adenomatous polyposis coli</i>) Clone CC-1	IgG _{2b}	a recombinant protein consisting of amino acids 1-226 of APC	oligodendrocytes, astrocytes	Calbiochem	1:100	NaBH ₄ (1 %)

2. MATERIALS AND METHODS

rPH (rat prolyl 4-hydroxylase)	ms IgG ₁	rat prolyl 4-hydroxylase	fibroblasts	Acris	1:200	NaBH ₄ (1 %)
CD4 Clone W3/25	ms IgG ₁	rat CD4 thymocyte membrane glycoprotein	helper T cells (weakly: monocytes, macrophages)	Serotec	1:100	Protease (0.05 %)
CD5 Pan T cells Clone Ox-19	ms IgG ₁	rat CD5 thymocyte glycoproteins	T cells, thymocytes and a subset of B cells (B ₂ -cells), macrophages, granulocytes	Serotec	1:100	Protease (0.05 %)
CD8 Clone 15-11C5	ms IgG ₁	rat CD 8 thymocyte glycoproteins	cytotoxic T cells, natural killer cells, dendritic cells	Hycult Biotech	1:100	Protease (0.05 %)
Pan B-cell marker	ms IgG	rat B-cell surface proteins	B-lymphocytes	Serotec	1:100	Protease (0.05 %)
MBP Clone 1	ms IgG _{2a}	myelin basic protein (early myelination marker)	myelin basic protein	Chemikon	1:50	Citrate buffer
TH (Tyrosine Hydroxylase)	rb IgG	tyrosine hydroxylase	dopaminergic neurons	Abcam	1:750	-
5-HT (5-Hydroxy-tryptamine) Serotonin	rb IgG	serotonin	neurotransmitter in PNS and CNS	Biologo	1:30	-
CGRP (Calcitonin gene-related peptide)	gt IgG	CGRP	CGRP-containing sensory neurons	Serotec	1:1500	-

2.2.2.2 Secondary Antibodies, Reagents and Tracer Substances

A list of secondary antibodies, reagents and tracer substances used in the course of the experiments is given in Table 2.1.

Table 2.3: Secondary antibodies, reagents and tracer substances.

Substance	Class	Manufacture	Dilution
anti-mouse IgG	hs IgG (biotinylated)	Vector Laboratories	1:150
anti-mouse IgG	gt IgG (biotinylated)	Vector Laboratories	1:150
anti-rabbit IgG	gt IgG (biotinylated)	Vector Laboratories	1:150
anti-goat IgG	hs IgG (biotinylated)	Vector Laboratories	1:150
Alexa Fluor® 594 anti-mouse	dk IgG	Molecular Probes	1:200
Alexa Fluor® 488 anti-mouse	dk IgG	Molecular Probes	1:200
Alexa Fluor® 594 anti-rabbit	dk IgG	Molecular Probes	1:200
Alexa Fluor® 488 anti-rabbit	dk IgG	Molecular Probes	1:200
Alexa Fluor® 594 anti-goat	dk IgG	Molecular Probes	1:200
Alexa Fluor® 488 anti-goat	dk IgG	Molecular Probes	1:200
Avidin-Biotin-Peroxidase-Complex (ABC-Elite Kit)		Vector	1:100
Biotinylated Dextran Amine (BDA) MW 10,000		Molecular Probes	10%
Oregon Green® 488		Molecular Probes	1:1,000
Streptavidin, Alexa Fluor® 405		Molecular Probes	1:200
Streptavidin, Alexa Fluor® 647		Molecular Probes	1:200
Sudan Black B		Fluka	0.3 %
DAPI (4',6-Diamidino-2-phenylindole)		Roche	1:10,000

2.3 Experimental Setup

2.3.1 Experimental Animal Groups

An overview of the different treatment groups is given in Fig. 2.1.

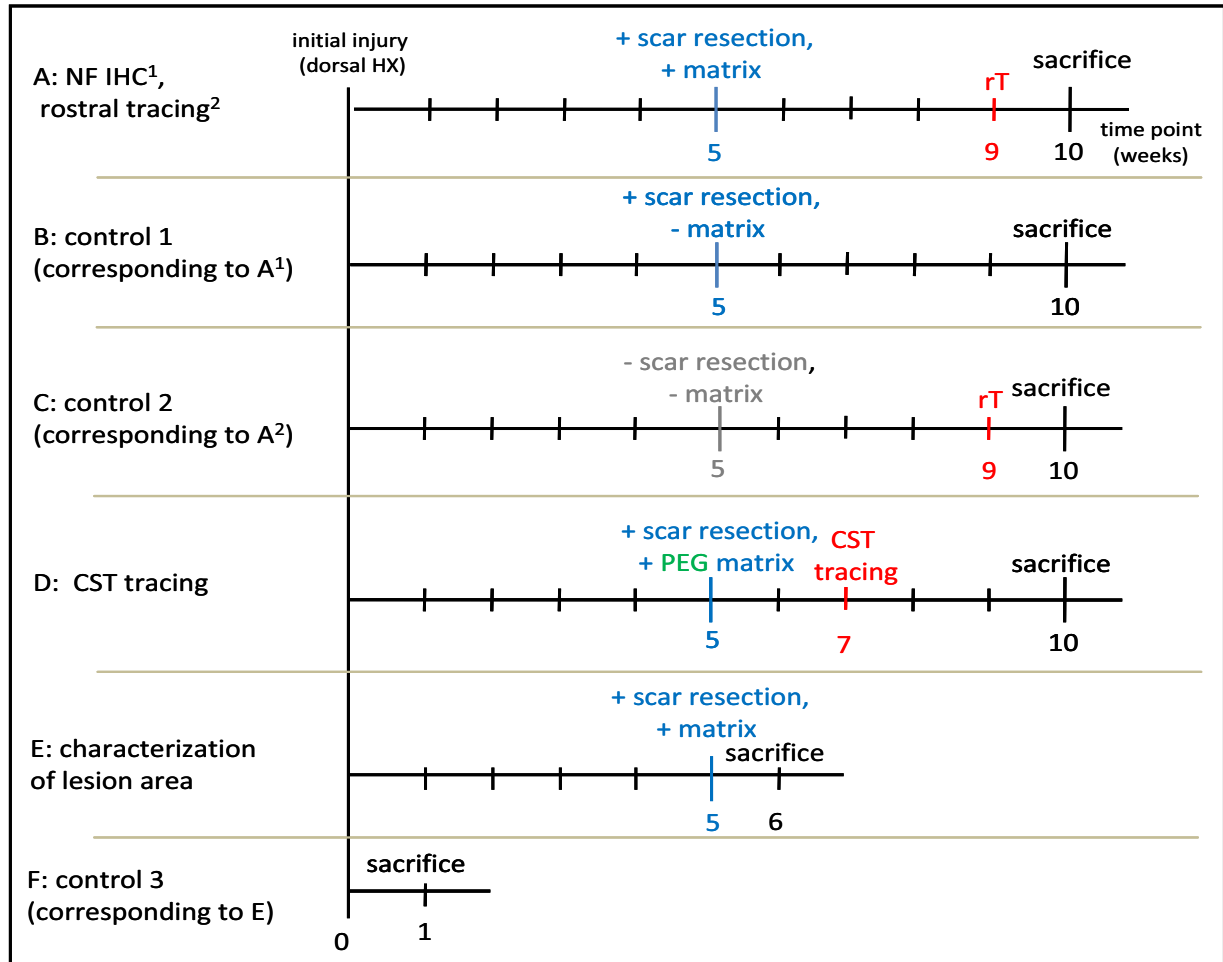


Fig. 2.1: Experimental treatment groups.

In Tab. 2.4, the animal numbers used for evaluation of the respective treatment approaches (shown in Fig. 2.1) are listed.

Table 2.4: Experimental animals analyzed for the respective treatment groups shown in Fig. 2.1.

Treatment Group	Survival Time	n
A1 _{ALG}	5 wpr	6
A1 _{PEG}	5 wpr	9
A2 _{ALG}	5 wpr	4
A2 _{ALG+BPY-DCA}	5 wpr	3
A2 _{PEG}	5 wpr	4
B	5 wpr	4
C	5 wpr	6

Treatment Group	Survival Time	n
D	5 wpr	5
E _{MG}	1 wpr	3
E _{ALG}	1 wpr	7
E _{PEG}	1 wpr	6
F	1 wpl	4
F	5 wpl	4

2.3.2 Surgical Procedures

2.3.2.1 Dorsal Transection Lesion

Animals were anesthetized with isoflurane (Forene; 2–3 % in O₂ and NO₂ at a ratio of 1:2). All instruments were disinfected using 70 % ethanol before usage. The skin overlying the Th6-Th12 vertebral levels was shaved and disinfected. An incision was made with a scalpel blade over the Th6-Th12 spinous processes exposing the underlying paravertebral muscles. Adipose tissue between the blade bones was carefully removed from the muscles. Care was taken not to damage any BV. Blunt dissection was utilized to expose the transverse processes at Th7-Th10, muscle tissue was forced apart using a muscle retractor, and a complete laminectomy was performed at Th8/Th9: Spines and vertebral arches were removed using a Friedman-Pearsons micro-rongeur (FST 16020-14). Care was taken not to damage the lateral spinal arteries. The spinous processes of Th7 and Th10 were clamped and stabilized using a stereotactic device (Small Animal Adaptor, David Kopf Instruments) to allow controlled operation procedure. The meninges (*dura mater*, *arachnoidea* and *pia mater*) were opened at the vertebral levels Th8/Th9 under microscopic control using iridectomy scissors via a longitudinal cut, and a dorsal hemisection injury was induced with a Scouten wire knife (SWK, Bilaney). The diameter of the opening of the bones was slightly larger than the opened SWK. The SWK was fixed on the stereotactic frame. The tip of the unopen knife was placed on the right side of the spinal cord, and from there the guidance canula was stereotactically inserted 1.2-1.5 mm deep into the spinal cord tissue. The knife was slowly extended semicircularly. Then, while counterpressure was applied with a fine spatula, the opened knife was lifted up, transecting the axonal tracts of the dorsal spinal cord. In Fig. 2.2, a schematic illustration of the area affected by the dorsal SWK-hemisection is presented.

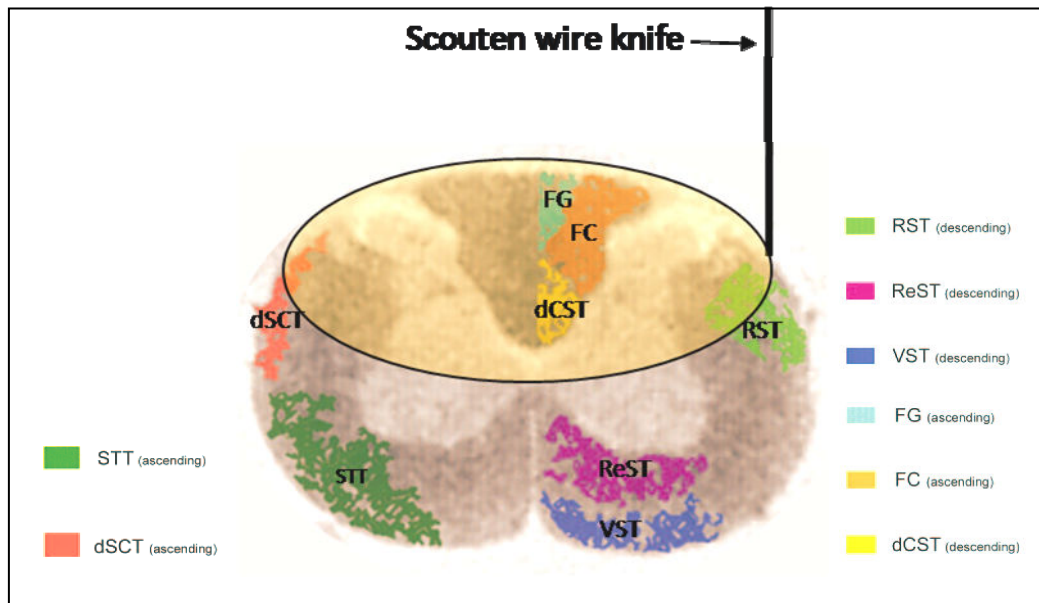


Fig. 2.2: Schematic illustration of the Scouten wire knife-lesion. In the MR image overlaid with a histologic spinal cord cross section (modified from Schwartz et al., 2005b) fiber tracts affected by the applied lesion are depicted; STT: spinothalamic tract, dSCT: dorsal spinocerebellar tract, RST: rubrospinal tract, ReST: reticulospinal tract, VST: vestibulospinal tract, FG: *fasciculus gracilis*, FC: *fasciculus cuneatus*, dCST: dorsal corticospinal tract.

In Fig. 2.3, a schematic drawing of the dura opening, which was performed in the course of the operation, is depicted. Contrary to other lesion models which are frequently applied in the Molecular Neurobiology Laboratory, the dura was not opened via a lateral cut, but instead a longitudinal opening was performed. This method was chosen because the extent of the tissue removal during the scar resection surgery amounted to 4 mm and would therefore require a larger opening of the meninges.

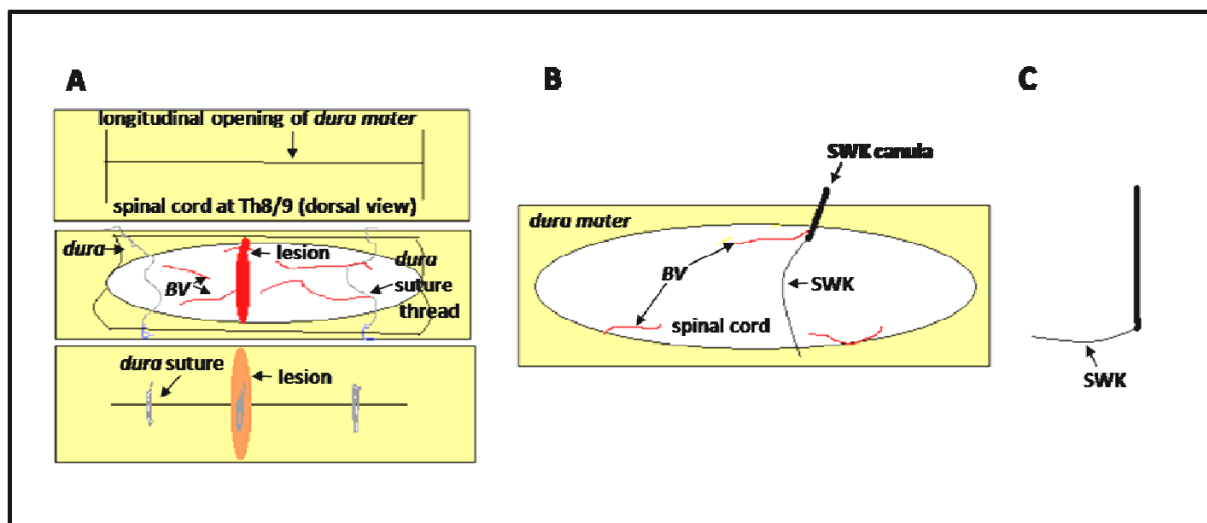


Fig. 2.3 (previous page): Schematic drawing of the longitudinal opening of the *dura mater* in top view. A: The *dura* was not opened via a transversal cut, but a longitudinal opening of the *dura* was performed instead. After lesioning the spinal cord, the *dura* was sutured (bottom drawing in A). B: A Scouten wire knife (SWK) was used to partially transect the spinal cord. C: To perform the dorsal hemisection lesion, an SWK was chosen which exhibited a flat, but wide extent to enable the dorsal hemisection lesion. BV: blood vessel, SWK: Scouten wire knife.

After suture of the *dura mater*, the lesion area was covered with a piece of Elvax (ethylene vinyl acetate) copolymer loaded with TRIS buffer. Finally, the overlying muscle and skin were sutured in layers. A schematic drawing of the dorsal hemisection lesion surgery is shown in Fig. 2.4.

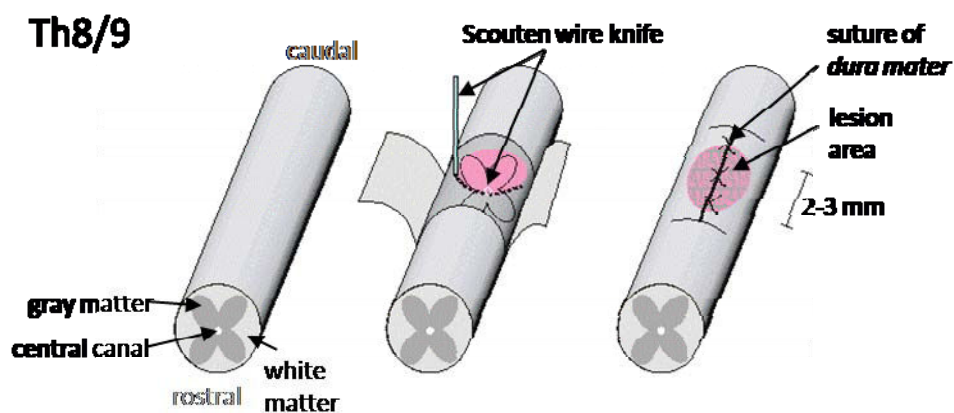


Fig. 2.4: Initial spinal cord lesion. Dorsal hemisection injury at thoracic level 8/9 (Th8/9) using a Scouten wire knife (SWK). The *dura mater* was sutured subsequently to the injury.

2.3.2.2 Scar Removal and Cavity Filling

Five weeks after the initial SCI, animals were re-anesthetized with isoflurane, and the lesion area was re-opened. The Elvax copolymer was removed and the sutures were cut open to expose the lesioned spinal cord. Two incisions on both sides of the spinal cord lesion, each 1.5 mm deep into the spinal cord, were made 4 mm apart from each other with iridectomy scissors. Spinal cord tissue was removed via gentle aspiration with a fine plastic tip attached to a vacuum pump. An area of 4 mm in length was aspirated until the central canal became visible or until all scar tissue (recognizable by its stiff texture) was removed, respectively. After the aspiration procedure, the cavity was filled with Gelastyp® (Sanofi) soaked in 0.9% sodium chloride solution for approximately 5-10 minutes to minimize bleeding during matrix implantation. After this time the Gelastyp® gelatin sponge was removed from

the spinal cord. After filling of the cavity with the respective gel matrix material, the lesion area was covered with a small piece of Nescofilm® (Roth), which was affixed to surrounding tissue with a few drops of tissue glue to prevent extensive leakage of the respective substance. Care was taken to prevent contamination of spinal cord tissue or gel matrix with the glue. Finally, the overlying muscle and skin were sutured in layers. Control animals either received a scar resection and no matrix injection (“RX only”), or they received the initial lesion and no scar resection, respectively (“lesion only”). A schematic drawing of the scar removal and matrix insertion procedure is shown in Fig. 2.5.

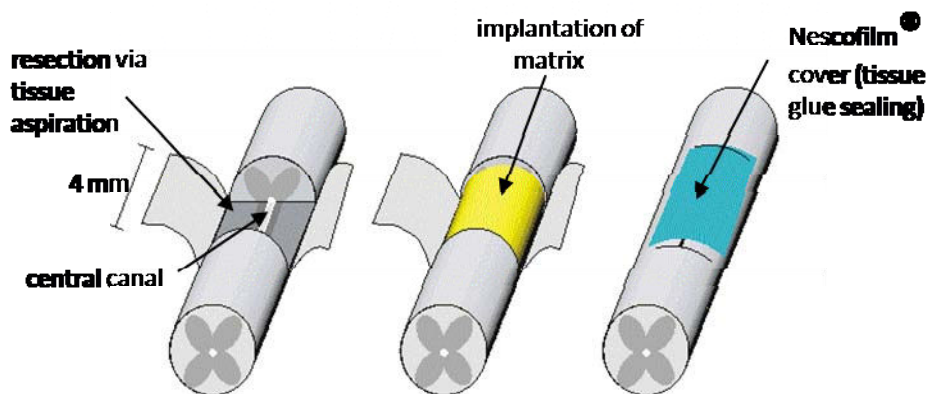


Fig. 2.5: Scar removal and subsequent gel matrix filling of resulting cavity. Scar removal via aspiration and resection five weeks post initial injury. Extent of dorsal spinal cord/scar tissue removal: 4 mm in rostro-caudal direction. Subsequent filling of cavity with matrix material in treated animals. Finally, covering of the lesioned area with Nescofilm® and sealing with tissue glue.

The schematic drawings in Fig. 2.6 show a comparison of the lesion extent in spinal cord cross section after initial SWK-transection and chronic SCI scar resection.

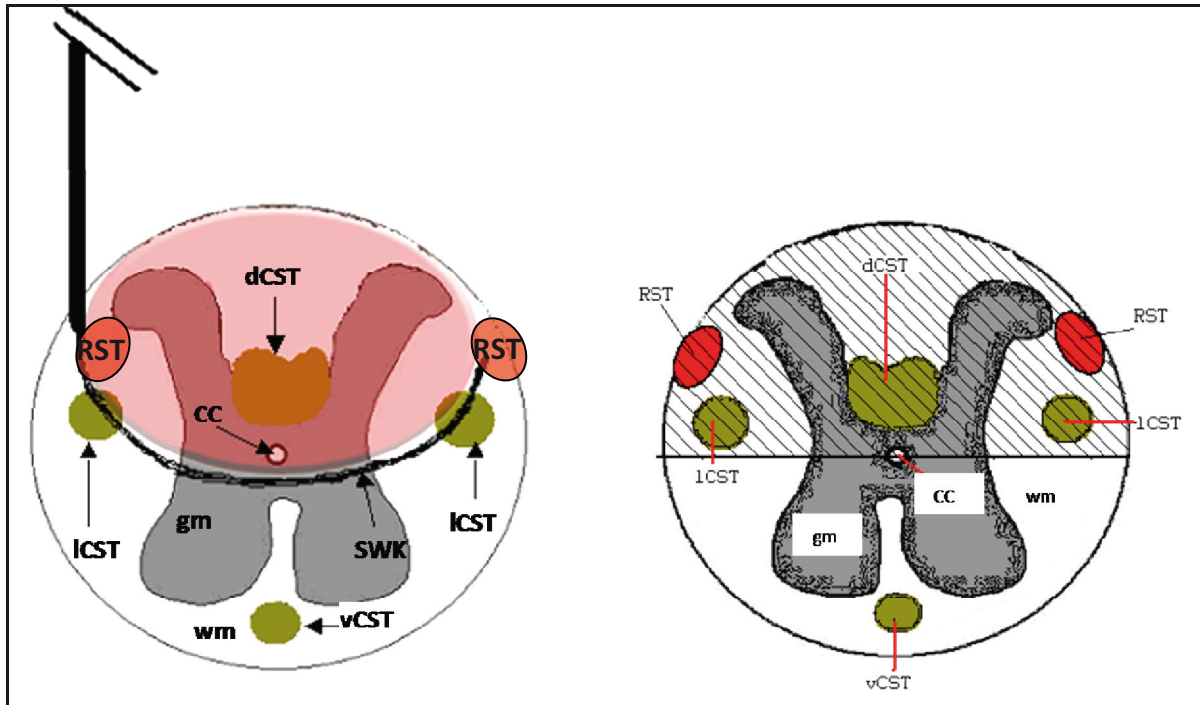


Fig. 2.6: Comparison SWK lesion vs. dorsal hemisection via aspiration in schematic cross sections. Left: Affected area after SWK lesion. Right: Affected area after tissue aspiration. dCST, ICST, vCST: dorsal, lateral, ventral CST; cc: central canal; gm: gray matter; wm: white matter; SWK: Scouten wire knife.

2.3.2.3 Matrix Preparation and Implantation

Subsequently to the scar removal, either MatrigelTM (BD Biosciences), or an ALG gel (Pronova UP LVM; NovaMatrix) or PEG 600 (Merck), respectively, were injected into the aspiration cavity.

Matrigel

Aliquots of MG were thawed on ice overnight for liquefaction. For MG injection, cooled pipette tips, syringes and canulas were used in order to prevent early gel formation. To fill the surgical cavity resulting from spinal cord injury scar aspiration, MG was injected using a stereotactic device to which a 10 μ l Hamilton syringe (#701 LT) with a blunt canula was attached.

Alginate and Alginate+BPY-DCA

For ALG hydrogel preparation, a 2 % (w/v) ultra pure low-viscosity mannuronic acid alginate in 150 mM sodium chloride (NaCl) solution was filtered with a sterile

syringe filter. Care was taken that ALG hydrogel was always freshly prepared to allow a constant viscosity.

To fill the surgical cavity resulting from spinal cord injury scar aspiration, ALG was injected using a stereotactic device to which a 10 μ l Hamilton syringe (#701 LT) with a blunt canula was attached. ALG was set by exposure to 0.1 M calcium chloride (CaCl_2) resulting in a solid ALG hydrogel.

For chelator-containing ALG solution, first a 40 mM solution of the iron chelator [2,2'-bipyridine]-5,5'-dicarboxylic acid (BPY-DCA) in distilled water was prepared. 150 mM NaCl was subsequently added to the solution. Then via addition of 2 % (w/v) ALG powder and subsequent filtration, the injectable ALG was created.

Polyethylene Glycol 600

Prior to implantation, PEG 600 was heated to 37 °C to allow liquefaction. To fill the surgical cavity resulting from SCI scar aspiration, PEG was injected using a stereotactic device to which a 10 μ l Hamilton syringe (#701 LT) with a blunt canula was attached.

2.3.2.4 Anterograde Labeling of Axons in the Thoracic Spinal Cord

One week prior to sacrifice, animals were re-anesthetized with isoflurane, and the thoracic area was re-opened. Biotinylated dextran amine (BDA) was injected into the spinal cord 3 mm rostrally to the lesion/implantation site, as shown in the schematic drawing in Fig. 2.7. Injections of BDA were applied: In the midline at 1.5 mm (ventral *funiculus*), 0.8 mm (dorsal CST), and 0.5 mm (cuneate and gracile *funiculi*) from the *pia mater*, at 1 mm laterally from the midline on each side at depths of 1.2, 0.8 and 0.4 mm (lateral *funiculi*) from the *pia mater*, using a grease-sealed glass canula attached to a Hamilton syringe.

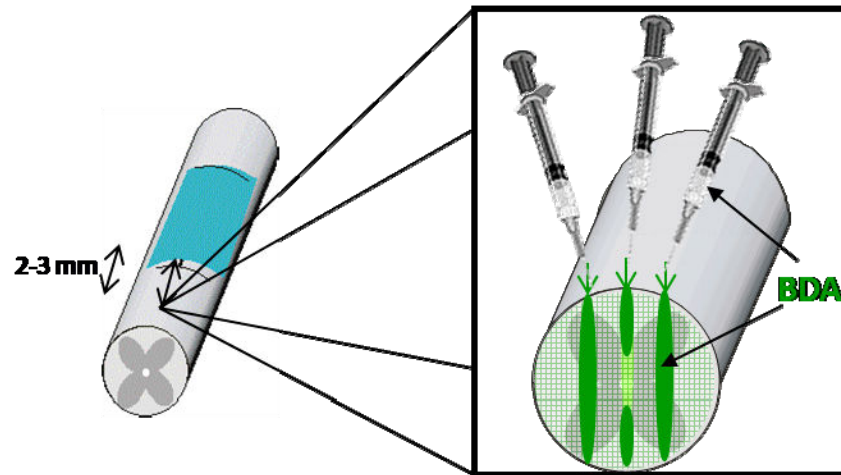


Fig. 2.7: Axonal tracing. Axons were labeled with biotinylated dextran amine (BDA) via tracer injections into the spinal cord 2-3 mm cranially to the lesion site.

2.3.2.5 Anterograde Labeling of Corticospinal Tract Neurons

Three weeks prior to sacrifice, the CST was labeled. The head of the anesthetized animal was fixed in the Small Animal Adaptor at both external acoustic *meati* and at the front teeth. The skull was shaved under precaution not to cut the whiskers and locked into the stereotaxic device. The *cranium* was exposed and the *periosteum* was removed. Two small „window“-openings along the sagittal and coronal suture were cut with a drill (\varnothing 1,4 mm, Fine Science Tools) to expose the brain. Bregma was determined according to Fig. 2.8.

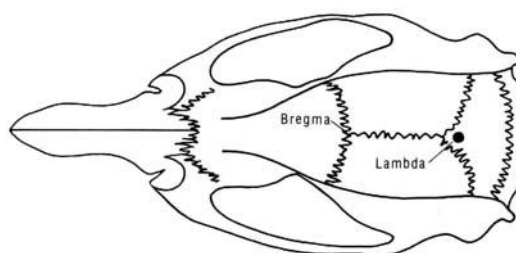


Fig. 2.8: Rat skull. Bregma, Lambda and the cranial fissures between the skull bones are important markers for orientation in the tracing procedure (Paxinos and Watson, 2005).

After craniotomy, tracing was performed by multiple small volume injections (0.2 μ l each) of BDA. For injection, a glass capillary (40-60 μ m in diameter) had been fixed with sealing wax onto a Hamilton microliter-syringe (10 μ l). 0.2 μ l BDA were pressure-injected at each target spot. Eight injections at a depth of 1.2 mm were made into the sensorimotor cortex of each hemisphere (Klapka et al., 2005). In table

2.5, the coordinates (in regard to Bregma) for injection into layer V of the sensorimotor cortex and marking of the corticospinal cellular bodies are shown. They were determined with the aid of Paxinos and Watson Stereotaxic Atlas of the Rat Brain (1982) and have been established by Susanne Hermanns in modification of a lab protocol of Dr. Ray Grill, University of Texas, Houston, TX (Hermanns, 2001). The coordinates for BDA injection are shown in table 2.5.

Table 2.5: Coordinates for BDA injections into layer V of the sensorimotor cortex in regard to Bregma. A/P: anterior/posterior, L: lateral

Bregma	left	left	right	right
A/P	L	L	L	L
-0.08	+0.20		-0.20	
-0.13	+0.22		-0.22	
-0.18	+0.24	+0.29	-0.24	-0.29
-0.23	+0.24	+0.29	-0.24	-0.29
-0.28	+0.24		-0.24	
-0.33	+0.24		-0.24	

Fig. 2.9 presents a schematic illustration of the BDA tracing.

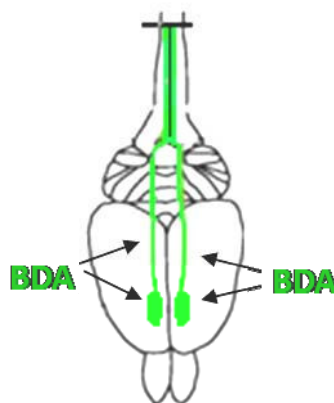


Fig. 2.9: Axonal tracing: Schematic drawing of the labeling of CST neurons via injection of biotinylated dextran amine (BDA, green) into the sensorimotor cortex. From there the tracer substance is transported anterogradely in the axons.

After the labeling procedure, the skin was closed using metal clips (Michel).

2.3.3 Post-Operative Care

Post-operative care included prophylactic daily oral Baytril® administration (Bayer Health Care) over one week. When necessary, animals received manual bladder expression. They were inspected for signs of infection, dehydration or autophagia, with appropriate veterinary assistance as needed.

2.3.4 Animal Sacrifice

Animals were deeply anesthetized. The thorax and the left ventricle of the heart were opened. A canula connected to a perfusion pump (505S, Watson-Marlowe) was inserted into the left ventricle and directed to be finally placed in the aorta where it was fixed with clamp forceps. Subsequently, the right ventricle was opened. With a pump rate of 25 ml/min, the blood was washed out of the circulatory system for 2 minutes with cold PBS (4 °C), followed by 15 minutes of perfusion with 4 % PFA to fix the tissue.

2.4 Tissue Processing

2.4.1 Paraffin Sections

Processing:

Immediately after perfusion, the Th4-Th11 part of the spinal column was removed and post-fixed ON/4 °C in the fixative (4 % PFA). On the following day, the lesion-containing piece of the spinal cord was dissected using fine bone scissors (FST 16109-14) and transferred into PBS ON/4 °C.

Paraffin-Embedding:

The tissue was dehydrated.

- Dehydration:
EtOH 70 %: 30'
EtOH 90 %: 60'
EtOH 100 %: 3x 60'
methyl benzoate: ON

Subsequently, after incubation in benzene for 15 minutes, specimens were incubated in a benzene/paraffin mix (10 % v/v) for 30 minutes/57 °C, followed by three further

incubations in pure paraffin (1 h/57 °C each). After a final incubation ON/57 °C the specimens were embedded in rubber moulds using liquid paraffin.

Sectioning:

Specimens in paraffin blocks were cut parasagittally into 10 µm thick sections on a paraffin-microtome (RM 2035, Jung). For mounting on HistoBond® slides (Marienfeld), sections were collected in ~40 °C-warm water. Finally, sections were baked in an oven at 56 °C.

2.4.2 Cryo Sections

Processing:

Tissue preparation was carried out as mentioned above. Specimens were transferred from PBS into 10 % sucrose/4 °C for 24 h, followed by incubation in 30 % sucrose/4 °C until the tissue had completely sunken in the solution. Finally, specimens were frozen in isopentane (-50 to -40°C) on dry ice and stored at -20 °C until sectioning.

Sectioning:

Specimens were frozen on tissue holder using Tissue-Tek® (Sakura). 10 µm or 20 µm, respectively, thick sections were cut using a cryotome (CM3000, Leica) at a specimen temperature of -32 °C and a chamber temperature of -40 °C. Sections were mounted on HistoBond® glass slides and stored at -20 °C until further usage.

2.4.3 Freezing-Microtome Sections

Processing:

Tissue preparation was carried out as mentioned above. Two to three days prior to sectioning, specimens were transferred from PBS into 10 % sucrose/4 °C for 24 h, followed by incubation in 30 % sucrose/4 °C until the tissue had completely sunken in the solution.

Sectioning:

The respective spinal cord pieces were cut on a freezing-microtome (HM 430, Microm) at 50 µm thickness for improved visualization of potentially regenerated

axon fibers and for improved stability of the matrix-containing area. Specimens were freeze-mounted onto the cutting area of the microtome (cutting temperature: -28 to -24 °C) in sagittal direction using Tissue-Tek® compound. Care was taken that the specimens were mounted in diagonal orientation with the dorsal part of the spinal cord pieces facing away from the steel knife.

2.5 Staining Protocols

2.5.1 Histological Stainings

2.5.1.1 Nissl Staining

- Deparaffinization and rehydration:

ROTI Histol: 3x 10'
EtOH 100 %: 3x 5'
EtOH 90 %: 1x 5'
EtOH: 70 %: 1x 5'
EtOH: 50 %: 1x 5'
PBS: 1x 5'

- Nissl Staining:

Nissl-solution: 5-7'/60 °C

- Dehydration:

rinse 3x (fast) *aq. dest.*
rinse 3x (fast) EtOH 50 %
rinse 3x (fast) EtOH 70 %
rinse 3x (fast) EtOH 90 %
rinse 6x (fast) EtOH 100 %
rinse 6x (fast) ROTI Histol
mount with DPX

2.5.1.2 Masson Trichrome Staining

Depending on the protocol, trichrome stain is a polychrome protocol which is used in histology and presents an easy and fast way to define connective tissue in histological preparations. The protocol used for this study slightly differed from the original Masson's trichrome stain protocol, since no staining of cell nuclei was performed. The trichrome was applied by immersion of fixated spinal cord tissue sections into three different solutions labeled A, B, and C. Solution A contains acidic red dye which is responsible for red/pink staining of muscle, keratin and cytoplasm as

well as for red stain of red blood cells. Solution B is necessary for the differentiation of the staining, and solution C causes the green fiber (i.e., collagen) staining. The principle use for trichrome is to differentiate collagen from other eosinophilic structures, such as muscle fibers, making trichrome stains especially useful for highlighting an accumulation of scar tissue.

- Solutions:

A:

1 g Acid Fuchsin
1 g Xylidine Ponceau
198 ml deionized water
2 ml acetic acid

B:

1 g Phosphomolybdic acid
200 ml deionized water

C:

4 g Light Green SF yellowish
4 ml acetic acid
200 ml deionized water

- Deparaffinization and rehydration:

ROTI Histol: 3x 10'
EtOH 100 %: 3x 5'
EtOH 90 %: 1x 5'
EtOH: 70 %: 1x 5'
EtOH: 50 %: 1x 5'

- Staining:

rinse deionized water
solution A: 1x 10'
rinse deionized water
solution B: 10'
rinse deionized water
solution C: 10'
rinse deionized water

- Dehydration:

EtOH 50 %: 1x 1'
EtOH 70 %: 1x 1'
EtOH 90 %: 1x 1'
EtOH 100 %: 2x 1'
ROTI Histol: 2x 3'

- Mounting:

DPX

2.5.2 Immunohistochemical Staining

The ALG used for the present studies was prepared and implanted as a hydrogel without freeze-drying after preparation. Thus, it was very sensitive to shear forces. Injection or cutting into pieces of pre-gelled alginate was hardly possible due to its immediate disintegration caused by the applied force. For this reason, after the ALG gel component was injected into the cavity, it was covered with CaCl_2 solution until gel formation had occurred. While it remained in place during the operation procedure, remaining ALG which had been spared from degradation *in vivo* frequently dissolved during tissue processing (e.g., embedding, cutting and staining procedures). Therefore, the scar-containing spinal cord pieces and lesion/matrix area-containing sections were collected in CaCl_2 -containing (100 mM) PBS solution.

2.5.2.1 DAB-Staining of Paraffin Sections

- Deparaffinization and rehydration

ROTI Histol: 3x 10'

EtOH 100 %: 3x 5'

inactivation of endogenous proteases: 200 ml MeOH+ 1.2 ml H_2O_2 : 10'

EtOH 90 %: 1x 5'

EtOH: 70 %: 1x 5'

EtOH: 50 %: 1x 5'

PBS: 2x 5'

- Methods for demasking of antigens (if required):

Protease XXIV:

0.05 % in TRIS buffer

incubation of sections: 7'/37 °C

PBS: 2x 5'

Citrate buffer:

buffer concentration: 10 mM

incubation of sections: 8'/microwave (600 W)

cooling-down period: 30'

PBS: 2x 5'

Triton X-100:

0.1 % in PBS/RT

incubation of sections: 10'/RT

PBS: 2x 5'

NaBH₄:

1 % in PBS/RT

incubation of sections: 10'/RT

PBS: 2x 5'

- Blocking:

3 % normal serum: 15'/RT

- Primary antibody:

incubation ON/4 °C

PBS: 2x 5'

- Secondary antibody:

45'/RT

PBS: 2x 5'

- Antibody detection:

ABC: 45'/RT

PBS: 1x 5'

0.1 M PB: 1x 5'

DAB: incubation for 1'

addition of 0.01 % H₂O₂

further incubation for 5'

aq. bidest.: rinse 5x

- Dehydration:

EtOH 50 %: 1x 5'

EtOH 70 %: 1x 5'

EtOH 90 %: 1x 5'

EtOH 100 %: 2x 5'

ROTI Histol: 2x 10'

- Mounting:

DPX

2.5.2.2 DAB-Staining of Cryo Sections

fix sections in ice-cold acetone

let sections dry at room temperature

PBS: 2x 5'

inactivation of endogenous proteases: 200 ml PBS + 600 µl H₂O₂: 10'/RT

PBS: 2x 5'

- Methods for demasking of antigens (if required):

as described in 2.5.2.1

- Blocking:

3 % normal serum: 15'/RT

- Primary antibody:

incubation ON/4 °C

PBS: 2x 5'

- Secondary antibody:

45'/RT

PBS: 2x 5'

- Antibody detection:

ABC: 45'/RT

PBS: 1x 5'

0.1 M PB: 1x 5'

DAB: incubation for 1'

addition of 0.01 % H₂O₂

further incubation for 5'

aq. bidest.: rinse 5x

let sections dry at room temperature

- Mounting:

DPX

2.5.2.3 Immunofluorescent Staining of Paraffin Sections

- Deparaffinization and rehydration:

Xylene: 2x 10'

EtOH 100 %: 3x 5'

EtOH 90 %: 1x 5'

EtOH: 70 %: 1x 5'

EtOH: 50 %: 1x 5'

PBS: 2x 5'

- Methods for demasking of antigens (if required):

as described in 2.5.2.1

- Blocking:

5 % normal serum: 1 h/RT

- Primary antibody:

incubation ON/4 °C

PBS: 2x 5'

- Secondary antibody + DAPI:

1 h/RT

PBS: 1x 5'

EtOH 70 %: 1x 5'

Sudan Black B: 1x 7'

EtOH 70 %: rinse 5x

aq. bidest.: 2x 5'

- Mounting:

Fluoromount-G™ (Southern Biotech)

2.5.2.4 Immunofluorescent Staining of Cryo Sections

fix sections in ice-cold acetone

let sections dry at room temperature

PBS: 2x 5'

- Methods for demasking of antigens (if required):

as described in 2.5.2.1

- Blocking:

5 % normal serum: 1 h/RT

- Primary antibody :

incubation ON/4 °C

PBS: 2x 5'

- Secondary antibody + DAPI:

1 h/RT

PBS: 1x 5'

EtOH 70 %: 1x 5'

Sudan Black B: 1x 7'

EtOH 70 %: rinse 5x

aq. bidest.: 2x 5'

let sections dry at room temperature

- Mounting:

Fluoromount-G™ (Southern Biotech)

2.5.2.5 Immunofluorescent Staining of Freezing-Microtome Sections

To ensure diffusion of the staining substance through the entire thickness of 50 µm-sections, a free-floating staining technique using 12-well-microtiterplates on a shaker was applied. First, sections were washed with PBS (3x 10'), followed by the staining procedures as described above. For fluorescent BDA-visualization, sections were incubated ON with Oregon Green® 488 at 4 °C. After the staining procedures, sections were mounted on glass slides with PBS. After sections were dried, they were cover-slipped with Fluoromount-G™ and stored at 4 °C.

In Table 2.2, antibodies which were applied and the used respective concentrations are listed. Antibodies against the animal type of origin of the first antibody were used as secondary antibodies. Normal serum of the animal type of origin of the secondary antibody was used as blocking agent.

2.6 Analysis and Documentation

2.6.1 Documentation of Immunohistological Stainings

Spinal cord slices with DAB-antibody-visualization or with either Alexa 488-, Alexa 594-, respectively Alexa 405-coupled secondary antibodies (immunofluorescent staining, IF) were analyzed using a BZ-8000 Keyence fluorescent digital microscope. Additional images of IF staining, were taken using a Zeiss LSM 510 confocal microscope. The digitalized pictures were saved in TIF format. Sections with antibody-IR visualization via use of DAB were analyzed using the Keyence BZ-8000.

2.6.2 Axon Quantification

The complete lesion area or resection area, respectively, was taken into account for evaluation, without exclusion of areas with increased tissue loss or matrix degradation.

For quantification of PAM-positive axon density or the number of BDA-positive axons, respectively, in the matrix/lesion site, on average at least every 5th 50 µm-spinal cord section was stained per animal, resulting in at least 8-12 stained sections

per animal. Three sections per animal were stained in the “RX-only” control group because due to consistent lack of regenerated tissue in the resection area of the respective animals, great variability was not expected. The assumption was proved correct by the respective quantification results. Different quantitative analyses were attempted to find a suitable method which would reflect observed results regarding axon in-growth into the lesion area.

2.6.2.1 Quantification of PAM-positive Axon Profiles via Pixel-Threshold in Image J

For PAM-IR signal quantification with the open source software Image J, microscopic color images were converted into grey scale images. A pixel threshold was set and the respective IR-positive area percentage per lesion area per image was quantified.

2.6.2.2 Quantification of PAM-positive Axon Profiles with Neuron J

For the quantification of axons in the lesion area with the Image J plug-in Neuron J (Meijering et al., 2004), the lesion area of the parasagittal center section, IF-stained with the neurofilament marker PAM, of each animal was analyzed. Microscopic images of the lesion area were taken at a 10x-magnification. After conversion into 8-bit images, neuronal structures were traced with the help of the Neuron J software. An illustrative model of the Neuron J axon tracing procedure is given in Fig. 2.10.

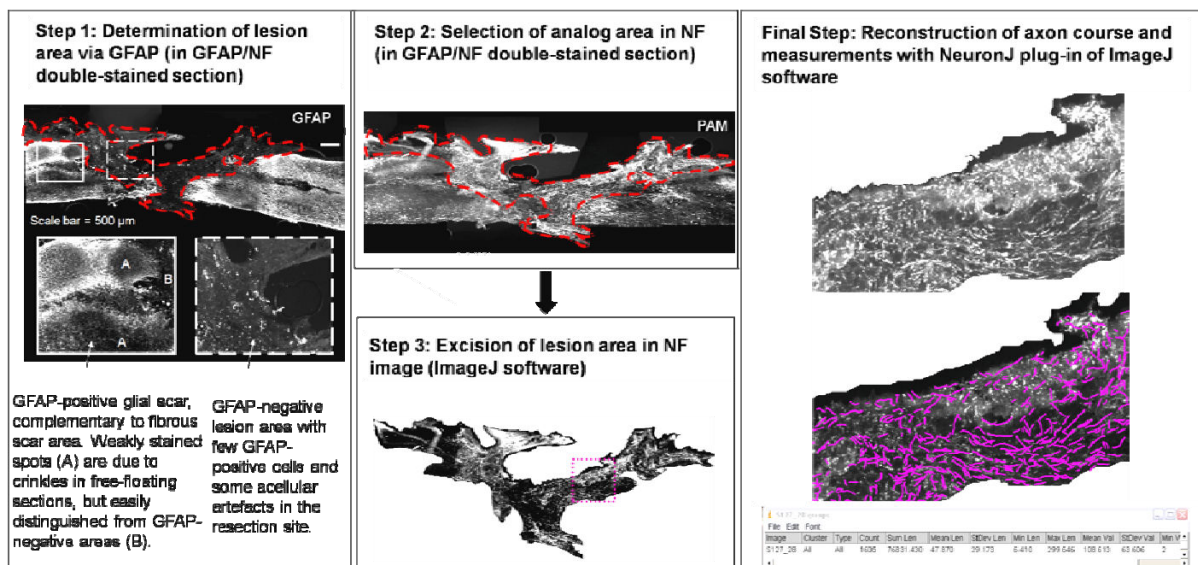


Fig. 2.10 (previous page): Illustrative model of scar determination and PAM-positive axon quantification with Neuron J. Example images of 50 μm thick spinal cord sections from a matrix-treated animal. Sections were stained for the neurofilament marker PAM and analyzed with Image J software plug-in Neuron J. After manual tracing of axons, the software calculates numbers, lengths and length distributions of axonal structures which can be further analyzed with Excel.

Additionally, in Fig. 2.11, a representative image of a “resection only” lesion area and the corresponding neuronal tracing with Neuron J is presented for comparison.

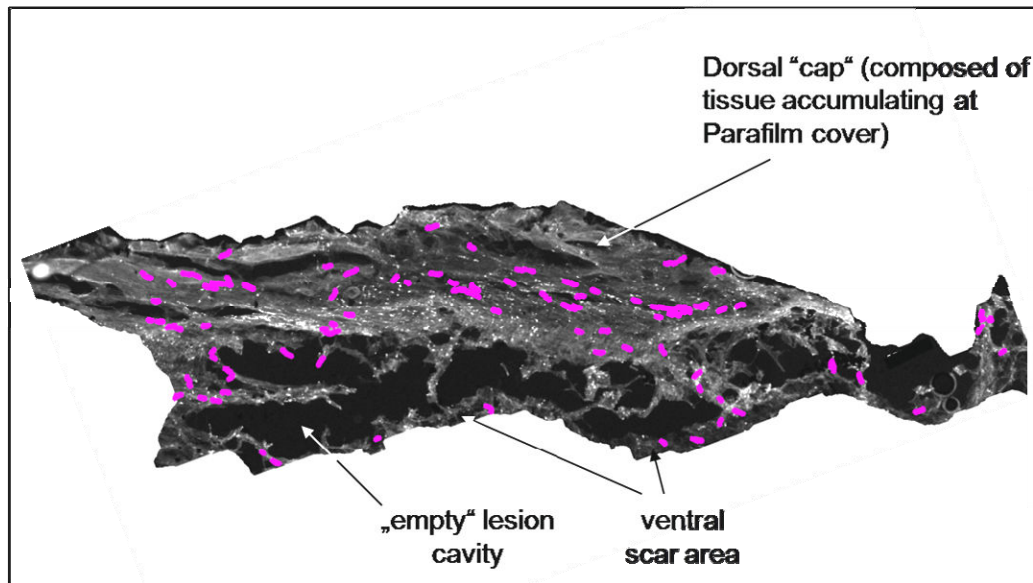


Fig. 2.11: Example of Neuron J axon tracing in a section from a “resection only” control animal. Quantitative data, e.g., axon profile number or profile length, were subsequently calculated by the software for each analyzed section.

2.6.2.3 Quantification of PAM-positive Axon Profile Density with Image J

Fig. 2.12 shows exemplary image areas of ALG- and PEG-treated resection sites at 5 weeks post resection (wpr). The presented images further illustrate why analysis via simply applying a certain pixel threshold in Image J (as described in chapter 2.6.2.1) was not a good quantitative method in this study: Background signal (arrows in Fig. 2.12A) oftentimes revealed similar or even higher intensities than axon profiles. While in PEG-matrix, PAM-IR was mainly restricted to clear axonal structures (Fig. 2.12B), in ALG matrix, axonal structures were often much thinner than those seen in PEG matrix (Fig. 2.12A), and they often revealed only weak IR to PAM. Therefore, simple quantification of IR-signal pixels would falsify the actual results. In order to eliminate some unwanted background signal recognition during

the evaluation, the eventual method of choice for the quantification was an Image J plug-in which can be used for the quantification of line-like structures, such as axons in images.

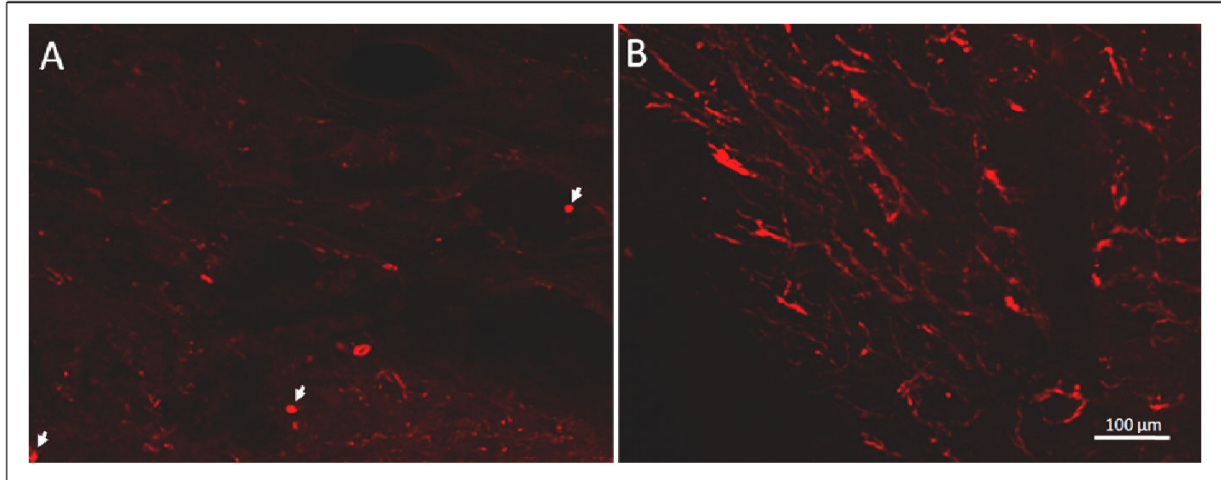


Fig. 2.12: Example images of PAM-IR in the matrix area at 5 wpr. A: ALG, B: PEG, arrows: unspecific background signal.

Immunohistological staining with PAM was used to identify axonal fibers. Double-labeling with GFAP antibody was performed to delineate the fibrous scar or the matrix borders, respectively. Images of PAM-IR of the complete lesion area or the matrix area, respectively, defined by lack of GFAP staining and/or by lack of Sudan Black B myelin staining (since the spinal cord lesion scar is virtually devoid of myelin), of the analyzed sections were taken using the 10-x-objective of a Zeiss LSM 510 confocal microscope in the focal plane with the highest PAM staining intensity. Three laser lines emitting at 405, 488 and 543 nm were used to excite DAPI, Alexa 488 and Alexa 594, respectively. Attention was given to ensure identical values for laser intensity, scan speed, amplifier gain and cut off, and pinhole size across all images. Using graphic editing software, precise excision of the respective area was carried out. In Image J, the TIF-original images were converted to 8-bit.

After image conversion, application of the “smallest Hessian eigenvalue” was performed using the Image J software and its java-based plug-in Feature J (Fig. 2.13). In the resulting image, unspecific background staining was eliminated using the Image J eraser tool. Background signal elimination presented the most time-consuming step of the analysis. Careful comparison of the original colored image with the black-and-white “Hessian eigenvalue” image had to be performed at 100 % image size. Correction was further achieved by setting the right pixel threshold

values. The overall aim of the correction was to get a resulting image in which the axon distribution matched that of the original color image.

The resulting images were converted to a binary image by setting a threshold for pixel intensity. Semi-automated quantification of axon density (Grider et al., 2006) in the lesion area was performed.

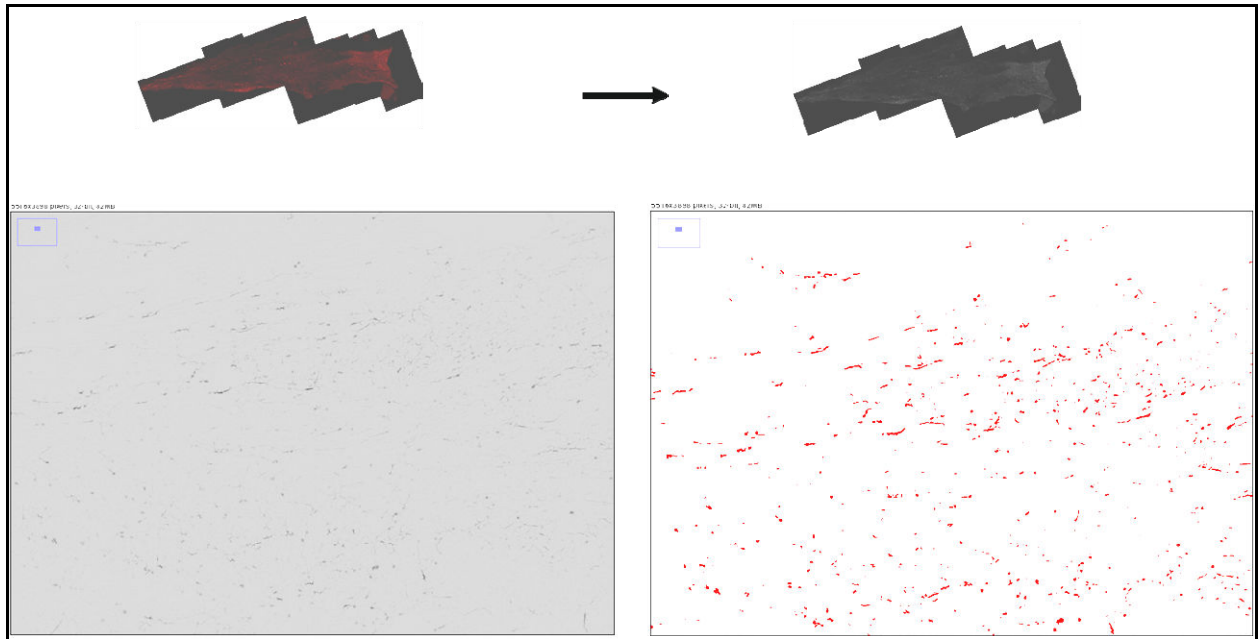


Fig. 2.13: Illustration of axon quantification procedure with Image J plug-In Feature J. Colored images (top left) were converted into binary 8-bit (top right), then binary images (bottom left). Subsequently a pixel threshold was set (bottom right) and the amount of pixels above threshold was quantified by the software. Exemplary areas of an image after its conversion (left) and after threshold application (right) are presented (bottom).

2.6.2.4 Quantification of BDA-positive Axon Profiles

Axons in the lesion area, which were labeled via BDA-injection into the spinal cord cranially to the lesion site, were visualized with Oregon Green® 488. BDA-positive axon profiles were manually counted. Respective sections were analyzed using the 10x-objective of a Nikon Diaphot 300 fluorescent microscope. Only BDA-positive structures which could clearly be defined as structures arising from regenerated axons due to certain characteristics described by Steward et al. (Steward et al., 2003) were taken into account for evaluation. In Fig. 2.14, an exemplary image area of BDA-labeled axons in a lesion area after chronic SCI scar resection is presented.

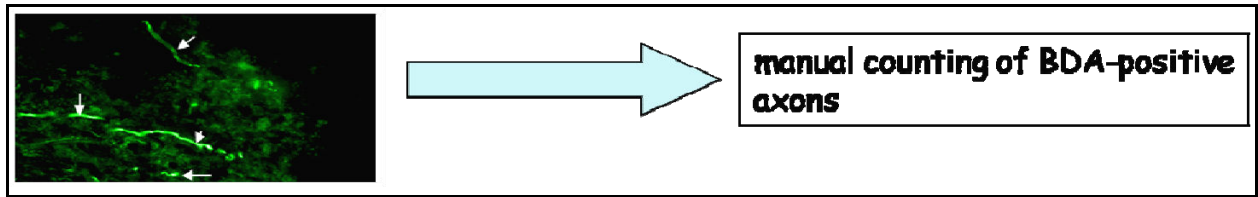


Fig. 2.14: Example of BDA-labeled axons after chronic scar resection and matrix implantation. Labeled axons were manually quantified.

2.7 Functional Testing

2.7.1 Open Field Observation of Locomotor Behavior

The overall locomotor behavior was assessed in an open field test using the Basso–Beattie–Bresnahan (BBB) score (Basso et al., 1995). Over a time period of four min per animal per trial the locomotor behavior was observed and analyzed.

Animals were placed in a rotund Plexiglas® open field (custom made by Febikon) with a diameter of 1 m. The open field’s floor was covered with a black rubber mat. All animals were tested weekly after initial SCI operation. Important steps of locomotor evaluation are listed in Table 2.6.

The rubber mat facilitated assessment of toe clearance. Whenever an observation could not be classified unambiguously, the lower possible BBB score was given. For evaluation, the BBB scores of both hindlimbs were averaged.

Table 2.6.: Basso Beattie Bresnahan locomotor rating scale (modified from Basso *et al.*, 1995).

BBB score	Attributes
0	No observable hindlimb (HL) movement
7	Extensive movement of all three joints of the HL
11	Frequent to consistent weight supported plantar steps and no FL-HL coordination
21	Consistent plantar stepping and coordinated gait, consistent toe clearance, predominant paw position is parallel throughout stance, consistent trunk stability, tail consistently up

2.8 Statistics

The Kruskal–Wallis test was used for all axon profile numbers, i.e., over all different experimental groups in total. As a *post hoc* test, the one-sided Mann–Whitney U-test was applied for paired comparison and Holm–Bonferroni correction for multiple testing with the type I error rate $\alpha = 0.05$. The paired comparisons were made to test for significant elevation in axon profiles of treated compared with control animals and for comparison of the control and matrix groups, i.e., three comparisons in the PAM analysis and six comparisons in the BDA analysis, respectively. The experimental groups were considered significantly different at $P \leq 0.05$.

3 Results

3.1 Chronic Spinal Cord Injury Model in the Adult Rat

3.1.1 Scar Removal

In preparation for the subsequent matrix application, the inhibitory chronic lesion scar needed to be removed. Scar removal via aspiration alone led to unsatisfactory results. The chronic lesion scar could not always be easily identified during surgery. The position of the scar was therefore determined by the position of the sutures which were made subsequent to the initial spinal cord lesion. After perfusion of the animals, completeness of the scar removal was checked by immunohistochemical staining of Col4. Fig. 3.2 shows example images of spinal cord sections of animals that were sacrificed subsequent to the aspiration procedure. Both staining methods, histological Nissl (Fig. 3.2A-C) and immunohistological Col4 antibody staining (Fig. 3.2D-F), demonstrate incomplete scar tissue removal after the use of aspiration alone.

Nissl staining with cresyl violet is a standard histological method for visualization of neurons in the brain and spinal cord. The Nissl substance (rough endoplasmic *reticulum*) appears dark blue, due to the staining of ribosomal RNA (Fig. 3.1).

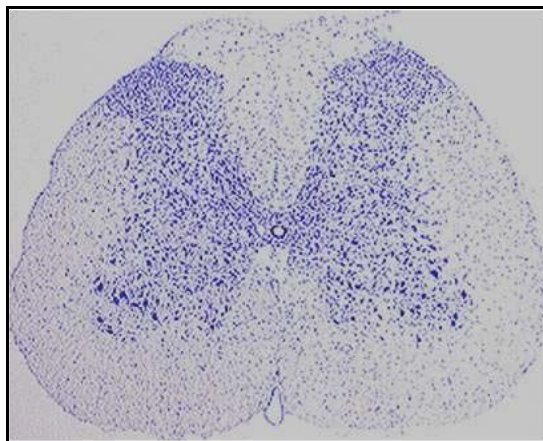


Fig. 3.1: Nissl-stained intact spinal cord cross section.

After axotomy, Nissl substance redistributes from the perikaryon to the proximal dendrites and is often reduced overall (central chromatolysis). Healthy cells possess well-defined borders and uniform stain density. In contrast, after SCI, there

is a notable accumulation of dark blue Nissl-stained chromatin clumps which are characteristic of apoptosis (see outlined dark blue areas in Fig. 3.2A,B).

The scar which develops after a spinal cord lesion (or a lesion in general) is rich in Col4-positive BM structures (Fig. 3.2C,D). BV are also stained positively with antibodies against Col4, since BM structures are also important for their function (Fig. 3.2C).

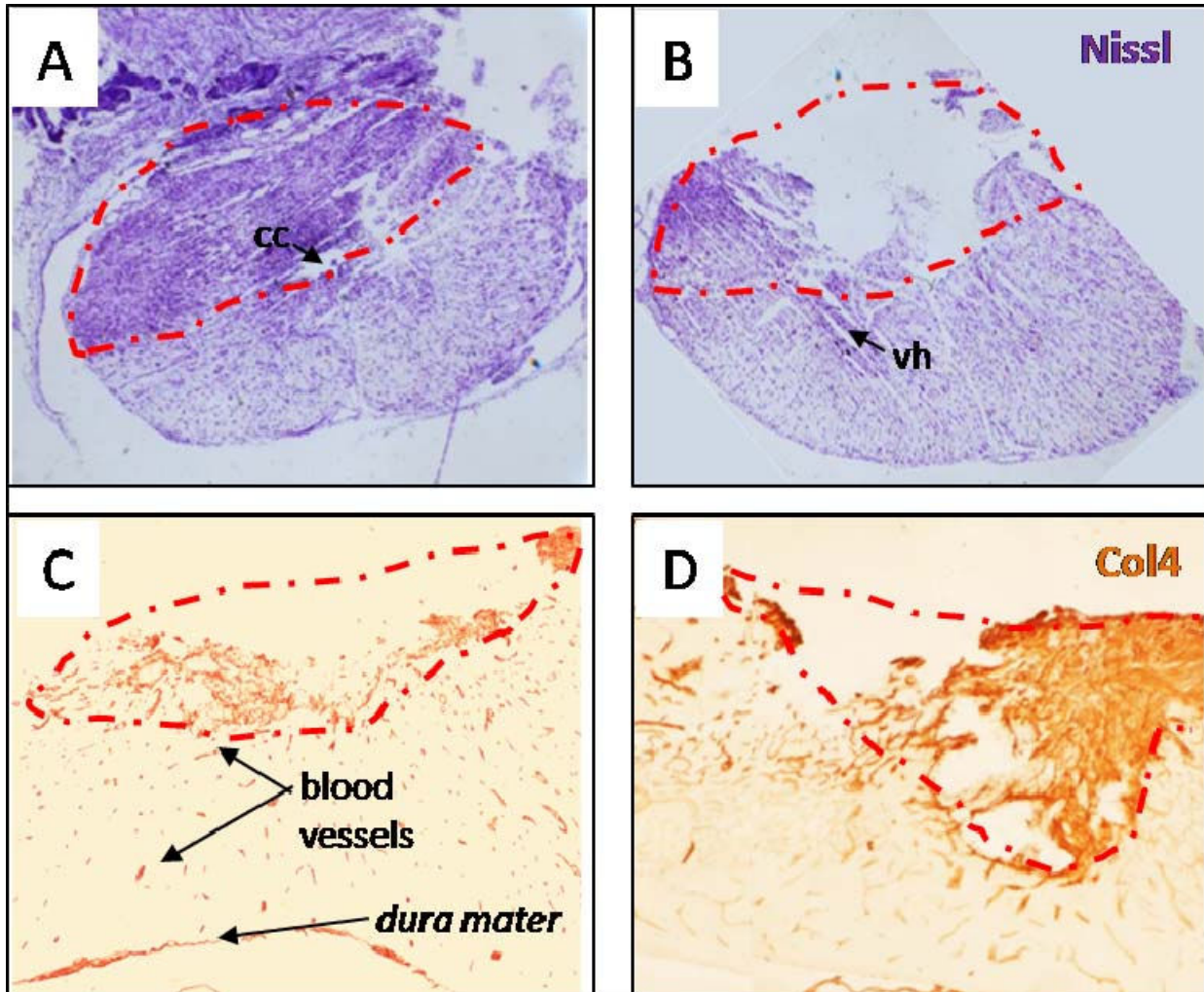


Fig. 3.2: A,B: Example images of Nissl-stained 10 μ m-thick paraffin spinal cord cross sections of the lesioned and/or aspirated area. Darker blue/purple areas correspond to lesioned spinal cord tissue, and also to ventral horn (vh) area. Dashed lines mark the lesion area. A: Complete lesion scar with callus formation in the dorsal part of the lesioned spinal cord. B: Partly removed lesion scar, callus formation and in large part the chronic SC lesion scar could be removed via aspiration of harmed tissue.

C,D: Example images of Col4-stained 10 μ m thick (paraffin-embedded) sagittal spinal cord sections of the lesioned and/or aspirated area. Brown staining is apparent in Col4-positive BM of lesion area, *dura mater* and blood vessels (BV). Dashed lines mark the lesion area. C: The lesion scar only covers approximately one third of the spinal cord depth, scar tissue was only partly removed dorsally. D: Partly removed lesion scar.

A combination of resection (by means of iridectomy scissors) *and* tissue aspiration proved to be the best and most reliable method for scar removal. Example images in Fig. 3.3A-C reveal that after the establishment of a good method, spinal scar tissue could be successfully removed. While there is still some callus formation visible in some of the sections (Fig. 3.3B), it is mostly restricted to the most dorsal part of lesion edges of the spinal cord, while the actual spinal cord tissue affected by scar formation has been successfully removed.

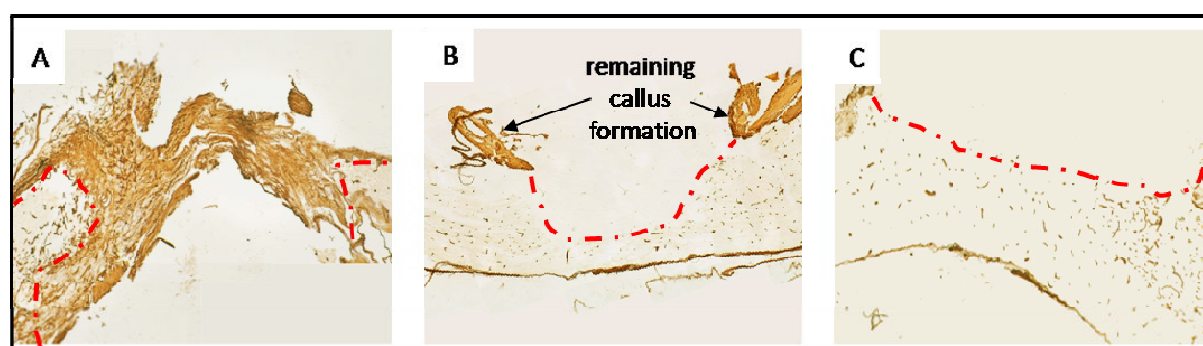


Fig. 3.3: Example images of Col4 stained 10 μ m-thick sagittal paraffin spinal cord sections of the lesioned and/or resected area. Brown staining can be noted in Col4-positive BM of lesion area, *dura mater* and BV. Dashed lines indicate the border between harmed and intact spinal cord tissue. A: Image of a stained section from an animal which developed strong bleeding during the scar removal procedure. Due to an insufficient view of the operation area the scarred tissue could not be removed. B,C: Example image of successful scar removal. In some cases, small parts of the callus formation were still visible (B).

3.2 General Applicability and Suitability of the Matrices

3.2.1 Matrigel™

MG proved to be a suitable matrix in regard to its handling and its general distribution in the aspiration cavity. The gel exhibited a good applicability regarding its injection into the lesion cavity resulting from scar resection. MG was insensitive to shear force. Gel formation occurred immediately after injection of the MG into the spinal cord lesion site. The gel remained in place, and no leakage was detected during the operation procedure. Immunohistological analyses of spinal cord sections from MG-treated animals could be done without further problems, e.g., loss of matrix area tissue. Care only needed to be taken not to cause early gel formation due to increasing temperatures.

Fig. 3.4 shows representative images of sagittal spinal cord sections with trichrome stain from three different animals that received MG as a matrix to fill the resection cavity. Collagen deposition in the lesioned area is noticeable (green

connective tissue staining). The collagen staining is visible in the whole lesion site, where it is most prominent in the dorsal spinal cord. The lateral rim areas of the lesion reveal a slightly reduced collagen accumulation as they are more weakly stained. The lesion center on the other hand shows a strong green staining of collagen deposition throughout the whole depth of the spinal cord. In the section shown in Fig. 3.4A some of the dorsal part of the lesion scar/matrix area was lost during tissue preparation. The image in Fig. 3.4B is an example for the phenomenon of encapsulation. Here, the scar/matrix area was not merely disrupted due to its fragility, but an obvious cyst/cavity formation or encapsulation of a foreign body had occurred, as can be identified by the well-defined bordered regions in the center of the lesion scar of this particular animal. Although the section in Fig. 3.4A also exhibits small holes, these are primarily found in the most dorsal part of the scar/matrix which can be considered part of the callus formation and not the actual spinal cord. The image shown in Fig. 3.4A further depicts areas of bleedings in the spinal cord (strongly red-stained areas in the center of the lesion/matrix) which were nearly absent in sections of the remaining two animals.

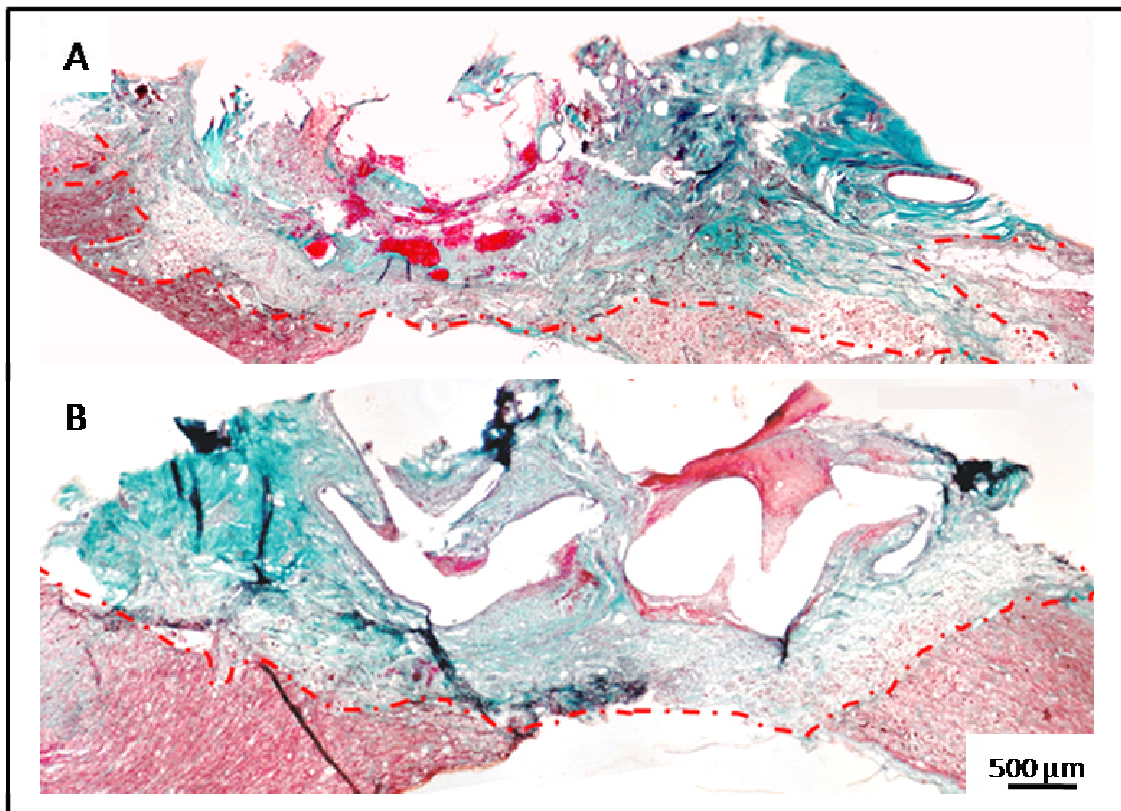


Fig. 3.4 (previous page): Representative example images of trichrome (+PAM) stained 10 µm-thick sagittal spinal cord sections (paraffin) from animals which received MG-filling of the resection lesion cavity. Representative images of trichrome stained sections from animals with MG implantation after chronic SCI scar removal. The area affected by the spinal cord lesion and/or scar removal is marked by dashed lines.

3.2.2 Alginate

The ALG used for the present studies was prepared and implanted as a hydrogel without freeze-drying after preparation. Thus, it was very sensitive to shear forces. Injection or cutting into pieces of pre-gelled alginate was hardly possible due to its immediate disintegration caused by the applied force (also see Materials & Methods). Intended dissociation of the ALG for minimization of background staining (which was frequently noted in ALG matrix in the course of this study) has previously been described (Yen et al., 2008). This method may be of advantage when ALG is simply used as a carrier for cellular delivery, but it is not applicable when ALG is used as a bridging substance. Immunohistological staining of matrix area-containing sections was carried out with care to prevent further damage of the ALG-containing area. ALG's susceptibility to impurity posed further problems. For this reason NaN_3 (0.1 %) was added to the tissue collecting solution. Generally, only a scaffold-like structure remained of the ALG matrix after tissue processing (Fig. 3.7, middle row). Remaining ALG fractions/scaffolds frequently revealed non-specific binding of antibodies resulting in background staining. Furthermore, ALG seemed not to be well integrated into the surrounding spinal cord tissue at the analyzed time points of 1 wpr or 5 wpr, respectively. Remaining ALG scaffold structures as well as bordering spinal cord tissue (note ventral matrix area in Fig. 3.5A) was found to exhibit collagenous staining (Fig. 3.5A). The resection area of ALG-treated animals frequently lacked matrix or tissue, respectively (Fig. 3.5A). Additionally, in several cases, encapsulation of the ALG-matrix appeared to have occurred (Fig. 3.5B).

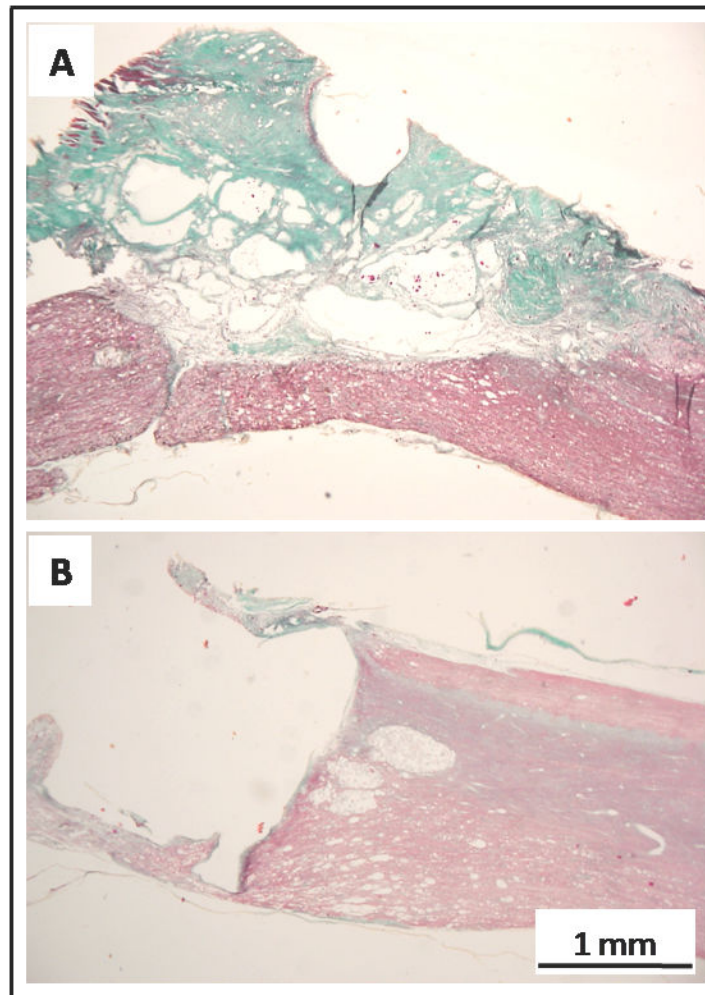


Fig. 3.5: Representative example images of trichrome stained 10 µm-thick sagittal spinal cord sections (paraffin) from animals which received ALG-filling of the resection lesion cavity. A: note the large callus formation on top of the dorsal spinal cord and the large holes in the area of ALG-implantation. B: A distinct collagen (green staining)-containing rim-formation was apparent in the area of implantation of the respective animal. Such observations are indicative of encapsulation of the inserted material.

3.2.3 Polyethylene Glycol

The PEG used for this study - i.e., PEG 600 - was chosen because of its viscosity. Other PEG tested were PEG 400 and PEG 1000. PEG 400 was suitable for injection due to its fluidity, but during the operation procedure strong leakage of the PEG from the resection area was observed. Therefore a more viscous PEG seemed more appropriate. PEG 1000 is a rather rigid PEG at RT but could well be injected once brought to higher temperature (temperature at the time of injection was 37°C). Cutting an appropriate amount of PEG 1000 and subsequently placing it into the lesion cavity to fill the aspiration site, where it quickly melted, was also tested. Since only very few axons were found to grow into a matrix of PEG 1000 and since

there also were indications for encapsulation of the material (Fig. 3.6A), PEG 600 turned out to be the PEG matrix of choice. PEG 600 is of soft rigid consistency at RT, but it becomes a slightly viscous injectable fluid when heated (temperature at the time of injection was 37°C). Leakage of PEG 600 from the aspiration cavity was also observed, but to a much lesser extent than it was the case after application of PEG 400. Tissue processing and IHC could be carried out without further problems or extensive loss of matrix/tissue because a stable tissue bridge had formed at the analyzed time points.

Application of PEG after acute compression SCI has previously been described to result in smaller lesions than in water (vehicle)-treated animals (Duerstock and Borgens, 2002), due to an increased volume of intact spinal cord tissue and reduced cystic cavity. Similar observations were made in the present chronic transection SCI study, where ALG-treated animals appeared to exhibit a more extended lesion area than PEG-treated animals. But since the size of the resulting scar removal area is not only dependent on the matrix used but also on the extent of the initial transection injury, and because the extent of the lesion area was not quantified, such observations can only be noted as impressions rather than definite results. In Fig. 3.6A-C, images of the lesion site of trichrome-stained parasagittal sections of PEG-treated animals are depicted. Insertion of PEG 1000 into the chronic SCI scar resection cavity was tested, but the indication of encapsulation of the material (note distinct rim of DAPI-positive nuclei surrounding the tissue-devoid area in Fig. 3.6A) led to the conclusion that PEG with a lower molecular weight and viscosity – was better suited as a matrix material for the intended purpose. Trichrome stain (shown in Fig. 3.6B,C) revealed partially decreased collagen deposition (green) in the matrix area of PEG-treated animals. In Fig. 3.6B, green staining in the matrix is scarce and limited to the most dorsal callus area. While there are some holes apparent, these are most likely due to tissue loss during tissue preparation. They do not indicate encapsulation since the respective areas do not exhibit distinct rims of collagen and are not completely devoid of tissue. In the trichrome stained section which is depicted in Fig. 3.6C, there is only a partial reduction in collagen deposition apparent. While the tissue in some areas exhibited only weak or no green collagen staining, other areas, especially the dorsal callus region, revealed the presence of collagen, recognizable by green staining.

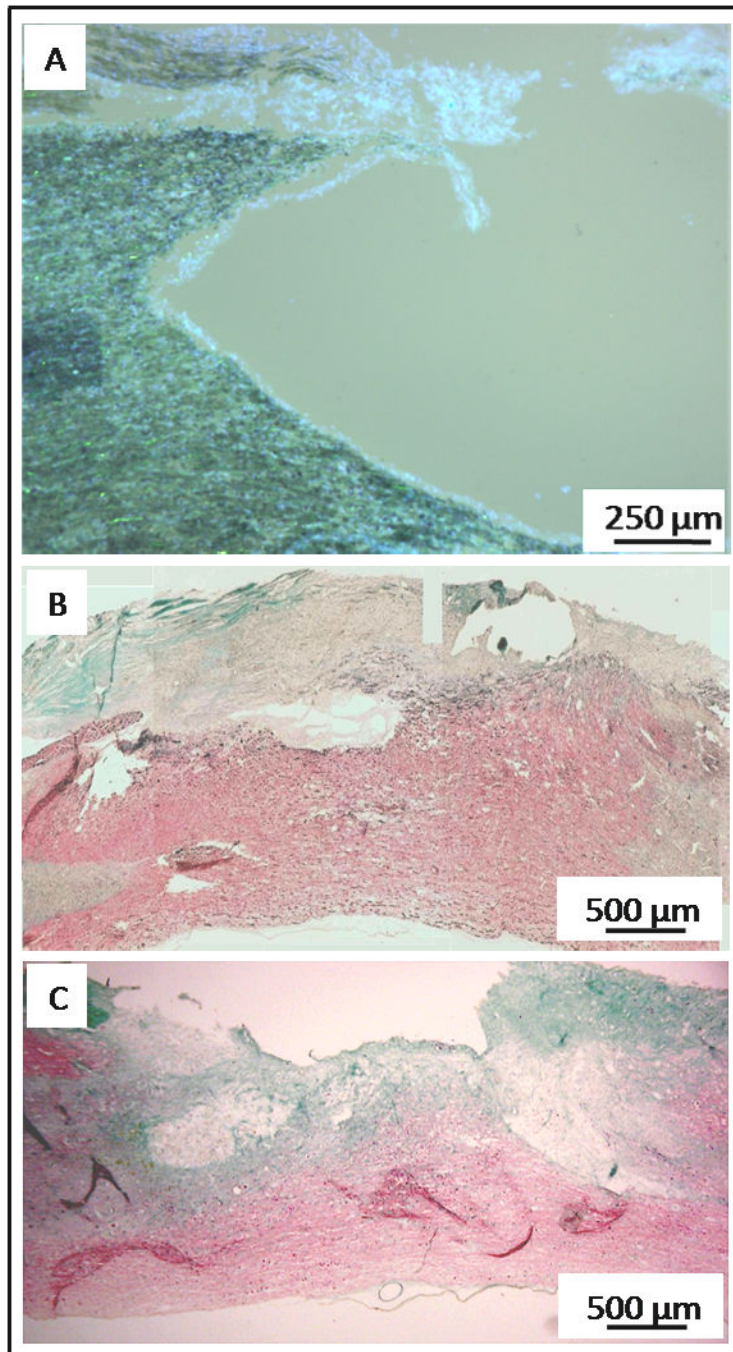


Fig. 3.6: Example images of the lesion area in 10 μm -thick parasagittal sections spinal cord sections of PEG-treated animals. A: Overlay of a fluorescent staining with a Sudan Black staining. The implanted matrix material was PEG 1000. Note the distinct rim of DAPI-positive nuclei surrounding the tissue-devoid area indicating occurrence of encapsulation of the material. B,C: Trichrome (+PAM) (B) and trichrome staining (C).

3.3 Tissue and Matrix Preservation

At 5 wpr (or 10 weeks post lesion (wpl), respectively, in the case of “lesion only” control animals), the lesion area or matrix area, respectively, was generally well preserved to a greater extent in animals which received PEG-filling of the resection

cavity compared to those with ALG-matrix or to “lesion only”-controls. This is shown in Fig. 3.7. While control animals exhibited generally insufficient preservation of remaining tissue at the site of injury and also in surrounding areas (Fig. 3.7, top), ALG-treated animals revealed varying degrees of tissue preservation. Remaining ALG fractions were often found only in the most ventral part of the chronic scar resection cavity and exhibited merely a scaffold-like structure (Fig. 3.7, center). In some animals, ALG or the newly developed tissue bridge, respectively, were found to exhibit good preservation. However, such observations did not necessarily coincide with increased incidence of axonal fragments in the lesion area of the respective animals. Generally good tissue preservation and formation of a stable tissue bridge in the lesion area was observed in PEG-treated animals (Fig. 3.7, bottom).

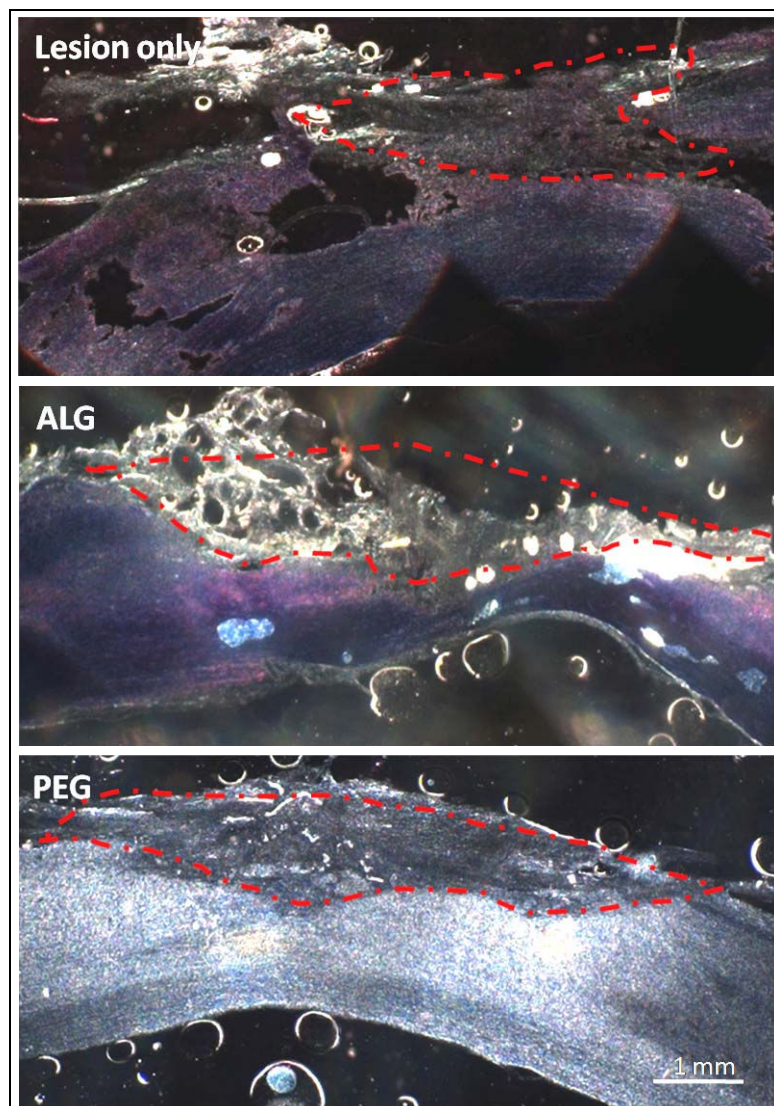


Fig. 3.7 (previous page): Comparison of tissue preservation at 10 wpl in lesion only controls (top), and at 5 wpr in ALG-treated (center) and PEG-treated (bottom) animals. Representative images of the lesion area in 50 μm -thick sagittal sections. In the dark field microscopic images the lesioned area can be easily distinguished from the surrounding tissue. Dashed lines delineate the lesion area.

3.4 Axonal In-Growth into the Lesion Area

3.4.1 PAM-Positive Axons

3.4.1.1 Axon Regeneration into Matrix at 1 wpr

For quantification of PAM-positive axon fibers in the matrix, animals which received a resection of the chronic lesion scar without subsequent matrix application (“RX only”) were used as controls. “Lesion only” controls were considered to be unsuitable for this particular analysis, since after a spinal cord injury the axonal debris, which is present in the lesion area even over a longer period of time (Klapka and Muller, 2006), also displays positive PAM-IR, resulting in falsified quantification of axonal in-growth into the lesion area in these animals. Focus was put on the investigation of spontaneous axonal regeneration into a scar or matrix, therefore “RX only” controls were chosen to be appropriate for this part of the experimental setting. In the remaining groups, only axons which have regenerated into the matrix are stained, since the lesioned tissue has been completely removed via the aspiration procedure.

A higher amount of PAM-positive axon fragments was found in the dorsal callus region of the spinal cord lesion of ALG-treated animals. In these respective areas an increased immunoreactivity of axon fragments was also observed in the remaining analyzed treatment groups, including the control group. In ALG-treated animals this respective region was generally larger than in the other analyzed groups. This is due to the performed tissue preparation. Because of the aforementioned fragility of ALG, care was taken not to induce further loss of matrix material by applying unnecessary force near the respective area. In animals of the other analyzed groups the normal proceedings could be carried out. The area which was taken into account for the evaluation only contained tissue/matrix material which was present in the original intact spinal cord area (see materials and methods).

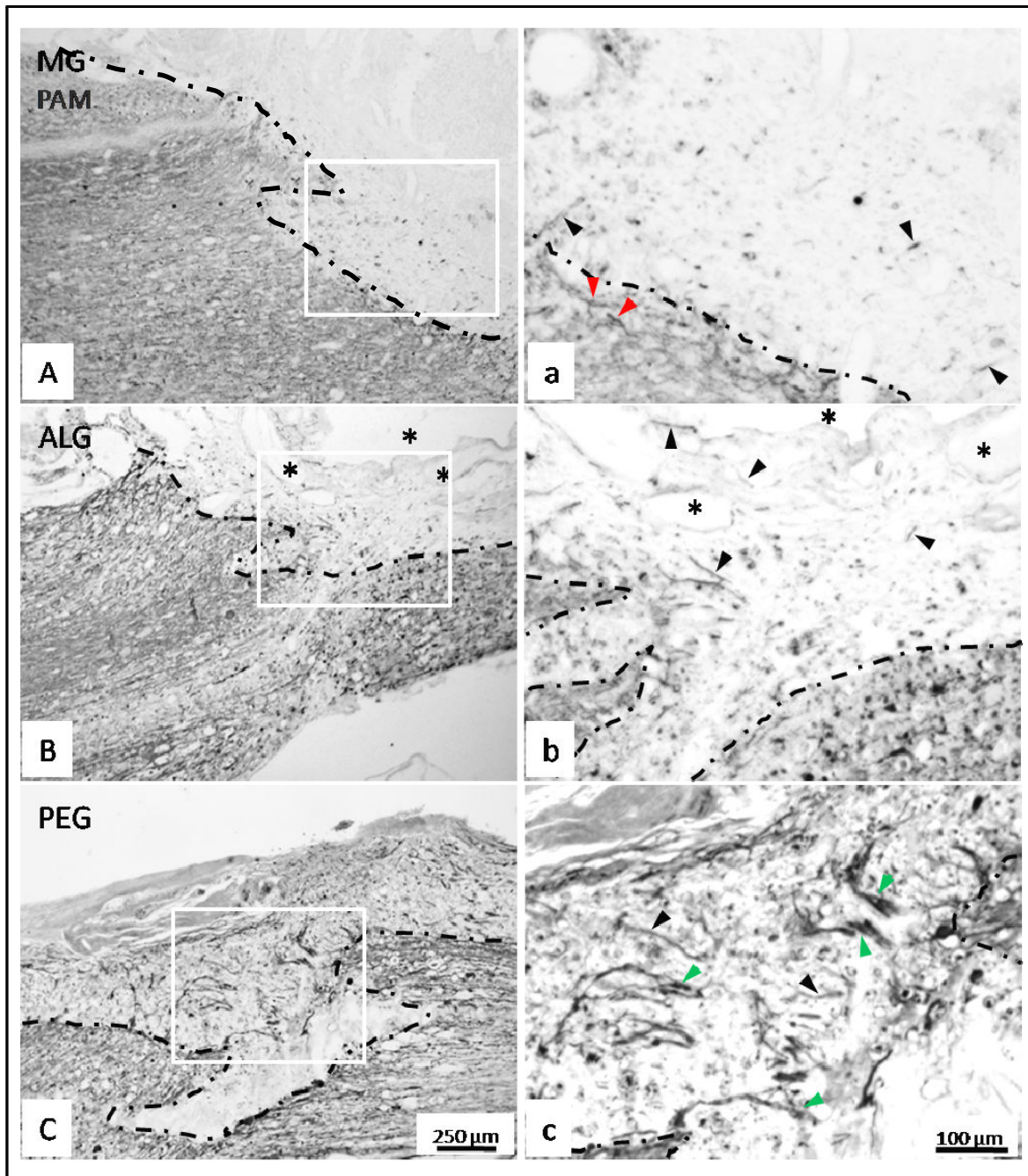


Fig. 3.8: PAM-IR in lesion area at 1 wpr. Increasing PAM-IR in the order of MG < ALG < PEG. Representative images of PAM-IR in the matrix visualized via DAB reaction in 10 μm -thick sagittal paraffin sections of the lesion area of MG- (A), ALG- (B) and PEG (C)-treated animals. Magnifications of framed areas in A-C are shown in a-c. Black arrowheads: Axonal PAM-positive structures; red arrowheads: axons which are repelled by the lesion site instead of growing into it in MG-animals; green arrowheads: axonal bundle-like structures in the matrix area of PEG-animals; dashed lines delineate the lesion border; note typical occurrence of holes or ALG-dissociation (asterisks) in B.

No or only scarce axonal in-growth into the matrix after chronic scar resection was found in the MG group (Fig. 3.8A,a) at 1 wpr. Some axon terminals even appeared to be repelled by the lesion area, as they were found to be turning away to grow around the lesion area (Fig. 3.8a, red arrows). PAM-IR inside the MG was mostly seen in structures which resembled macrophages, but only rarely in axonal

fibered structures. Short axon fiber fragments inside the matrix were only observed at the lesion margins. Due to this observation, MG was considered an unsuitable matrix for the intended purpose and was excluded from further analyses.

Compared to MG, an increase in the amount of PAM-positive axon fibers in the gel matrix could be noted in the ALG group (Fig. 3.8B,b). Although at the analyzed time point of 1 wpr the ALG matrix in the majority of cases contained several (large) holes, some axon fiber fragments, which appeared to be longer than those found in the MG matrix, were still able to grow into the matrix area. For the most part, these axons were located in the callus region as well as in the ventral, cranial and caudal border areas of the lesion. Only few axon fragments could be observed in the center of the ALG matrix.

The most prominent axonal in-growth at 1 wpr was noted in PEG-treated animals (Fig. 3.8C,c). The axon fragments were not only observed in the border areas of the matrix, but they were also frequently located in the complete matrix area including the lesion center. The axonal structures oftentimes displayed a bundle-like assembly in the PEG-filled area.

3.4.2 Axon Quantification

Quantification of PAM-positive axons at 5 wpr via Image J threshold-analysis was attempted (see Fig. 3.10), but it was obviously not a suitable method due to the variations in staining intensity and to staining caused by unspecific binding of antibody. Cellular debris in the lesion area, as well as the matrix materials, in particular ALG, were observed to be prone to exhibit such unwanted staining. Such “background signal“ was not restricted to axonal fiber structures and should therefore preferably not influence the final quantitative evaluation. Example images in Fig. 3.9 demonstrate the described variations in staining intensity and background signal. The image which is shown in Fig. 3.9A shows an exemplary area of PAM-IR in a “lesion only“-control animal. Although this animal group was not taken into account for the actual quantification of PAM-stained axon profiles in the lesion area, this image is presented here to illustrate emerging problems due to staining variability. While there were only few axonal structures detected in the respective area, there is a high amount of non-specifically stained structures or areas distributed throughout the entire analyzed area. Similar patterns were frequently observed in ALG-animals (Fig. 3.9B). The exemplary image reveals high amounts of non-specific “background-

staining”, especially in ALG-containing areas, whereas interface areas of ALG/spinal cord tissue – the areas where occurrence of axonal fragments were usually detected in ALG-animals - exhibited a rather “normal” staining pattern, which was also characteristic for PEG-matrix (Fig. 3.10C, note the clearly identifiable fiber-structures). However, in the analyzed images of PEG-treated animals, variability was also apparent due to differences in lighting/exposure (Fig. 3.10C). Such differences became apparent when the individual pictures which were taken of the lesion area of an animal were photomerged.

However, quantification via Image J threshold analysis was initially attempted using respective images of fluorescent PAM-IR taken with a fluorescent microscope at a 5x-magnification (see Fig. 3.9), but the quantification did not at all reflect the observed differences regarding regeneration into the lesion area (see results of the quantitative analysis presented in Fig. 3.10), presumably due to the described issues. Only the “RX-only”-group revealed realistic results, as there was generally not a lot of tissue (and thus no unspecific binding of antibody) in the resection cavity (Fig. 3.10, ca. 0.6 % PAM signal/lesion area). Although a slightly increased PAM-IR was detected for PEG- compared to ALG matrix with the Image J threshold method (Fig. 3.10, ca. 2 % PAM signal/area in PEG vs. ca. 1.8 % PAM signal in ALG), this difference was only very small, not at all reflecting the observations.

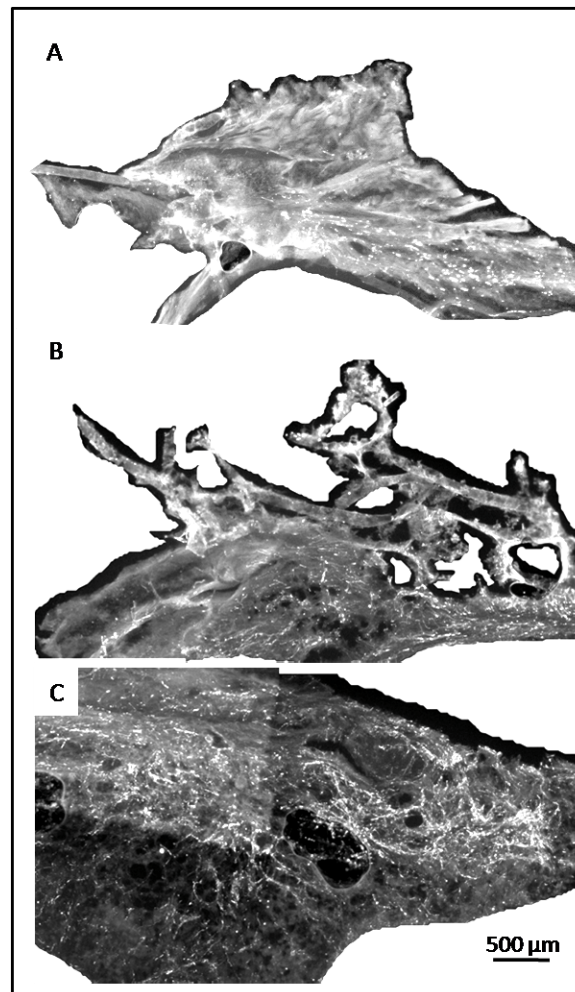


Fig. 3.9: Representative example images of PAM-IR in areas of the lesion site in 50 μm -thick parasagittal sections taken at 5x-magnification. The lesion area was cut out in the image using a graphics editing program. A: lesion only control, B: ALG, C: PEG.

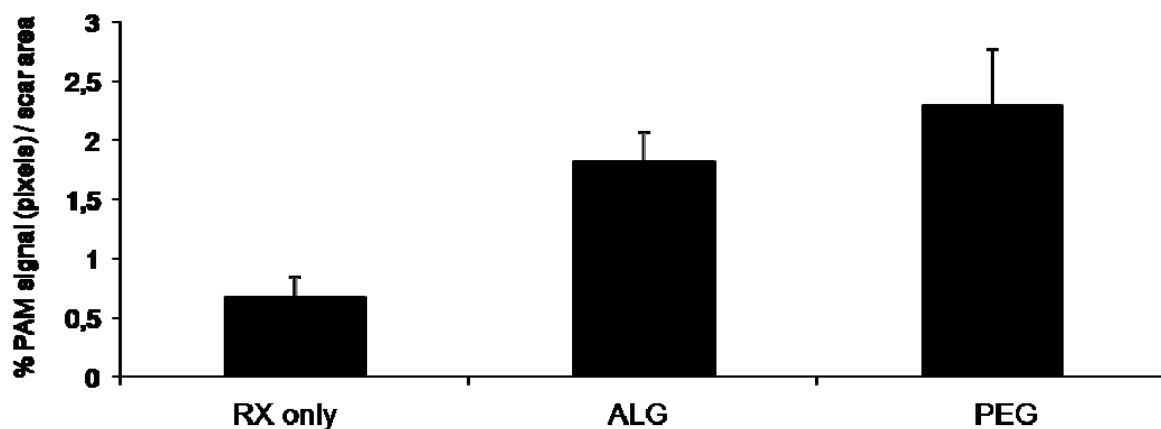


Fig. 3.10: Results of the Image J pixel-threshold analysis of PAM-signal in the lesion area. This method did not at all reflect previously made observations; n: RX only: 9 sections/3 animals; ALG: n = 42 sections/6 animals; PEG: 27 sections/5 animals; mean values are presented with SEM; no statistical differences were determined between the groups with Kruskal-Wallis and *post-hoc* Mann-Whitney U-test with Holm-Bonferroni correction.

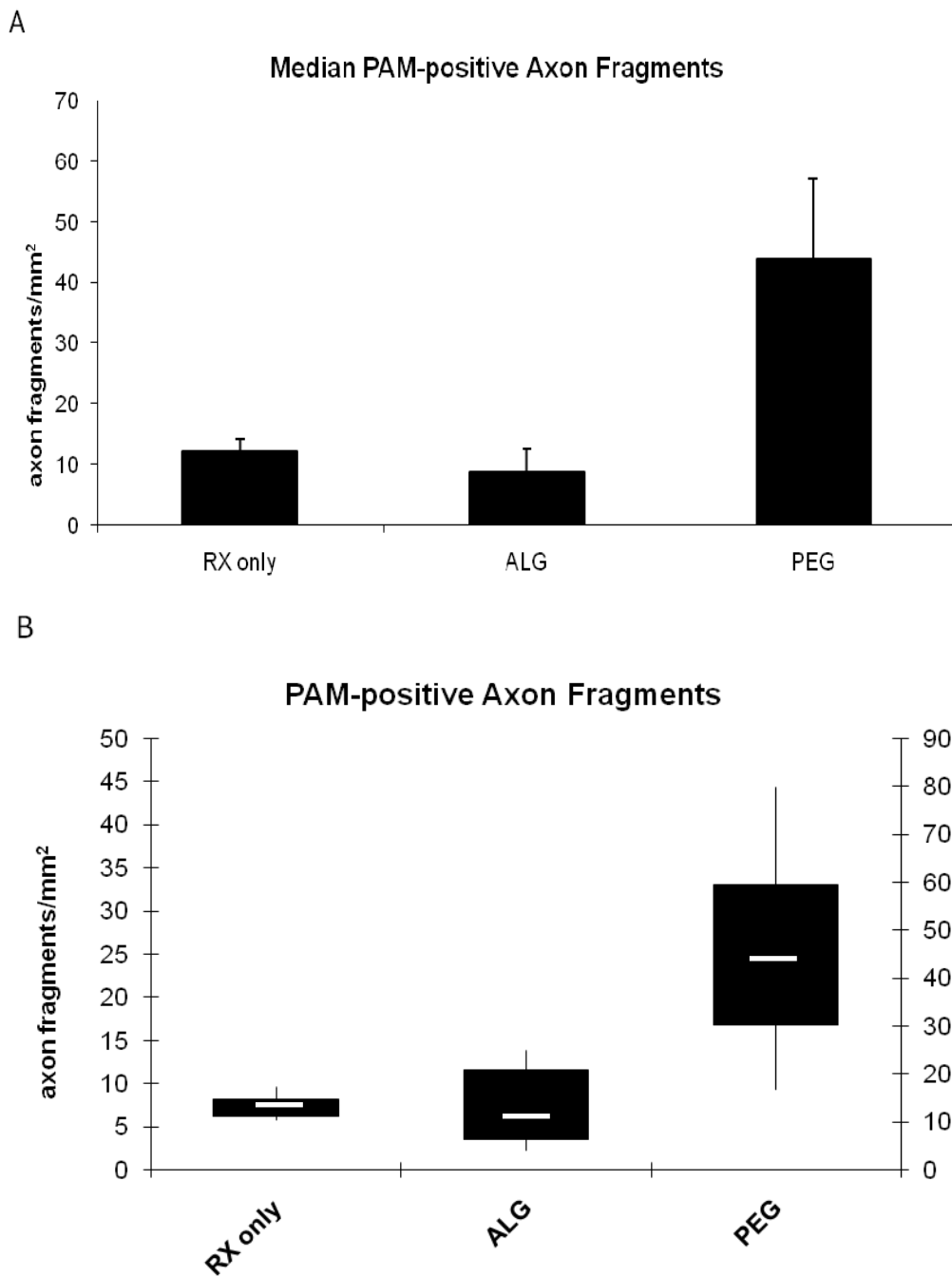
3.4.2.1 Quantitative Analysis with Neuron J

The quantification of PAM-positive axon profiles in the lesion area via Neuron J revealed a positive trend regarding axonal regeneration into the lesion area of PEG-treated animals compared to ALG-treated and “RX-only”-control animals (Fig. 3.11). A priori, possibly significant differences between the animal groups were not determined due to the low amount of sections which were used for this analysis ($n = 1$ center section per animal). The reason for analyzing such a small number of sections lies in the elaborate and extremely time-consuming Neuron J method which was applied. However, the evaluation revealed PEG as a possibly very suitable matrix for axonal regeneration after chronic SCI removal, compared to ALG-treated animals and “RX-only”-controls (Fig. 3.11A,B). On average, 44 PAM-positive axon profiles were detected at the respective magnification in the matrix area of the center slice of PEG-treated animals. In contrast, only 12 axon profiles were counted in “RX-only” lesions. The Neuron J tracing method revealed an even slightly lower number of axon fragments for ALG-treated animals: On average, only 9 axons were detected.

In addition to the number of regenerated axons found in the lesion area, the mean lengths of the fragments and also the sum of the axon lengths in the lesion area were determined (Fig. 3.11.C,D). While the mean length of axonal fragments was found to be relatively similar in ALG and PEG matrix (Fig. 3.11.C), the total sum length of axonal fragments present in the lesion area was detected to be highly increased in PEG matrix. Such results are in accordance with the observed increased presence of axons in PEG matrix compared to ALG matrix.

Presentation of the median value was chosen instead of presentation of the mean in the Fig. 3A,B. As can be seen in the presented boxplot diagram in Fig. 3.11B, the determined data showed a broad distribution, especially in the case of the PEG-group. One section per animal therefore appeared to be insufficient for the analysis of axonal regeneration into the lesion area, since the quantitative results indicated that the in-growth may not be equally distributed in respective areas of the spinal cord lesions site. For this reason, although the applied Neuron J method of axon quantification is a quite accurate method for computational axon tracing and subsequent quantification, a faster, semi-automated method was desired which enabled the analysis of higher numbers of sections in a shorter time period.

It should further be noted that for the presented quantifications via Image J threshold and Neuron J tracing, the entire affected area (including the dorsal callus region which generally exhibited increased occurrence of axonal fragments) was taken into account. Because axons in the callus region would not be expected to regenerate according to their original courses or even be able to make functional synaptic re-connections, such respective areas were not taken into account for further analyses (i.e., Feature J quantification, quantification of BDA-labeled axons).



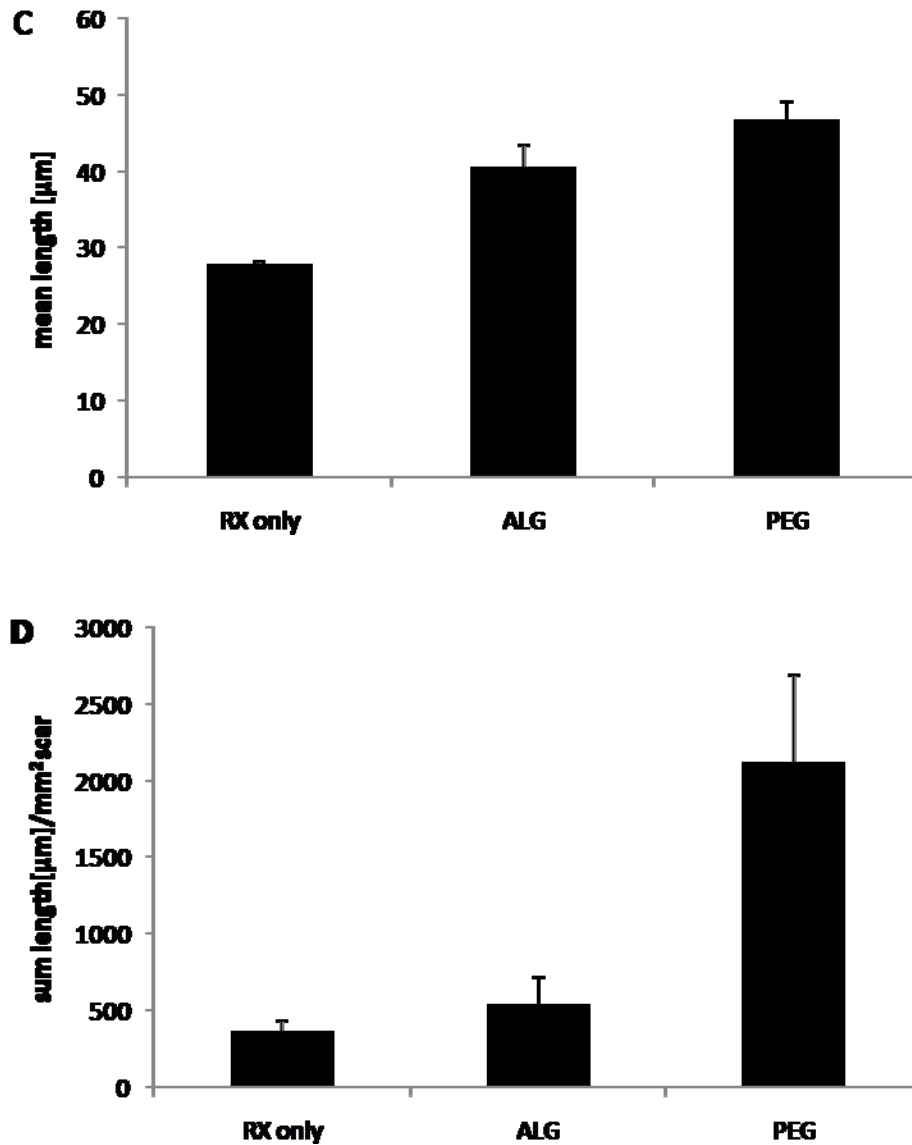
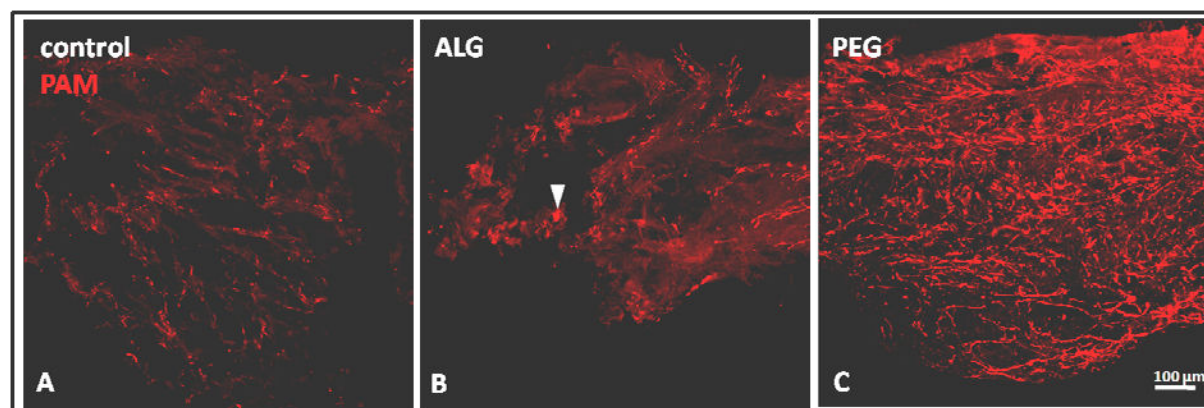


Fig. 3.11: Results of the quantitative analysis with Neuron J software. A: Median values of the respective groups are presented with SEM. B: The boxplot diagram reflects the broad distribution of the data obtained with this method, median values are presented by white bars; median values: RX only: 12.11, ALG: 8.73, PEG: 43.68. C,D: mean lengths (C) and sum lengths (D) of axonal fragments in the lesion area; mean values are presented with SEM; analysis was performed without the calculation of significant differences due to the low number of sections analyzed ($n = 1$ section/animal); RX only: $n = 3$; ALG: $n = 6$; PEG: $n = 4$.

For the quantitative analysis with Feature J software (see next chapter), confocal images were therefore taken at 10x-magnification in order to reduce occurring problems as much as possible.

3.4.2.2 Quantitative Analysis with Feature J

The Feature J quantification of PAM-positive axon fragments in the resection area after a longer survival time of 5 wpr further revealed clear differences regarding the growth-promoting qualities of ALG and PEG (Fig. 3.12A-D).



D Quantification of PAM-positive Axons in Lesion

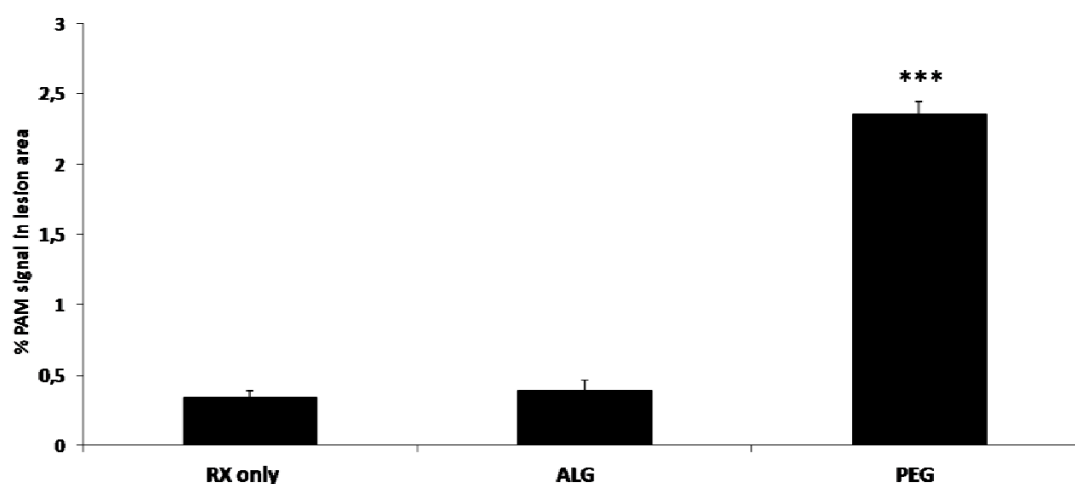


Fig. 3.12: Investigation of spontaneous axonal regeneration into lesion area via PAM-IR at 5 wpr. PAM-IR in the lesion area of “RX only” (A)-, ALG (B)- and PEG (C)-treated animals at 5 wpr. A-C: Representative images of the IF-stained lesion area in 50 μm -thick sagittal sections of the lesion area. D: Results of quantification of PAM-signal (after background elimination) in the lesion area via semi-automated analysis using the Image J plug-in Feature J. Bars represent mean + SEM. Spontaneous axonal in-growth into the lesion area was highly significantly increased after insertion of PEG ($n=64$) compared to ALG ($n=53$) or “RX only” ($n=12$). No statistical differences were found between ALG and “RX only”-controls. Arrowhead in B: Exemplary structure or area, respectively, exhibiting great extent of unspecific PAM-IR, but hardly any neuronal morphology. Such structures would have been eliminated in the course of background elimination and would not have appeared in the final quantification. Statistics in D: Kruskal-Wallis and *post-hoc* Mann-Whitney U-test with Holm-Bonferroni correction. * $p \leq 0.05$, ** $p \leq 0.01$, *** $p \leq 0.001$.

In “RX only”-animals, the resection area for the most part lacked sufficient tissue regeneration, resulting in a cavity filled with blood cells and some spongy scar tissue. PAM-positive axon fragments were therefore mainly found in the callus region which consisted of tissue which had formed underneath the Nescofilm® cover. Since the greater part of this region was not included in the evaluations, quantification in the “RX only” controls resulted in only low numbers (0.34 % PAM-signal in the scar area).

The signal intensity of PAM-positive axon fragments in the matrix area of ALG-treated animals was only inconsiderably higher than that of the control group. Only 0.39 % of the scar area in animals of this respective group revealed PAM-staining of regenerated axon fibers in the matrix. The ALG used in these studies further posed a problem in regard to tissue preparation and staining of the ALG-containing spinal cord sections: ALG matrix to a great extent exhibited unspecific antibody binding, resulting in high background staining, which complicated the analyses. Also, ALG, in the applied preparation, seemed to be easily contaminated leading to impurities which could then lead to further deterioration of the gel.

3.4.3 General Anterograde Labeling of Descending Axons

For quantification of BDA-labeled axon fragments in the lesion area, “lesion only” animals were used as controls. Since via the injection of BDA into the spinal cord only descending axons cranially to the lesion area should take up the BDA, all axon fragments found inside the lesion/matrix area can be considered regenerated axons. Therefore the situation in “lesion only” animals reflects the spontaneous axonal regeneration capacity at the analyzed time point without further intervention. An automated analysis of the in-growth of BDA-labeled axon fragments was not possible due to the oftentimes high background signal in the lesion area in sections of the BDA-traced animals (Fig. 3.13). This strong IR was exhibited by cellular debris structures as well as macrophages in the analyzed area (see red arrows in Fig. 3.13). Positive staining of such structures was oftentimes found to be of higher intensity than that observed in axonal structures (white arrow in Fig. 3.13), thereby making automated quantitative analyses impossible. In 20 µm-thick sagittal cryo sections of the lesion-containing spinal cord, there appeared to be less unwanted IR and BDA-positive axon profiles in the lesion area could be identified more easily.

However, the thickness of 50 μm of the analyzed sections was eventually chosen due to the increased loss of lesion area tissue/matrix, particularly in sections from animals of the ALG-group. Besides, the course of axonal structures can better be followed in 50 μm -thick sections. Since the quantification of regenerated axons in the matrix was an important point of the present study, the unwanted side effects had to be accepted.

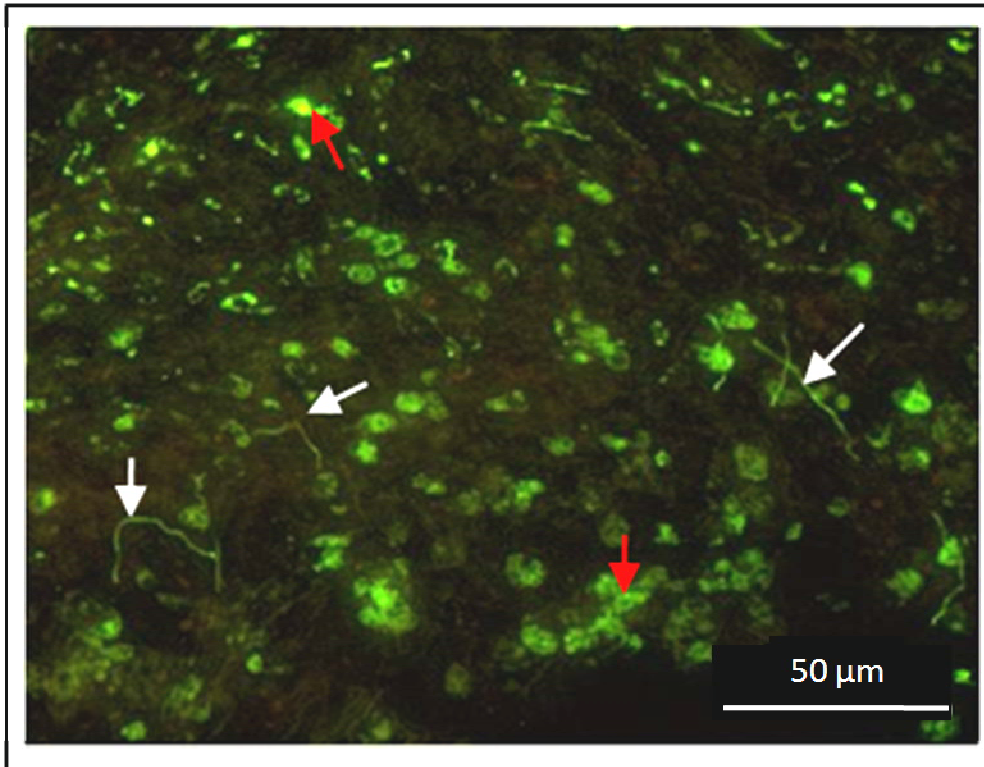


Fig. 3.13: Representative image of BDA-positive structures in the lesion area in a 50 μm -thick sagittal spinal cord section. BDA was visualized with OregonGreen® 488. White arrows: BDA-positive axon profiles, red arrows: BDA-positive non-axonal structures and cells.

In Fig. 3.14A, a schema of the general BDA-labeling of axons is presented. Images of respective areas “1” and “2” from sagittal sections of an animal which received this tracing are further depicted in Fig. 3.14B.

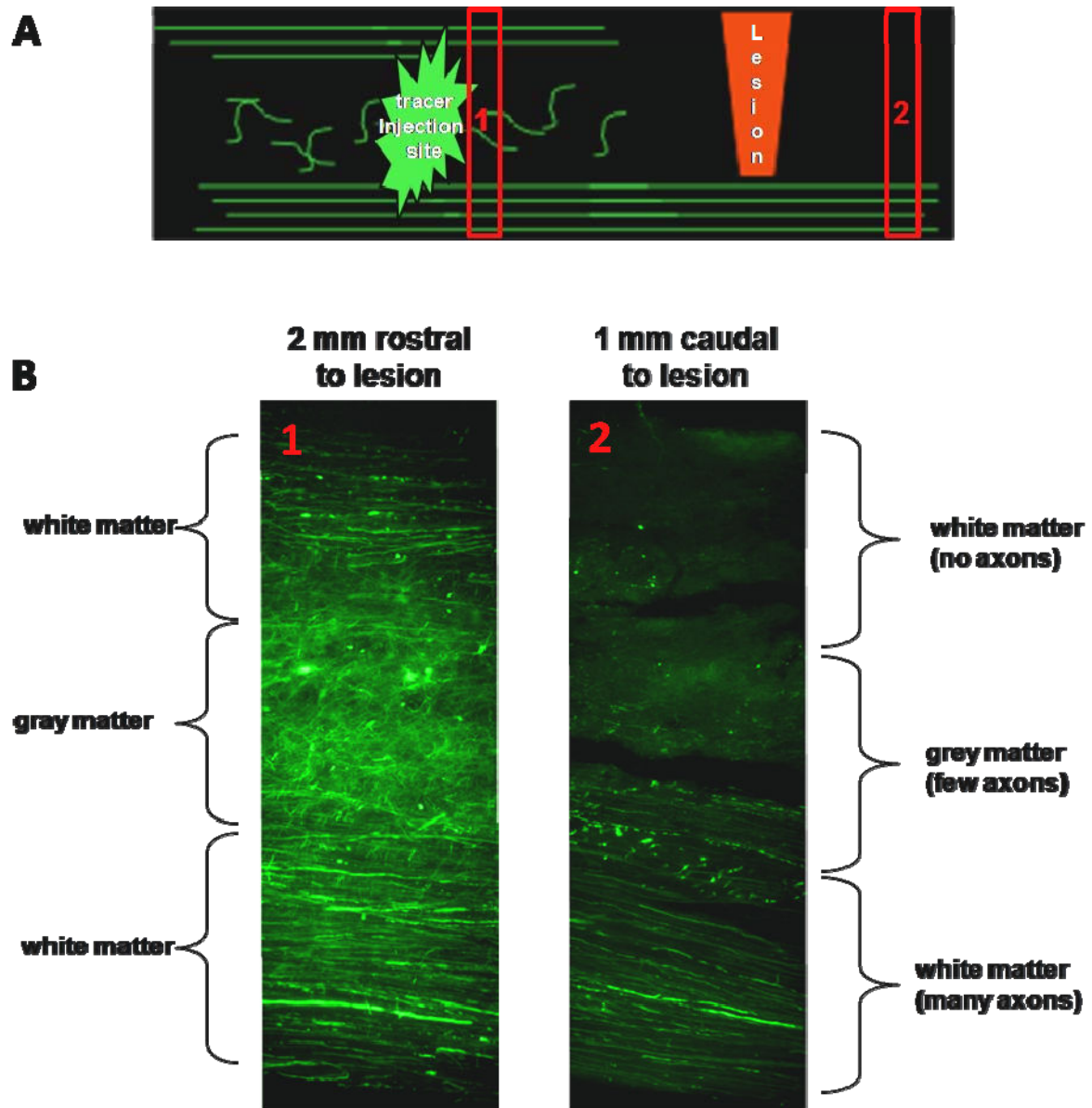


Fig. 3.14: General BDA-Labeling. A: Schematic illustration of the BDA-injection into the spinal cord in a sagittal section. Images of regions “1” and “2” from a spinal cord section are shown in B. B: BDA-labeled axons and neurons are distributed throughout the entire depth of the spinal cord after successful tracer injection into the spinal cord. Image sections from the same 50 μ m-thick histological section are depicted. Region 1: BDA distribution at the injection site approximately 2 mm cranially from the site of injury. Region 2: In spinal cord tissue caudally to the lesion site, BDA-labeling is restricted to axons in the ventral half of the spinal cord.

3.4.3.1 Quantitative Analysis of Regenerated Axons in the Lesion Area via Manual Counting of BDA-Labeled Axons

Comparable to the results of the quantification of PAM-positive axon signal in the lesion area, a higher amount of BDA-labeled axons was found in the dorsal matrix/callus region of the spinal cord lesion. In these areas, increased numbers of

axon fragments were also observed in the other analyzed treatment groups including the control group.

Only BDA-labeled structures which could clearly be identified as axonal fragments were counted. The quantification of the axonal fragments in the lesion area of “lesion only” controls or in the matrix area of treated animals, respectively, revealed further differences regarding axonal in-growth into the lesion area of chronic SCI-animals: Although the scar area of control animals was not completely devoid of axons which had regenerated into the lesion site, mainly background staining and only rare occurrence of BDA-positive axon profiles were detected in the respective areas of these animals (Fig. 3.15K, 1.7 BDA-labeled axon fragments/scar area/section). An even slightly (although not significantly) reduced mean axon number (1.5 BDA-labeled axon fragments/scar area/section) was detected in the matrix area of animals of the ALG-treated group. Only few, generally thin and short fiber fragments could be visualized in the lesion area of the respective animals. However, addition of the iron chelator BPY-DCA to the ALG resulted in an axonal in-growth into the matrix which, in comparison to “lesion only” controls was increased (3.5 BDA-labeled axon fragments/scar area/section). This increase was not significant according to the results of the applied statistical analysis with subsequent Bonferroni-correction. When only ALG and “lesion only” groups were taken into account for statistical analysis, there was a significant difference found for “lesion only” and ALG+BPY-DCA (* $p = 0.015$). After complete statistical analysis and comparison of all analyzed groups as is shown in Fig. 3.15K, the observed increase in axon in-growth after chelator addition to ALG, can only be noted an observed trend. However, axon profiles in the lesion area were further found to be longer than those found in the ALG alone. The highest amount of BDA-labeled axon fragments in the lesion area was detected in PEG-treated animals: Several long (Fig. 3.15E) and branched (Fig. 3.15F) axon profiles could be detected. Some axons further exhibited the bundle-like alignment (Fig. 3.15E) which was also revealed by PAM-staining in PEG-matrix (as shown in Fig. 3.8C,c). Compared to the remaining analyzed groups, the increase was highly significant (15.5 BDA-labeled axon fragments/scar area/section, *** $p < 0.0001$). The axonal fragments were distributed throughout the whole lesion area and at times even revealed a course with tract-like alignment. Similar observations were not made in any of the remaining groups.

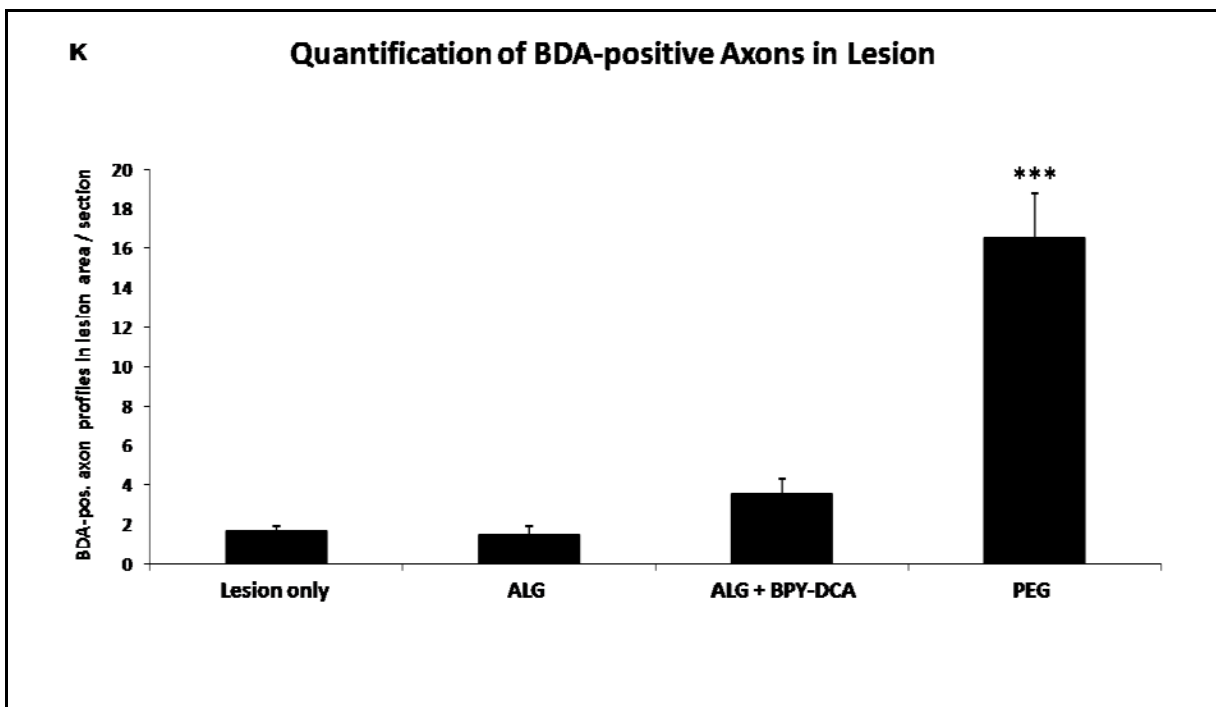
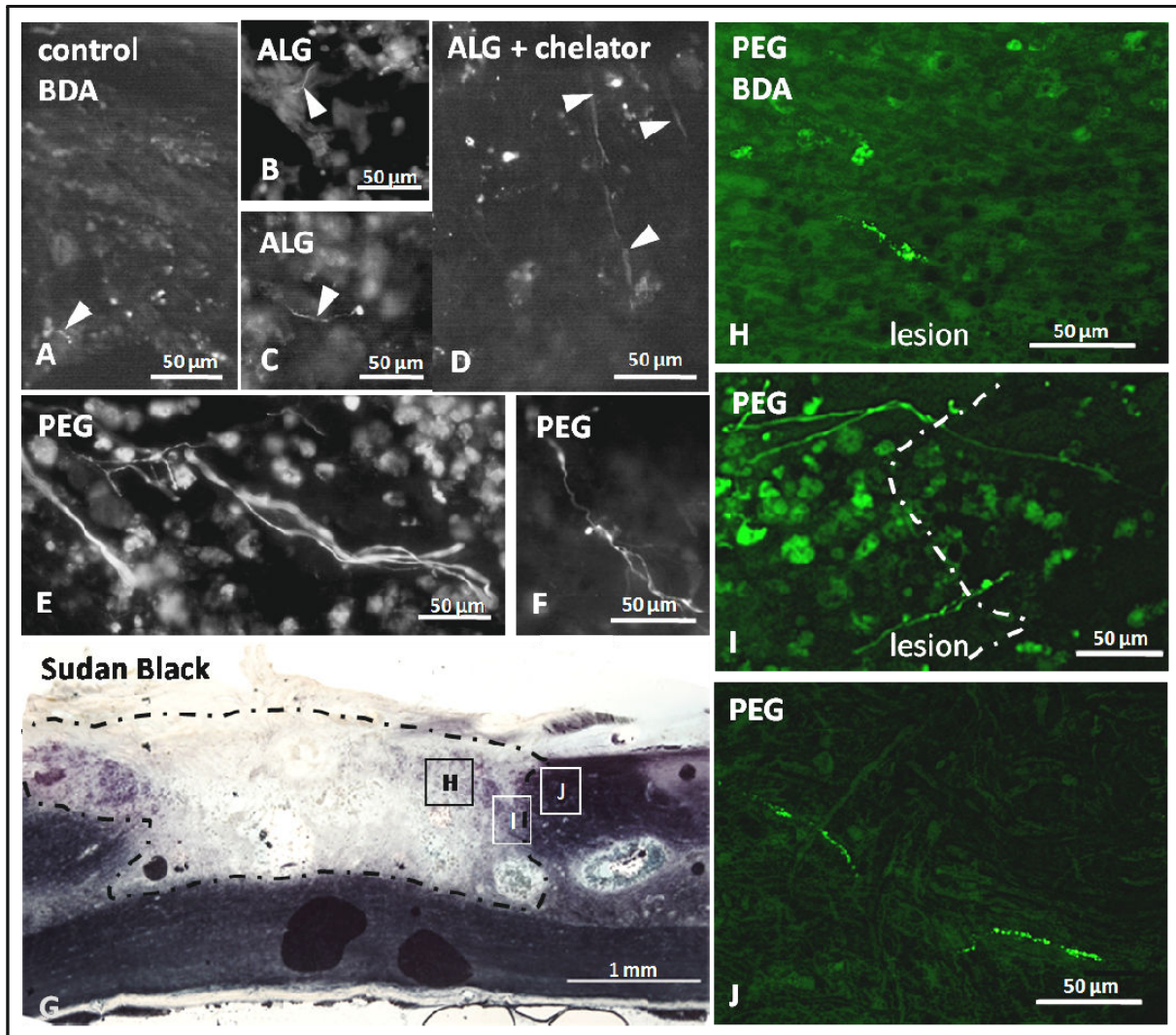


Fig. 3.15 (previous page): Investigation of spontaneous axonal regeneration into lesion area via axonal BDA labeling at 5 wpr. Spontaneous axonal regeneration of BDA-labeled axons into the lesion area of “lesion only” (A)-, ALG (B,C)-, ALG+BPY-DCA (D) and PEG (E,F)-treated animals at 5 wpr (“lesion only” controls: 10 wpl). A-F: Representative images of BDA-positive structures in the lesion area in 50 μm -thick sagittal sections of controls, ALG-, ALG+BPY-, and PEG-treated animals. Arrowheads in A-D: BDA-positive axonal structures. G: Exemplary image of Sudan Black staining. Areas devoid of Sudan Black staining correspond with lesion extent. Delineated Sudan Black-negative area represents area which was taken into account for evaluations. Boxed areas H-J in G: Areas in which BDA-positive axons (shown in H-J) were detected: Regenerated axons were found to grow inside the lesion area (H), from the lesion area into the distal spinal cord (I) and in dorsal spinal cord gray matter distal to the lesion site, but in close proximity (J). Dashed line in I: Transition from lesion to intact area. K: Results of quantification via manual counting of BDA-positive axon fragments in lesion. Bars represent mean + SEM. Spontaneous axonal regeneration into lesion area was highly significantly increased after insertion of PEG (n=31) compared to ALG (n=35), ALG+BPY (n= 39) or “lesion only” (n=46). Positive trend in the comparison of ALG+BPY with “lesion only” controls. Statistics in K: Kruskal-Wallis and *post-hoc* Mann-Whitney U-test with Holm-Bonferroni correction. *p \leq 0.05, **p \leq 0.01, ***p \leq 0.001.

3.5 Characterization of the Lesion Area at an Early Time Point

The matrix area of ALG- and PEG-treated animals was compared via immunohistological staining with special focus on (ECM) composition, vascularization, and cellular invasion of the lesion area. Since only few sections per animal (i.e., two sections minimum per animal from the central region of the lesion) were stained and analyzed, the described observations result from a qualitative rather than a quantitative analysis. It should once again be noted that the ALG’s characteristic to non-specifically bind antibody complicated the analyses, because immunohistological staining of ALG oftentimes resulted in false-positively stained structures. Detailed microscopic evaluation was therefore carried out very carefully.

For analysis the time point of 1 wpr was chosen. Because an increase in spontaneous axonal regeneration into the lesion area of PEG-treated animals was observed at the time point of 5 wpr, early evidence to explain the observed differences in the regeneration capacity of the respective treatment groups was of great interest. The chosen time point is also the time point in acutely injured animals at which, without further treatment, axonal regeneration is inhibited due to a fully developed fibrous lesion scar (Klapka et al., 2005). Therefore, a comparison of the situation in the lesion area of acutely injured animals vs. chronically injured and subsequently re-injured animals was drawn.

3.5.1 Extracellular Matrix Composition

The composition of the ECM (the fibrous scar) at the lesion site was investigated via immunohistological staining of Col4.

“Lesion only” control animals at 1 wpl - the time point at which the lesion scar is fully developed in untreated animals - revealed the highest IR to Col4 in the fully developed lesion scar (Fig. 3.16A). The majority of the stained structures revealed a sheet like Col4 accumulation. Some blood-vessel-like structures (marked by arrowheads) were also apparent. While some of the positively stained structures resembled BV, a strong Col4-IR was further noted to be distributed throughout the whole lesion scar, as has also been described previously by Klapka *et al.* (Klapka *et al.*, 2005).

A similar Col4 distribution was observed in “lesion only”-control animals at 5 wpl (Fig. 3.16B). At this chronic time point, the intensity of the staining was slightly reduced, but similar structures to those seen in the seven days post lesion-control animals revealed positive Col4-IR. However, fewer clearly defined structures and a rather homogenous staining of the whole lesion scar were noted in the chronic SCI scar. Once again, note the large holes in the ALG-matrix, some of which contained sparse ALG-residues (blue arrowheads).

In animals which received an ALG-filling of the resection cavity, the intensity of the Col4 staining was weaker than that in control animals at 1 wpl, but it was comparable to that in control animals at 5 wpl (Fig. 3.16C). Homogenous staining of the lesion area and few blood vessel-like structures were detected. Instead, several structures lined with a Col4-positive rim became apparent. Some of these encapsulation-like structures generally did not contain Col4 positive tissue even if they still contained ALG. In others with only incomplete Col4-lining, remaining ALG fibers revealed weak Col4 staining of individual cells.

The lesion area of PEG-treated animals exhibited a reduced Col4-IR intensity (Fig. 3.16D) compared to the other analyzed groups. Not only was the intensity of the staining reduced, but in comparison with control- and ALG-groups, as strong decrease in sheet-like Col4 accumulation was noted. There was also a striking increase in the amount of structures resembling BV. Furthermore, similar structures were also noted to be surrounding the lesion area.

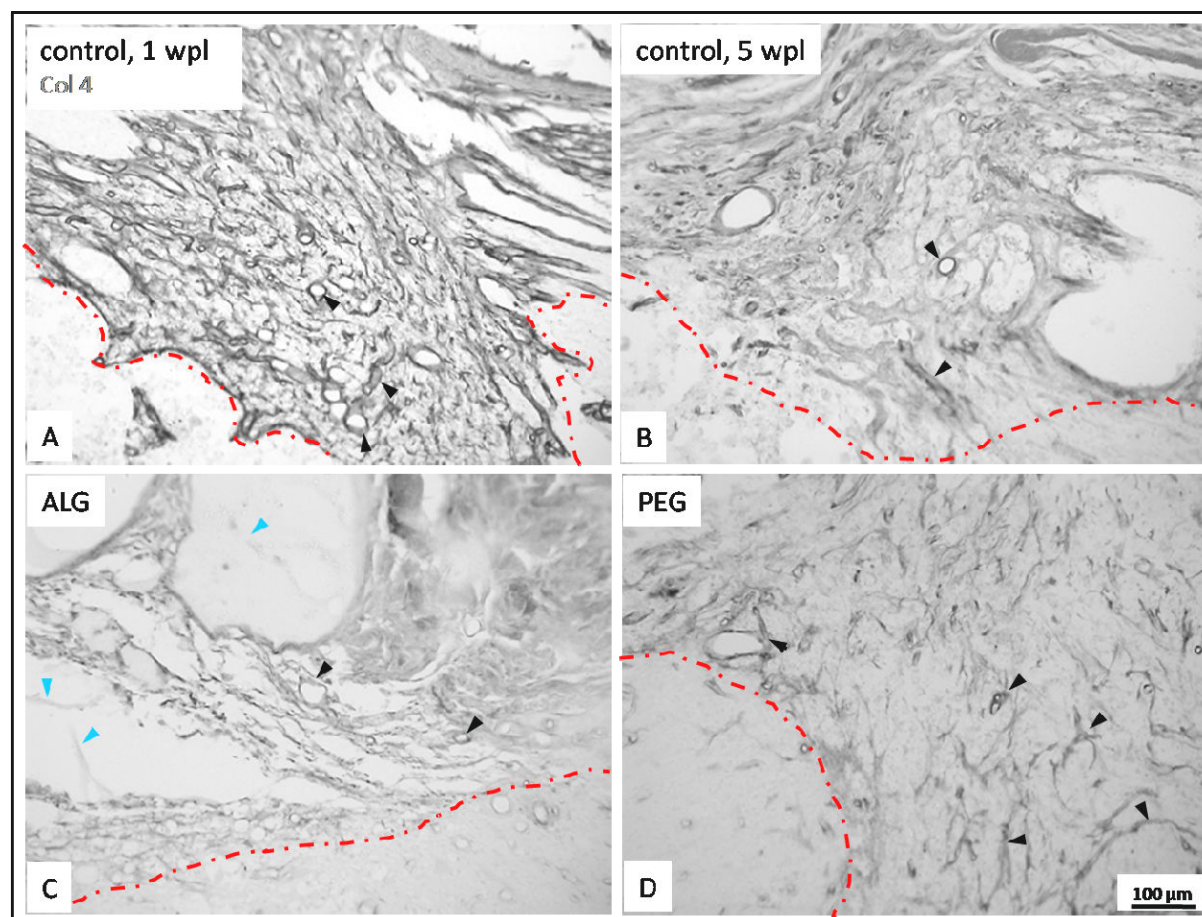


Fig. 3.16: ECM-composition in lesion area. Representative images of Col4-IR visualized via DAB-reaction in the lesion area in 10 µm-thick sagittal paraffin sections of “lesion only”-controls (A,B), and of ALG (C)- and PEG (D)-animals visualized via DAB reaction. Dashed lines delineate lesion area. Note large holes in ALG-matrix, some of which contained sparse ALG-residues (blue arrowheads); black arrowheads: BV-resembling structures.

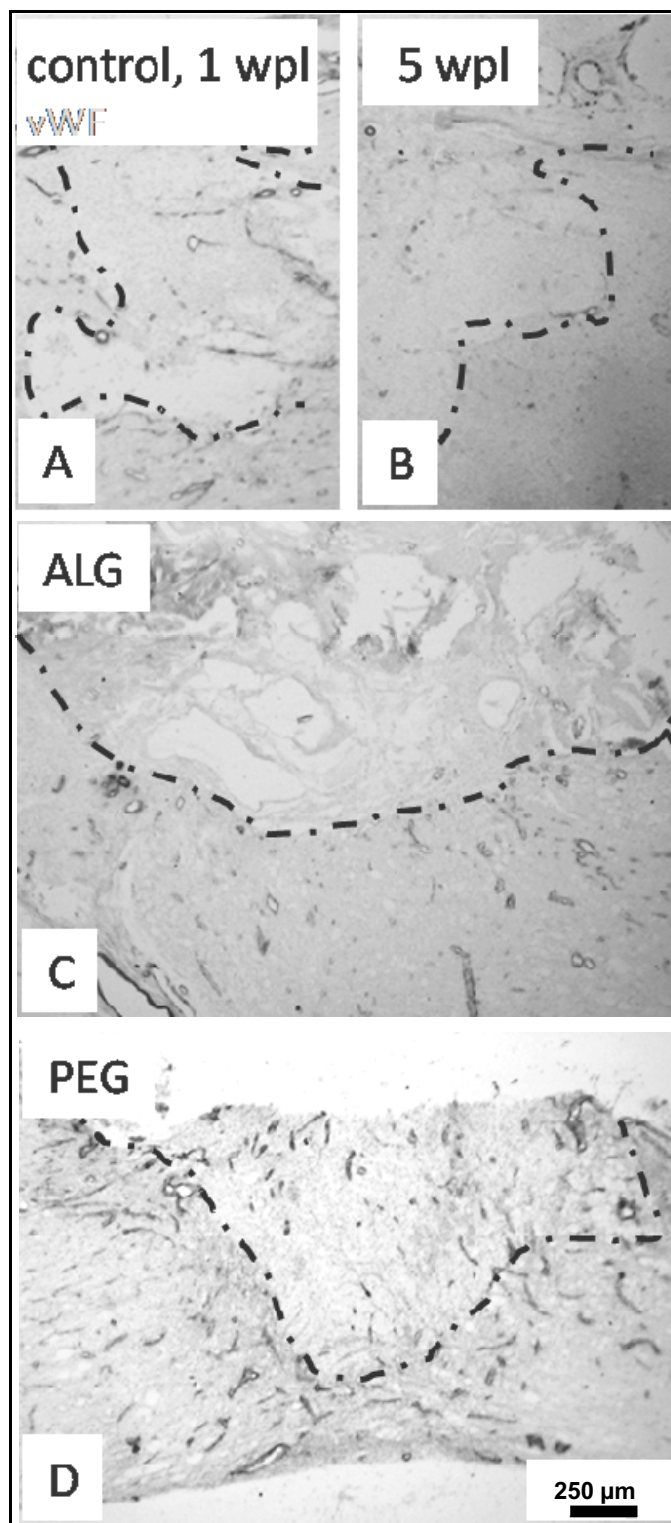
3.5.2 Vascularization

Vascularization of the lesion area was analyzed via antibody staining with an antibody against the endothelial marker von Willebrand factor (vWF) (Fig. 3.17).

Occurrence of BV was observed in animals of all treatment groups (Fig. 3.17). Increased numbers of BV were generally apparent in surrounding spinal cord areas (Fig. 3.17A-D) with increased BV numbers after treatment with PEG (Fig. 3.17D). The lesion area of animals which received PEG matrix after chronic SCI scar resection further revealed the highest number of BV (Fig. 3.17D,I), whereas the lesion area of “lesion only” controls at 5 wpl and of ALG-treated animals at 1 wpr showed the weakest IR to vWF (Fig. 3.17 B,C,F,G,H). In the lesion areas of animals of the control groups and of ALG-treated animals, PAM-positive axon fragments were generally not found to be present, and the few fiber fragments which were detected

were not found to be associated with BV (Fig. 3.17E-H). The fiber structures of the ALG-scaffold turned out to be misleading at times, since they also exhibited slight background staining which was probably due to unspecific antibody binding. Comparison of vWF-IR and of these ALG-structures with the morphology of the more intensely stained vWF-positive BV, however, elucidates the observed differences and helps with the clarification of the results of the immunohistological staining (Fig. 3.17G). Even when some regeneration into the lesion area of ALG-treated animals had occurred, association of regenerated axons with BV structures was not observed (Fig. 3.17H).

vWF-staining in the lesion area of PEG-treated animals demonstrated BV to be distributed throughout the whole lesion scar of animals of this respective group (Fig. 3.17D,I). These BV appeared to be of normal or even slightly increased size when compared to those in intact spinal cord tissue. Large and intensely stained blood vessels were numerous present in the lesion center (Fig. 3.17I). Regenerated axons were frequently found in BV-rich areas of the PEG matrix (Fig. 3.17I) where close association of the two cell types was detected, as can be seen in a confocal image shown in Fig. 3.17J. Such observations were not made in any of the remaining experimental groups.



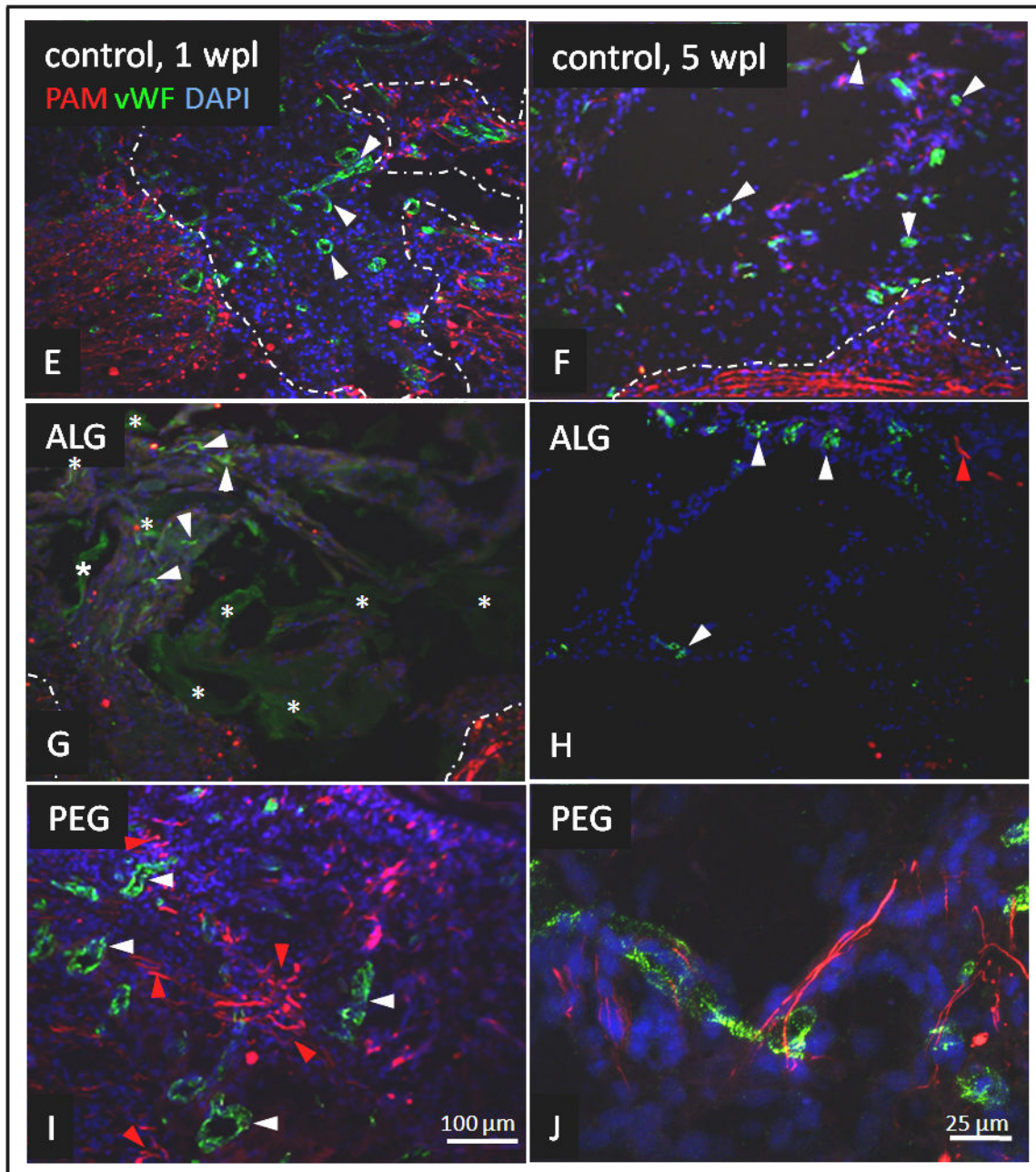


Fig. 3.17: Vascularization of lesion area. Representative images of vascularization in the lesion area in 10 μm -thick sagittal sections of “lesion only” controls (A,B,E,F), ALG (C,G,H)- and PEG (D,I,J)-animals. BV-occurrence was assessed via IR to endothelial marker vWF. A-D: IR-visualization via DAB reaction; E-I: IF; J: confocal image. Dashed lines delineate the lesion area. White arrowheads: vWF-positive BV and structures (green); red arrowheads: PAM-positive axonal structures (red); asterisks: areas of background staining exhibited by ALG; note scaffold residues in the lesion center of ALG-animals. Scale bar in D also applies for DAB-stained images, scale bar in I also applies for E-H.

3.5.3 Cell Invasion of the Lesion Area

3.5.3.1 Astrocytes

The fibrous lesion scar is surrounded by the glial scar. While in the fibrous lesion scar IR for the glial fibrillary acidic protein (GFAP) is absent, the glial scar is

characterized by the presence of reactive astrocytes which strongly express this protein resulting in strong GFAP-IR.

To find out whether insertion of a matrix after chronic SCI resection would alter the behavior of astrocytes, sections were stained with an antibody against GFAP. Much fewer GFAP-positive astrocytes were detected in the lesion area of “lesion only” controls at 1 wpl (Fig. 3.18A) or 5 wpl (Fig. 3.18B) or of ALG-treated animals (Fig. 3.18C), respectively, in comparison to PEG-treated animals (Fig. 3.18D). In Fig. 3.18A, a representative image of GFAP-IR of the lesion area of an acutely injured animal at 1 wpl is shown. Some astrocytic processes were found to have entered the lesion area in “lesion only” control animals at 1 wpl. Although the lesion area was mainly devoid of positive GFAP-IR, there were a few GFAP-positive structures in the border region of glial and fibrous scar, and even some structures in the center of the otherwise GFAP-free fibrous lesion scar.

In chronically injured control animals, on the other hand, the glial scar was found to be fully developed (Fig. 3.18B): The rim area was accurately closed by the GFAP-positive astrocytes. No invading or remaining GFAP-positive cells were observed in the fibrous lesion scar of the respective animals. While in the lesion area of control animals at one week post lesion some astrocytic processes appeared to be present in the lesion center, in animals of the ALG-treated group there was an increased number of GFAP-positive resembling astrocytes (Fig. 3.18C). In the analyzed parasagittal sections such structures were mainly detected in the lateral border regions of the lesion.

PEG-treated animals revealed the strongest GFAP-IR in the lesion area (Fig. 3.18D). Some of the positively stained structures could clearly be identified as astrocytes which had invaded the PEG-matrix. Because both cell types, i.e., reactive astrocytes and some Schwann cell populations are known to express GFAP, the analysis of the morphology of the respective cells can serve as a distinction feature. Just like in the ALG-group, the majority of astrocytic processes, which had entered the lesion area, were found to be located in the lateral border areas of the lesion site in the parasagittal sections. But in contrast to ALG-treatment, filling of the aspiration cavity with PEG matrix further promoted invasion of astrocytes or GFAP-positive structures, respectively, further into the lesion area, where they were frequently found to be widely distributed throughout the entire affected area. A slightly decreased

GFAP-IR was further noted in spinal cord tissue bordering the matrix area of these animals indicating a decreased glial scar formation.

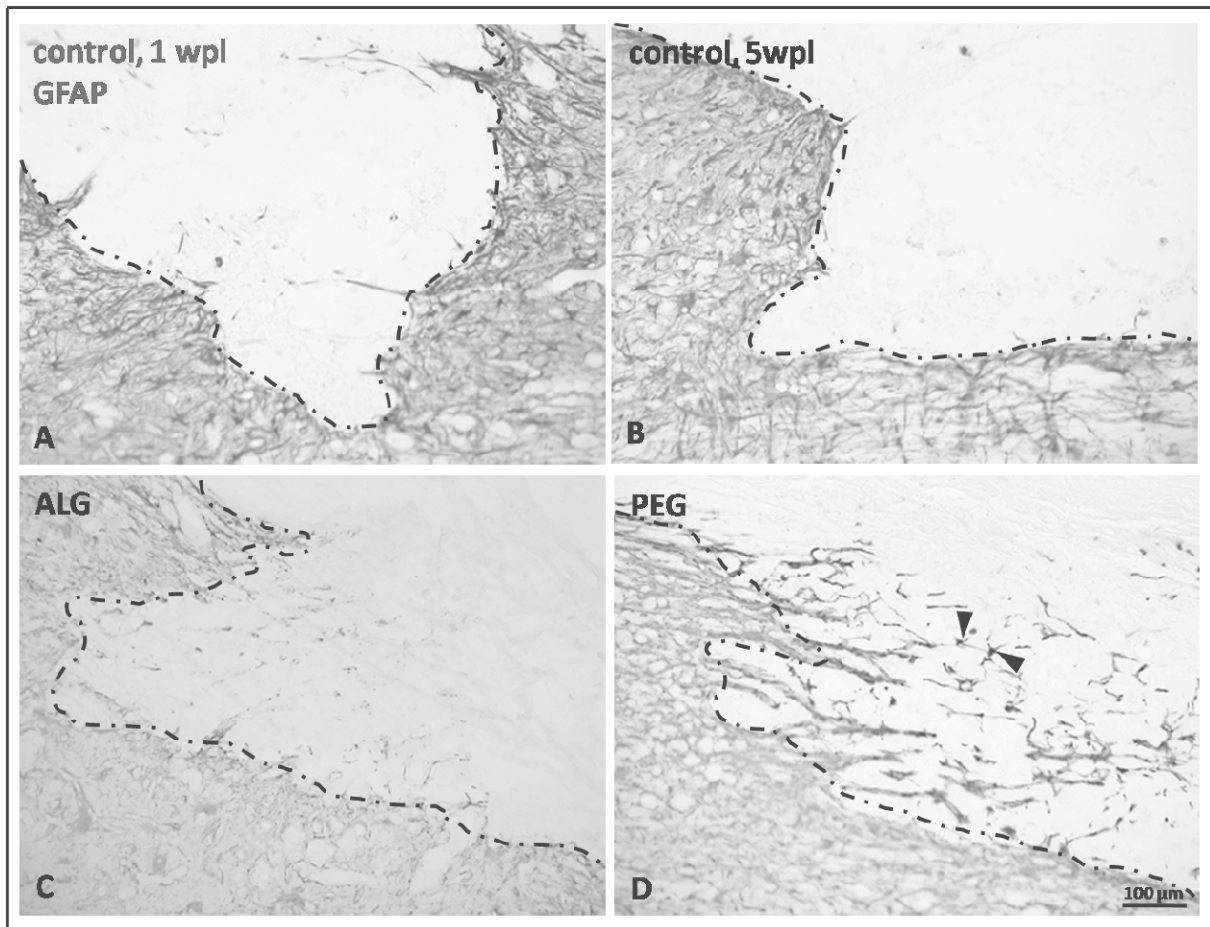


Fig. 3.18: Invasion of GFAP-positive cellular structures into the lesion area and astrogliosis. Representative images of astrocyte invasion and astrogliosis assessed via IR to GFAP in the lesion area in 10 µm-thick sagittal sections of acute (A) and chronic (B) “lesion only”-control animals, ALG-treated (C), and PEG-treated (D) animals. Dashed lines delineate the lesion area; arrowheads: GFAP-positive cells clearly exhibiting astrocyte morphology.

A similar observation regarding invasion of GFAP-positive structures was made in PEG-treated animals at the time point of 5 wpr (Fig. 3.19). These animals, too, frequently exhibited GFAP-IR in the lesion area, whereas in animals of the remaining analyzed groups at the same time point such an observation was not made.

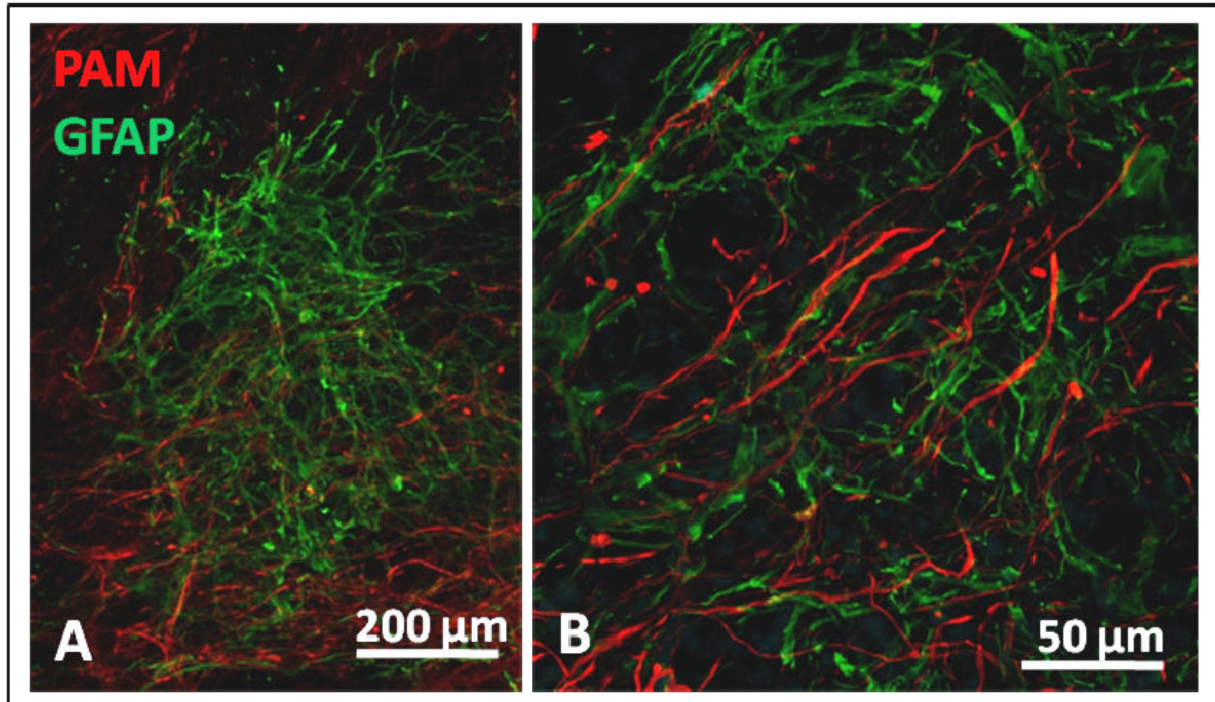


Fig. 3.19: Confocal images of PAM-positive axons and GFAP-positive structures in the lesion area in 50 μm-thick sagittal sections of a PEG-treated animal at 5 wpr. Close association of the two cell types is revealed in the magnification image (B) from the same section.

3.5.3.2 Fibroblasts

Since meningeal fibroblasts are known to secrete Col4 and thus contribute to a large extent to the Col4 accumulation in the fibrous lesion scar, it was investigated whether the two tested matrices revealed differences in the invasion of meningeal fibroblasts. As a marker for fibroblasts, an antibody against rat prolyl 4-hydroxylase (rPH), the key enzyme in the biosynthesis of collagens, was used. In comparison to PEG-treated animals, a striking increase in rPH-IR was observed in the lesion area of ALG treated animals (Fig. 3.20). While both matrices – as expected - exhibited strong IR to rPH in the dorsal areas of the lesion, ALG-treated animals further revealed a strong staining of fibroblasts distributed throughout the entire lesion area (Fig. 3.20A-C). In animals which received PEG-filling of the resection cavity such an increase was not apparent. Considerably less positively stained cells were present in the lesion area of the respective animals (Fig. 3.20D-F).

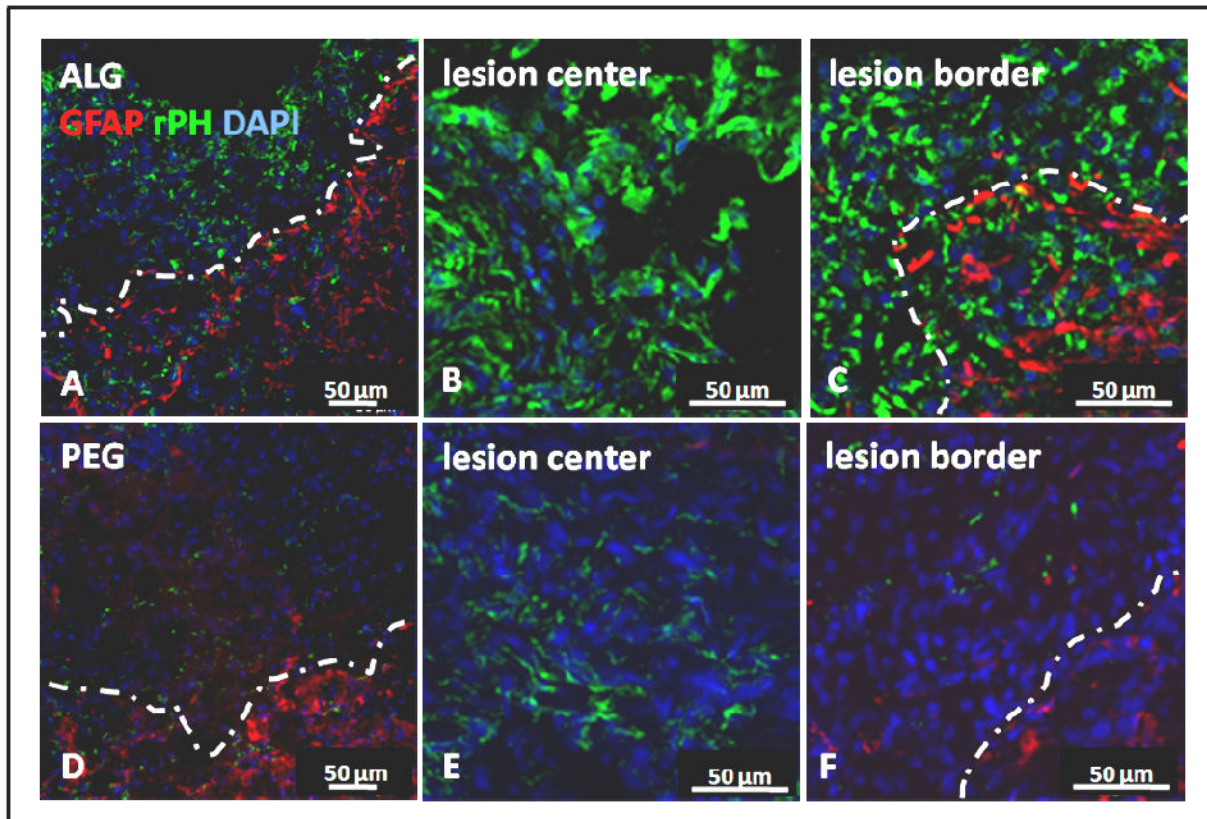


Fig. 3.20: Comparison of the extent of fibroblast invasion of the lesion area of ALG- and PEG-treated animals. Representative images of fibroblast invasion assessed via IR to rPH in the lesion area in 10 µm-thick sagittal sections of ALG-treated (A-C) and PEG-treated (D-F) animals. Dashed lines delineate the lesion area.

3.5.3.3 Oligodendrocytes

To investigate whether either of the matrices promoted the invasion of mature oligodendrocytes, the myelinating cells of the CNS, sections were stained using an antibody against *Adenomatous Polyposis Coli* (APC). Because APC is not a marker restricted to oligodendrocytes but also labels some astrocytes, the distinction was again made on the basis of differences in the morphology of the two cell types.

No obvious differences were detected in the lesion area of ALG-treated and PEG-treated animals (Fig. 3.21A-D). In both treatment groups there was an accumulation of oligodendrocytes detected in the GFAP-rich area of the lesion border. Invasion of mature oligodendrocytes was not or only very rarely observed in either of the analyzed matrices.

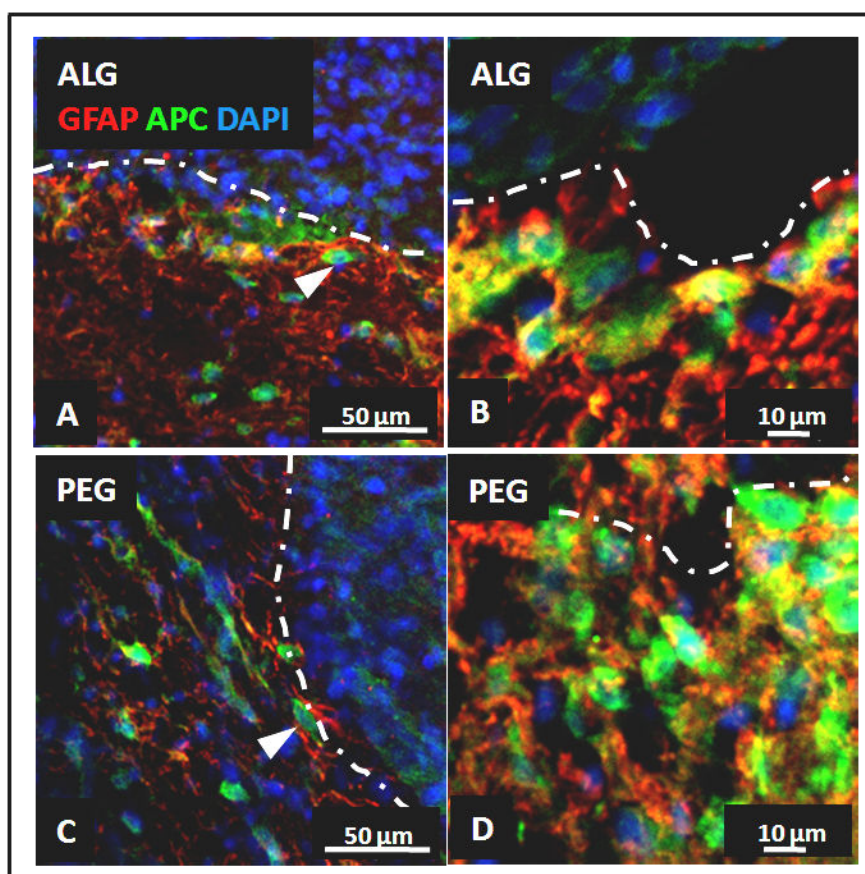


Fig. 3.21: Comparison of oligodendrocyte invasion of the lesion area of ALG- and PEG-treated animals. Representative images of oligodendrocyte invasion assessed via IR to APC in the lesion area in sagittal sections of ALG-treated (A,B) and PEG-treated (C,D) animals. Dashed lines delineate the lesion area.

3.5.3.4 Schwann Cells

Since Schwann cells are known to elicit positive regeneration-promoting effects after SCI (Ban et al., 2008; Black et al., 2006; Boyd et al., 2005; Cai et al., 2007; Oudega, 2007; Someya et al., 2008; von Euler et al., 2002; Xu et al., 1997), the lesion area of the analyzed groups was examined for the presence of Schwann cells. The antibody S100 β was used as a marker for Schwann cells. S100 β is further expressed by astrocytes. In immunofluorescent PAM+S100 β double-staining, S100 β -IR could therefore be used for the determination of the border of the glial scar (Fig. 3.22E,F).

No or only very few S100 β -positive cells were detected in the lesion area of control animals at 1 wpl (Fig. 3.22A). At 5 wpl, although the intensity of the staining generally appeared to be higher than at 1 wpl, control animals frequently revealed loss and degeneration of tissue in the lesion center. Such respective areas often

exhibited background staining of remaining tissue debris (Fig. 3.22D; note the lack of DAPI staining in the center of the lesion area), while the border areas of the lesion revealed S100 β -IR in only few cellular structures.

Some of the ALG-treated animals exhibited S100 β -IR in some cellular structures, which were located in the lateral border regions of the ALG matrix (Fig. 3.22B) in sagittal spinal cord sections. In the lesion area or ALG, respectively, in sections of other ALG-treated animals, S100 β -positive cellular staining was found to be completely absent, indicating that invasion of S100 β -positive cells had not occurred at the analyzed time point.

Only in the lesion area of the animals of the PEG-treated group, increased numbers of S100 β -positive cells were found to be distributed throughout the entire lesion site (Fig. 3.22C, also note GFAP-positive structures in the lesion area). These structures expressed either GFAP (red) or S100 β (green), whereas double-stained structures were only very rarely detected. S100 β -positive cells were furthermore found to be frequently associated with PAM-positive axonal fragments, indicating a close association of the two cell types in the PEG-matrix (Fig. 3.22F).

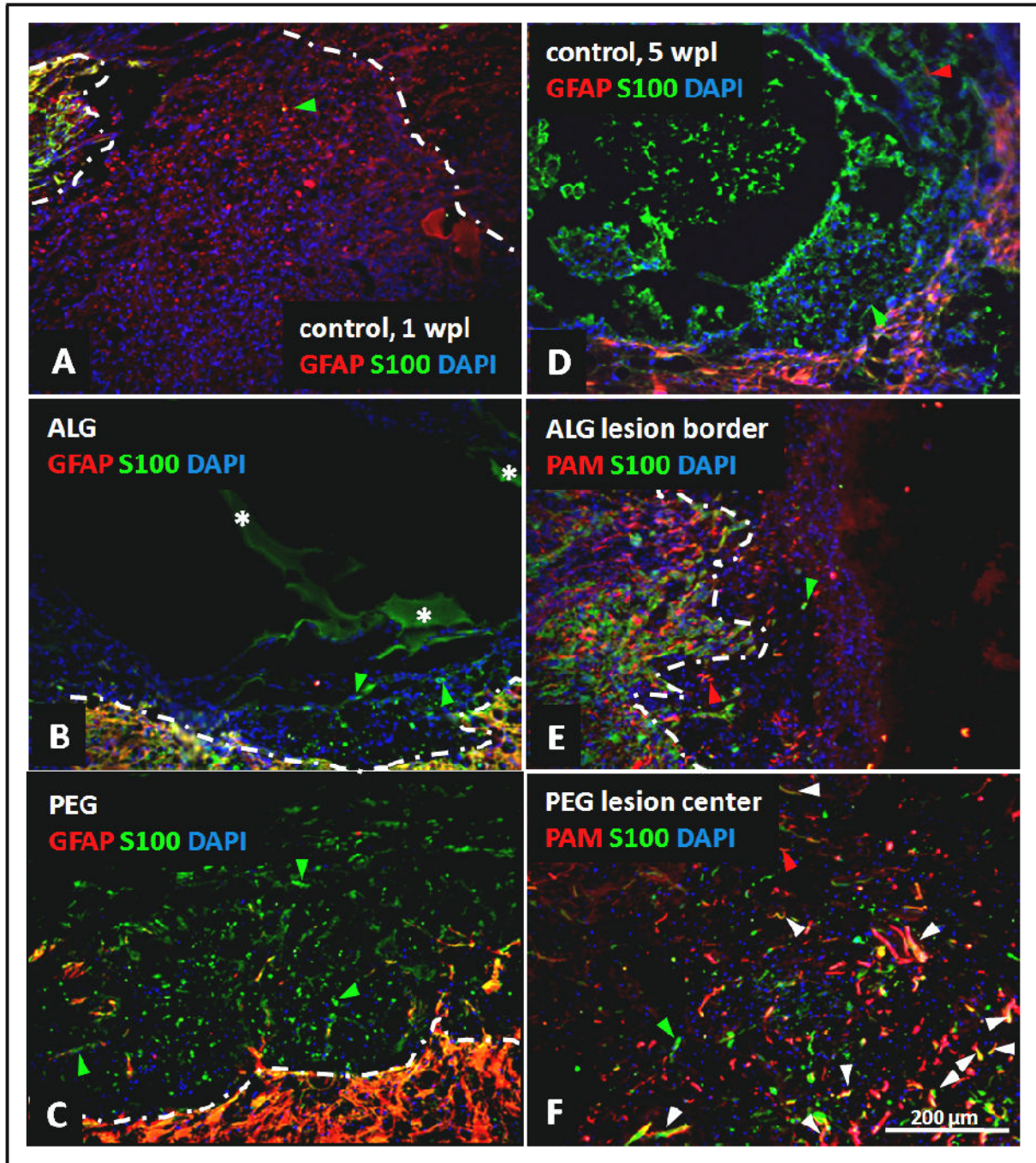


Fig. 3.22: Schwann cell invasion of the lesion area. Representative images of Schwann cell invasion assessed via IR to S100 β in the lesion area in 10 μ m-thick sagittal sections of acute (A) and chronic (D) “lesion only”-controls, ALG-treated (B,E) and PEG-treated (C,F) animals. Survival time of matrix-treated animal: 1 wpr. Dashed lines delineate the lesion area; arrowheads. Green arrowheads: S100 β -expressing cells, red arrowheads: PAM-Expressing cells, white arrows: possible association of S100 β - and PAM-positive cells; asterisks: ALG-residues.

3.5.4 Inflammatory Response

3.5.4.1 Activated microglia, monocytes and macrophages

Since DAPI staining in the IF-stained sections from animals of all experimental groups revealed the presence of many cells in the lesion area or matrix area, respectively, the lesion area was further characterized via immunohistology in regard to invasion of immune cells into the respective areas. A general immune cell staining with an antibody against ED1, the rat homologue of human CD68, was performed. In control animals at both analyzed time points, an extensive accumulation and distribution of ED1-positive cells throughout the entire lesion area was noted (Fig. 3.23A,B). Further, a large portion of cells with DAPI-staining of their nuclei were also found to express ED1.

The distribution of ED1-positive cells in the lesion area of ALG- or PEG-treated animals, respectively, appeared to be comparable (Fig. 3.23C or Fig. 3.23D, respectively). While the matrix area of the respective animals also contained many cells (as indicated by nuclear DAPI staining), only some of these cells revealed IR to ED1. Such ED1-positive cells were observed to accumulate mainly in the border areas of the lesion or matrix area, whereas the lesion center widely remained devoid of ED1-IR. Very high ED1-IR was also observed in the border areas of the lesion in control animals, but there, no or only weak decrease in ED1-IR (unless due to tissue loss) in the lesion center was noted.

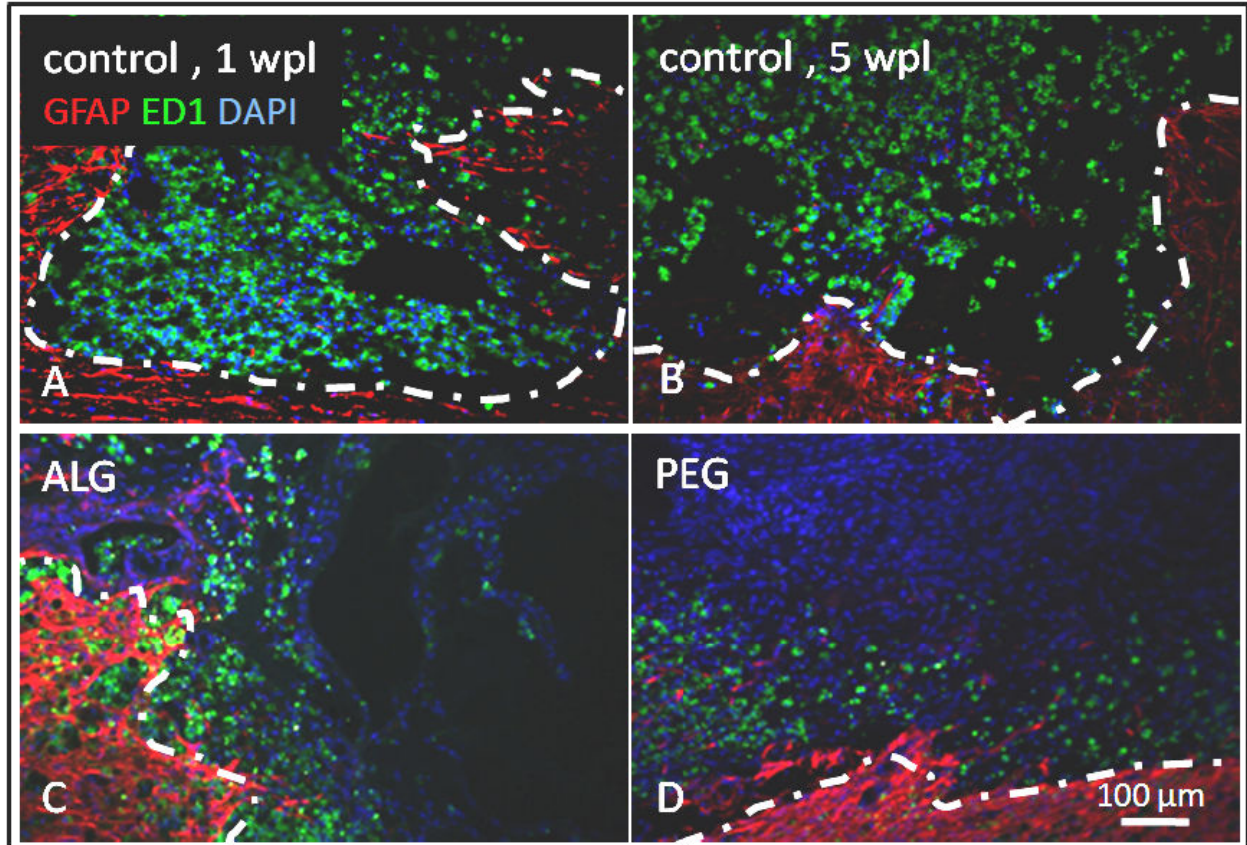


Fig. 3.23: Inflammatory response after matrix implantation in chronic SCI. Invasion of possibly inflammatory cells was assessed via IR to ED1. Representative images of the lesion area in 10 μ m-thick sagittal sections of “lesion only” controls at 1 wpl (A) or 5 wpl (B) and of ALG (C)- or PEG (D)-treated animals. Dashed lines delineate the lesion border.

3.5.4.2 T- and B-Lymphocytes

Additional analysis was carried out via antibody staining against B- and T-cells. A higher amount of positively stained CD4⁺ (Fig. 3.24A) and CD5⁺ (Fig. 3.24C) T-cells appeared to be present in the lesion area of “lesion only” controls at 5 wpl compared to matrix-treated animals, while occurrence of CD8⁺ T-cells (Fig. 3.24B) and of B-cells (Fig. 3.24D) was only rarely detected in these animals at the analyzed time point of 5 wpl.

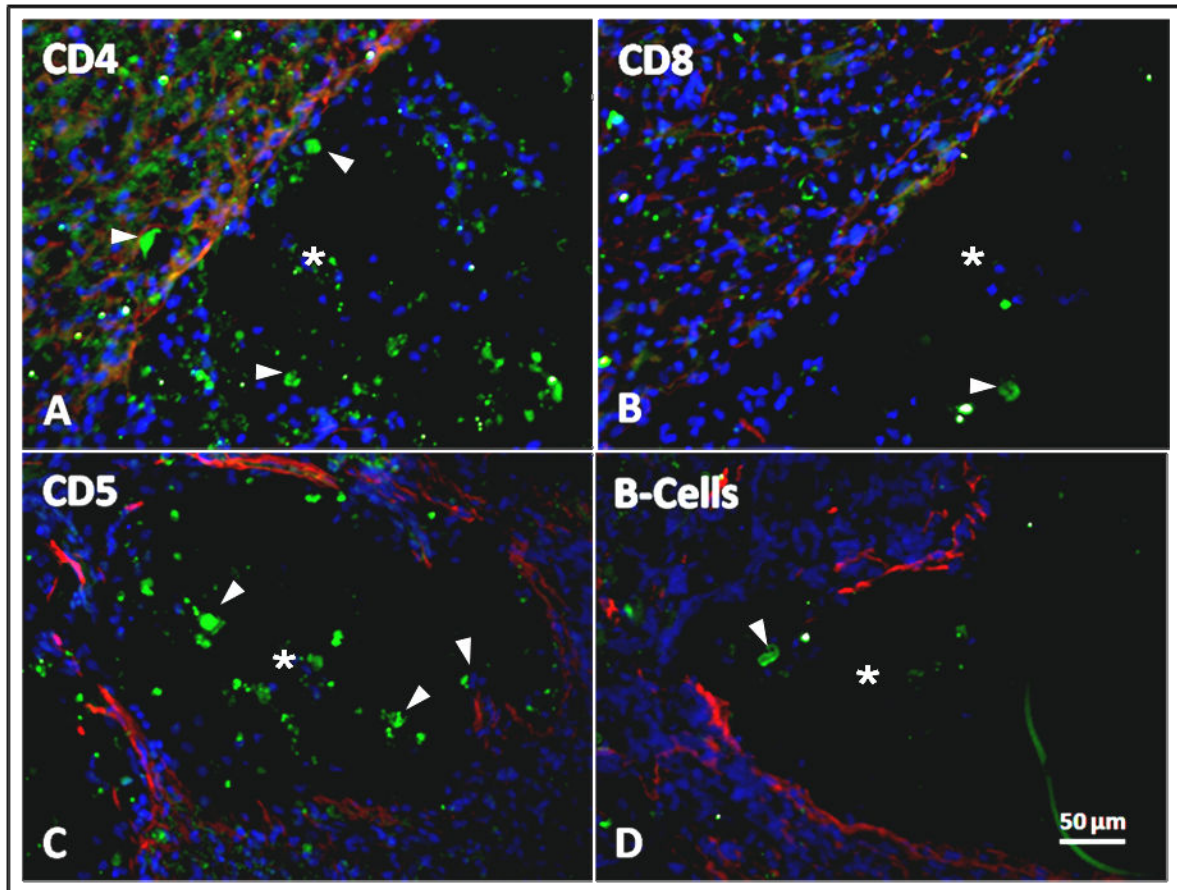


Fig. 3.24: T- and B-cell occurrence in the lesion area in 10 μm -thick sagittal sections of lesion only control animals at 5 wpr. The respective cells are visualized by green staining (red: GFAP, blue: DAPI); asterisks mark lesion area, arrowheads: IR-positive T- or B-cells, respectively.

In and around the lesion site, no obvious differences regarding invasion of cells from these populations were detected between sections of ALG- or PEG-treated animals (Fig. 3.25A-D). In all analyzed sections, cells revealing positive IR to the respective antibody were only rarely found. Furthermore, CD4^+ cells were not found in the matrix area of treated animals, but only in surrounding areas of the spinal cord (Fig. 3.25A).

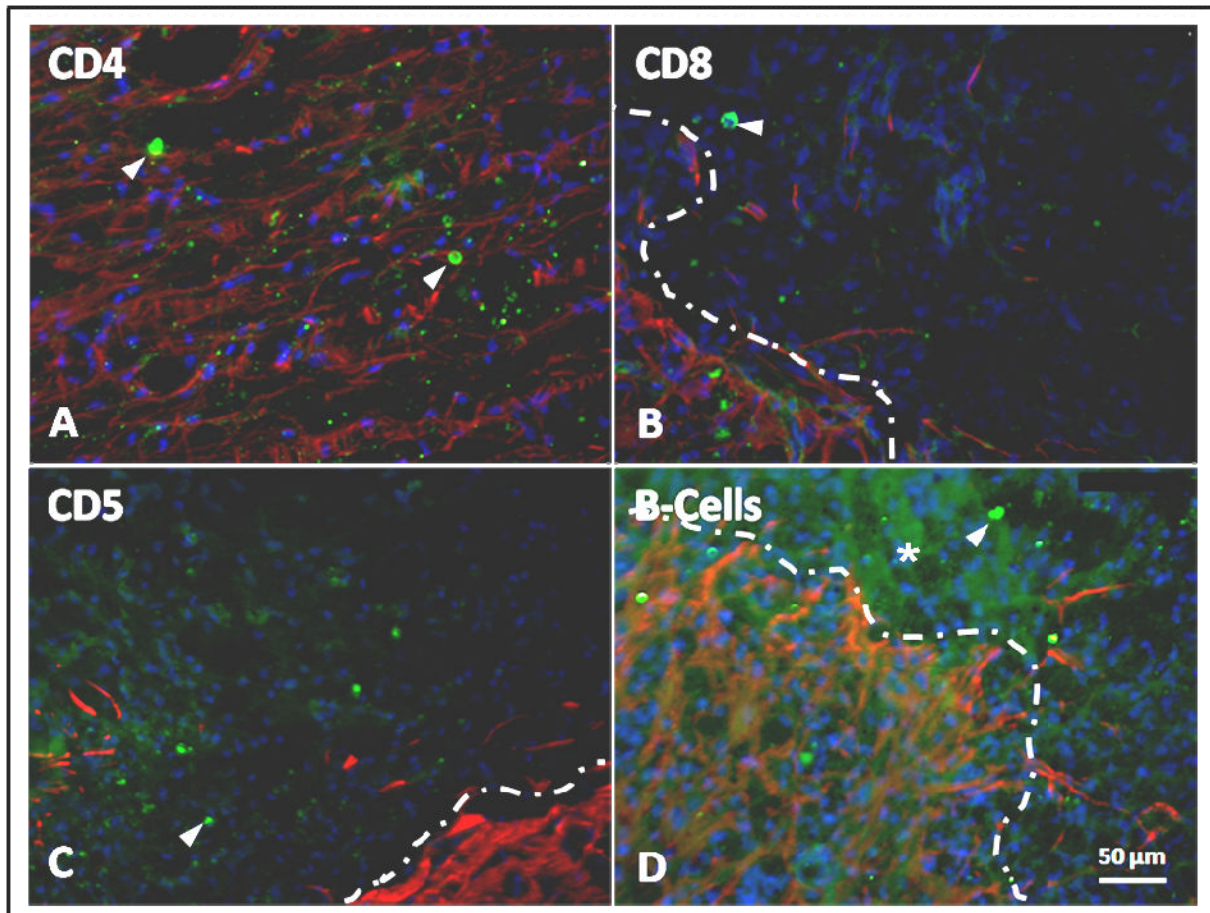


Fig. 3.25: T- and B-cell occurrence at 5 wpr in the lesion area in 10 μm -thick sagittal sections of animals with scar resection and subsequent filling of the cavity with either ALG or PEG. The respective cells are visualized by green staining (red: GFAP, blue: DAPI). Representative images of respective IR in the lesion area (dashed lines); arrowheads: IR-positive T- or B-cells, respectively.

3.5.5 Association of Regenerated Axons with Growth-Supporting Schwann Cells

To investigate whether the S100 β -positive cells, which were frequently found in the lesion area of PEG-treated animals, and to a much lower extent in animals of the ALG-group (see Fig. 3.22), were associated with PAM-positive axon fragments, immunofluorescent double labeling with antibodies against PAM and S100 β was performed.

In the lesion area of ALG-treated animals both, in-growth of PAM-positive axons as well as invasion of S100 β -positive cells, presented rather rare events. There was no indication found for the association of the two cell types in the analyzed sections of the respective animals (Fig. 3.22E).

In PEG-treated animals, on the other hand, PAM-positive axonal structures (red) frequently appeared to be closely associated with areas containing S100 β -positive cells (green) (Fig. 3.22F), indicating interaction of axons with Schwann cells. To further analyze such interaction in more detail, confocal analysis of the respective structures in the PEG-treated chronic SCI resection area was performed. Confocal microscopy further confirmed the previously mentioned observations of close associations and direct interactions of the two cell types (Fig. 3.26A-C). Although the occurrence of GFAP-stained structures was frequently detected in the lesion area of PEG-treated animals, triple staining with antibodies against PAM, S100 β and GFAP revealed S100 β -positive cells associated with PAM-positive axons being Schwann cells, rather than astrocytes (confocal images in Fig. 3.26C,D): Cells with S100 β -staining (green) only, rather than those with GFAP staining (red) only, were found in close association with PAM-positive axon fragments (Fig. 3.26C). Furthermore, myelin-staining with an antibody against myelin basic protein (MBP) showed that some of the axon fragments found inside the PEG-matrix after chronic SCI scar removal were closely associated with myelinating Schwann cells at the analyzed time point of 1 wpr (confocal images in Fig. 3.26E-G).

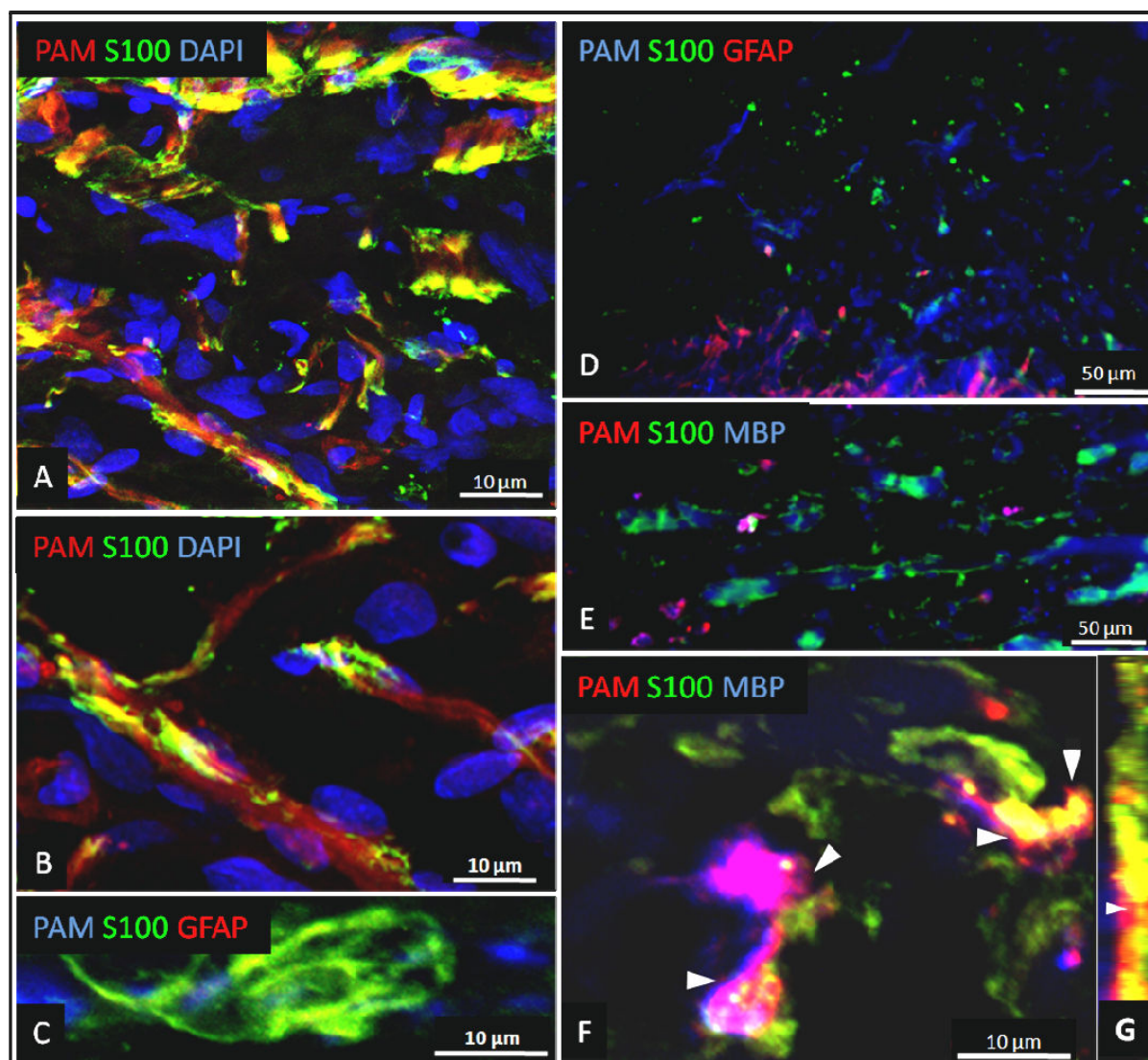


Fig. 3.26: Association of S100 β -positive cells with PAM-positive axons in PEG matrix. In the PEG-matrix in 10 μm -thick sagittal sections PAM-positive axon fragments (red; blue in C,D) revealed frequent close association with S100 β -positive cells (green), some of which were found to be myelinating Schwann cells (blue in E,F). A,B: Yellow appearing structures in images A,B reveal direct association of Schwann cells with axons. C: Lack of GFAP (red) in S100 β -positive cells (green) which are associated with axon fragments (blue) indicates that these cells are SC rather than astrocytes. D: Many cells in the lesion center of PEG-treated animals expressed S100 β (green), but only few were found to express GFAP (red), or both markers, respectively. E: The majority of S100 β -positive cells (green) were found to be myelinating SC (blue MBP staining). F: higher magnification of PAM-positive axon fragments (red) in direct association with myelinating (blue) SC (green); respective axon structures appear pink (PAM+MBP) or yellow. A-C,F: confocal images, G: confocal Z-stack; arrowheads in F,G: Close association of myelinating SC with axon fragments.

3.5.6 Regeneration of Axons from Different Neuronal Populations into PEG Matrix

In the study presented here, it was investigated whether the tested PEG matrix would allow the spontaneous regeneration of previously analyzed axon populations (corticospinal tract (CST) labeled with BDA; dopaminergic axons identified with an

antibody against tyrosine hydroxylase (TH); serotonergic axons identified with an antibody against 5-hydroxytryptamine (5-HT); and ascending sensory axons identified with an antibody against calcitonin gene-related peptide (CGRP) into the lesion area of chronic SCI animals. Immunohistological staining revealed that axons from all analyzed populations were able to grow through the GFAP-positive glial scar and readily entered the PEG matrix (Fig. 3.27A-D).

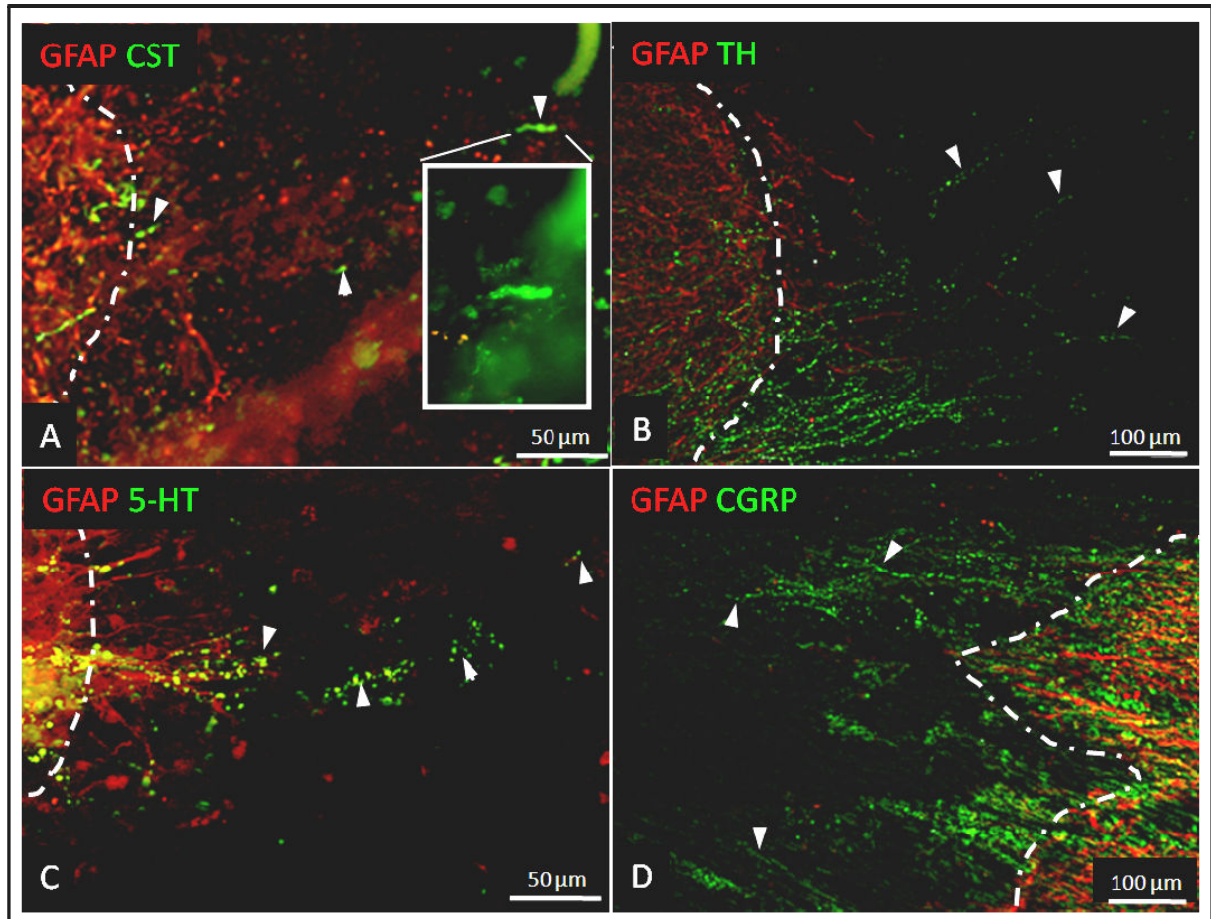


Fig. 3.27: Characterization of regenerated axon populations in 50 µm-thick sagittal sections of the lesion area of PEG-treated animals at 5 wpr. Axons from all analyzed populations were able to regenerate into a chronic SCI scar removal site filled with PEG 600. Examined axonal populations in the PEG-matrix area in sagittal sections were the corticospinal tract (CST; A), dopaminergic axons identified via tyrosine hydroxylase-IR (TH; B), serotonergic axons identified via 5-hydroxytryptamine-IR (5-HT, C) and sensory axons expressing Calcitonin Gene-Related Peptide (CGRP, D). Arrows: positively stained axonal structures (green) in the matrix area. Note also GFAP-positive (red) structures invading the lesion site.

3.6 Behavioral Analysis

3.6.1 Basso, Beattie & Bresnahan Open Field Locomotor Analysis

The locomotor behavior of all animals was assessed using open field observation and rating of the general locomotion according to Basso *et al.* (Basso *et al.*, 1995). While the majority of animals exhibited hindlimb locomotion at a BBB score of 11 at 5 wpl, some animals revealed more functional deficits, resulting in maximum BBB scores of 8 at the time of resection. To allow better comparison, only animals with a BBB score of 11 at the time of chronic scar resection were taken into account for the comparative evaluation (Fig. 3.28A). Due to low animal numbers in the treatment groups (significant behavioral analyses require higher animal numbers), determination of significant differences was not attempted.

The average score achieved by animals of all analyzed matrix groups at 5 wpr and the control group at 10 wpl (“lesion only” controls), respectively was rated to be 11 (Fig. 3.28B). At this time point, “resection only” controls revealed an average BBB score of 9 (Fig. 3.28B). The resection procedure resulted in a slight decrease in the first 2-3 weeks after operation, but animals with matrix implants were able to recover soon from the insult to reach similar BBB-values as the ones seen in “lesion only” controls.

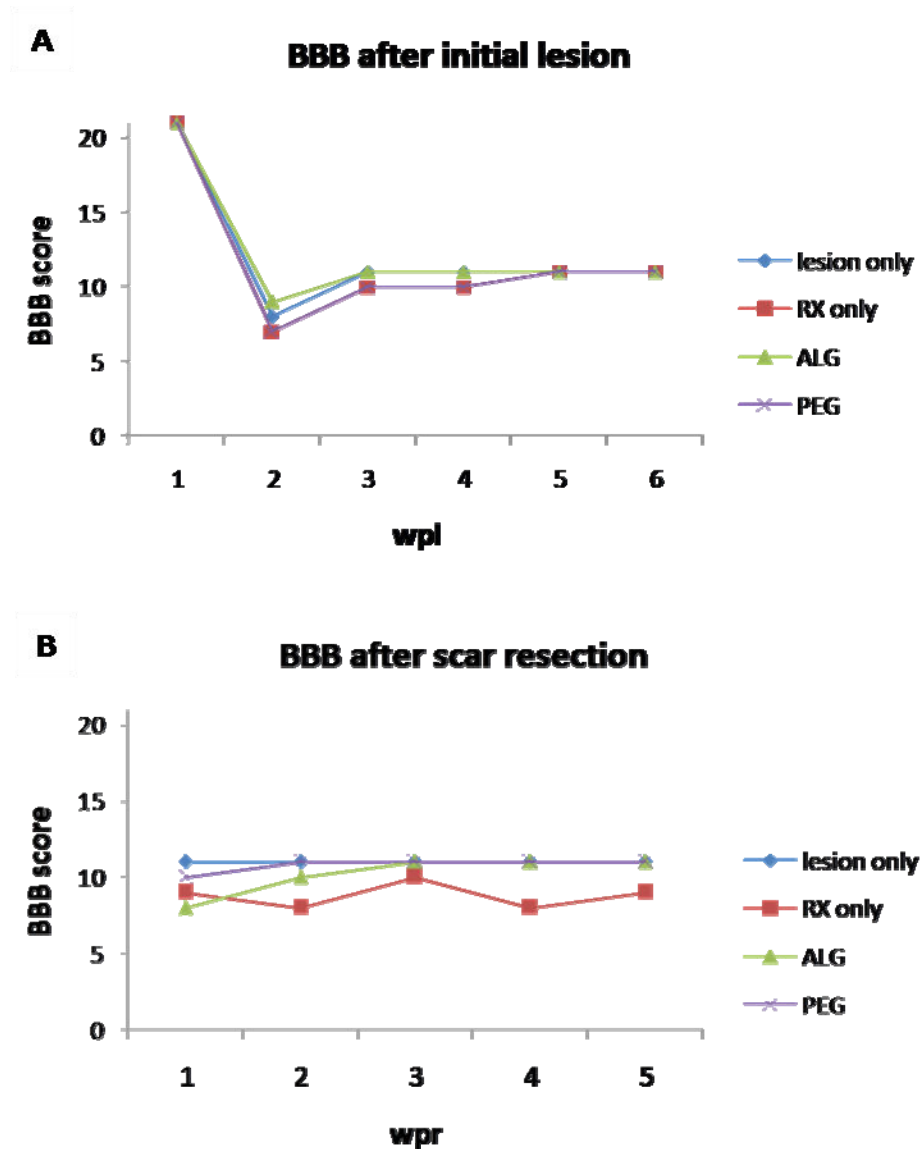


Fig. 3.28: BBB scores after initial SCI (A) and after chronic SCI scar resection (B). Data legend in A refers to treatment after chronic scar resection, as animals received no treatment after initial SCI; lesion only: n = 6; RX only: n = 9; ALG: n = 5; PEG: n = 7.

4 Discussion

4.1 Defining the Time Point for Chronic SCI

While for human patients a chronic spinal cord lesion could be clinically defined by the end of hospitalization (Ditunno and Formal, 1994), such a determination is difficult to make for spinal cord injured rats. Pathological changes still occur in the late phases of SCI in both humans and rodents. Even though most of the degenerative processes are stabilized in the chronic stage of SCI, there is evidence that suggest degeneration even long after the injury (Ellingson et al., 2008). In the literature dealing with chronic spinal cord injury, the experimental “chronic” time point is defined at periods ranging from two weeks post initial injury (von Meyenburg et al., 1998), over five weeks post initial injury (Houle and Ziegler, 1994;Jin et al., 2002) to several months post initial injury (Grill et al., 1997;Kwon et al., 2002b) and even as long as twelve (Kwon et al., 2002b) or 15 (Kadoya et al., 2009) months after initial injury.

For the present study regarding chronic SCI, a delay of five weeks between initial injury and scar removal was chosen. After this time both, the fibrotic and the astrocytic scar are fully developed at the injury site, new production of most CSPG forms has subsided (Tang et al., 2003), and spontaneous behavioral recovery has reached its plateau (Ung et al., 2007).

4.2 Removal of the Spinal Cord Injury Lesion Scar as a Suitable Lesion Model

Aspiration of the chronic lesion scar proved to be a suitable method for scar removal. Harmed tissue could be identified by its appearance (Imaizumi et al., 2000;Rasouli et al., 2009) which differs from that of unharmed spinal cord tissue. Furthermore, chronically scarred spinal cord tissue is denser than intact spinal cord tissue and can therefore easily be distinguished. Due to the scar tissue’s density, iridectomy scissors were used to cut the scar tissue from the intact spinal cord when necessary. For the aspiration procedure a longitudinal extent of 4 mm was chosen. Thus, it was certain that the whole length extension of scar tissue, which was determined in prior pilot experiments, was removed. It was further intended to also remove small fractions of intact spinal cord directly adjacent to the lesion scar in

order to re-injure previously injured axons – which may have retracted by the time of the resection (Busch et al., 2009; Davies et al., 1999; Ramer et al., 2005; Schwartz et al., 2005a) - to mimic an acute injury situation. Such imitation of acute SCI was desired because after SCI, a genetic regeneration program is switched on (Kruse et al., 2008). Stimulation of genetic reprogramming may therefore also be useful after chronic SCI.

The main focus of the present study was laid on finding a suitable matrix material which could be used to fill the cavity after scar removal. A suitable matrix should not impede but rather promote both, general tissue regeneration and axonal regeneration. Such a matrix could in future studies be further combined with other therapeutics, e.g., an iron chelator for transient inhibition of fibrous scar formation, which has led to axonal regeneration and functional recovery after acute SCI in previous studies (Klapka et al., 2005), or SDF-1 α , which, after local application via osmotic minipump, increased axonal sprouting after acute SCI (Opatz et al., 2009).

While MG and ALG, applied either alone or in combinatory treatments, have been tested as bridging materials in the acutely injured spinal cord, PEG has so far proven to effectively ameliorate the outcome of acute SCI when applied at early stages after insult, but has never been considered as a bridging material in acute or chronic SCI. This is probably due to the fact that the membrane-sealing, as well as the neuroprotective mechanisms attributed to its effectiveness in acute SCI require the acute injury situation to result in beneficial outcome. In contrast to regenerative therapies, which can improve functional recovery in both, acute and chronic SCI, neuroprotective therapies will mainly help in acute SCI. However, neurons whose axons are re-injured by the procedure of chronic SCI scar removal could also benefit from neuroprotective effects elicited by PEG. On the other hand, simply the nature of the polymer as well as deleterious side effects of a prolonged exposure to PEG which have been reported (Cole and Shi, 2005), may have led to the reluctance to use PEG as a bridging material.

4.3 Evaluation of Axonal Regeneration after Chronic SCI Scar Resection

Two methods of axon labeling were applied for quantitative analyses. The first was the general immunohistochemical axon staining with an antibody against PAM.

PAM is expressed by many (but not all) descending and ascending axons. Therefore, the quantification of PAM-IR signal can be considered a general axon labeling.

The anterograde BDA-labeling after tracer injection into the spinal cord cranially to the lesion also presents a general axon labeling compared to the normally applied labeling of specific axonal tracts. The labeling in the lesion area is, however, restricted to descending axons. Such axons may either arise from projecting neurons of descending tract systems involved in motor function, or they can be interneuron axons.

4.3.1 Axon quantification requires detailed analyses

Axon quantification was aspired to reveal observed differences in axonal regeneration into the chronic lesion area. However, detailed quantitative general analysis is difficult. Many studies therefore describe axon quantification by means of determining the number of axons crossing a certain line in the area of interest (Schiwy et al., 2009). This method is applicable if the determination of axon in- or out-growth is desired. However, for quantification of a total axon number in an area of interest, it cannot be used. If lower axon numbers are expected in the respective area, counting of axonal profiles is possible in the case of individual axon populations, arising from, e.g., CST or RST, which can be labeled by a tracer substance. For the quantitative determination of higher numbers of axon profiles, signal density measurements, as applied in the course of the described study for the general axonal marker PAM, are therefore more suitable. Nevertheless, this kind of analysis remains difficult. Different problems were encountered in the course of the analysis: Simple analysis via setting of a pixel threshold (also see chapter 2.6.2.1, and Fig. 3.9, Fig. 3.10) presents a fast and easy quantification method. However, this method proved to be not suitable for the quantification of immunohistochemically stained fiber-like axon profiles in the here presented study. This is mainly due to the presence of unspecific background staining of non-axonal structures (see Fig. 2.12, Fig. 3.10, Fig. 3.12). While such unspecific binding of antibody was exhibited only to a small extent in the lesion area of PEG-treated animals, it was a dominant feature of the ALG-containing resection site. This is explicable due to various contributing factors:

- Unlike PEG, which was for the most part well integrated into the surrounding spinal cord tissue, ALG hydrogel may exhibit varying thickness in the 50 μm -thick cryo sections, as it might be squeezed during cutting procedure.
- In contrast to PEG, ALG itself was noticed to exhibit unspecific binding of antibody, resulting in relatively high degrees of unwanted (often fiber-like) background staining (also see vWF-staining of ALG in Fig. 3.17). Such staining could be identified via careful manual analysis. However, with an automated or semi-automated method of quantification, such discrimination is hardly possible.
- Since ALG-containing sections were observed to be prone to impurities during tissue preparation and storage, it is possible, that biofilm formation also occurred post-operatively on the ALG implant *in vivo*, resulting in the presence of organisms or metabolites which then revealed false-positive IR.
- The thickness (50 μm) of the analyzed sections may further have led to the described observations. If such unwanted structures or signals, respectively, are present in the ALG, the respective staining signal intensity would have been multiplied in thick sections. However, the reason for choosing the respective thickness of the sections has already been mentioned.
- Furthermore, the quantification of IR to PAM, which is a rather general axon marker which recognizes all axons containing phosphorylated neurofilament, was performed in images which were taken at 10x-magnification. Therefore, the analysis can be exacerbated by high amounts of PAM-positive axon profiles in the analyzed area. However, since the same magnification was used for ALG- and PEG-treated spinal cord sections, this presents a negligible factor.

With the eventual quantification method - Image J plug-in Feature J after background signal elimination - it was, however, possible to screen the analyzed sections for regenerated axons in the resection area, while achieving results which further reflected previous impressions (Fig. 2.13; Fig. 3.12). At the same time, the method further confirmed the results which were already indicated by quantitative methods which were either found to be unsuited for analysis, such as a simple Image J threshold analysis (Fig. 3.9), or which were only done with small amounts of sections due to extremely time-consuming tasks, such as the Image J plug-in Neuron J (Chapter 2.6.2.2, and Fig. 3.11).

Just like in the case of the aforementioned method of PAM-IR quantification, the reason for choosing the described method of BDA injection into the spinal cord (see chapter 2.6.2.4) was to label as many neurons whose axons extended into the lesion/matrix area as possible. The use of BDA for axon tracing can achieve a greater amount of axonal labeling than some other tracers because not only regional neurons and their axons can be labeled but also passing axons within the injection area (Bamber et al., 2001; Hsu and Xu, 2005; Zahm et al., 1996). The applied BDA with a molecular weight of 10,000 kDa is preferably, although not exclusively, transported in an anterograde direction (Reiner et al., 2000). In the present study, the BDA injection site was easily recognizable due to strong labeling, visualized with Oregon Green®. A similar tracer distribution and labeling of necrotic tissue was seen by Lu *et al.* after the injection of the tracer fluororuby, a tracer with the same molecular weight as the BDA used in the present study, into the spinal cord (Lu et al., 2001). Davies *et al.* have also demonstrated the use of the described method for the anterograde BDA-labeling of axons as was applied in the course of the present investigations (Davies et al., 2006). However, the authors do not describe the extensive labeling of non-axonal structures by the BDA, possibly because of a markedly smaller lesion extent (lateral dorsal column white matter transection), an increased distance between BDA-injection site and lesion site (5 mm), and finally, because thinner sections (25 µm) were used for the respective analysis. As described earlier, in the present study, sections with a thickness of 50 µm were used because pilot experiments in which sections of varying thickness were prepared had shown that ALG-fractions were best-preserved in 50 µm-cryo sections. The observations of increased labeling may further result from a relatively high number of tracer injections into the spinal cord. Small injuries caused by the injections most likely lead to necrotic events at the sites of injection. The necrotic tissue at the site of pressure injection also exhibited extensive labeling as it has been described in the study of Lu *et al.* (Lu et al., 2001). Since the BDA-injection sites were in relatively close proximity to the lesion area, diffusion of the tracer substance into the surrounding spinal cord presents a conceivable possibility. This hypothesis is further supported by the observation of increased cellular (most likely macrophage) BDA-localization at the injection site also in the spinal cord cranially to the tracer injection site. This type of error would be equally distributed in the different groups, but while in the matrix groups every axonal fragment found in the lesion site must be

considered to be originated from regenerated axons (due to prior tissue removal), in control animals which received only the transection lesion but no removal of the harmed tissue, BDA-positive axons could either have regenerated into the lesion area or these axons may have been merely stretched and not cut by the applied method (Steward et al., 2003). Because of the generally low axon fragment numbers (average 1.7 fragments per scar in “lesion only” control animals, Fig. 3.15B,C,K), the possibility of tracer-diffusion was considered a negligible factor in the axon quantification. Uptake of the tracer and cellular debris by macrophages attracted by the small needle stab injuries caused by the injection procedure may likely have contributed to the observed increase in background signal and therefore made automatic quantification not feasible. It had no influence, however, on the final quantification results. The presence of macrophages in the analyzed sections is presumably caused by the tracer injections. This can be concluded since spinal cord sections from animals, which received a scar resection operation and subsequent filling of the resulting cavity with a matrix, did not reveal increased presence of ED1-positive macrophages and microglia in the lesion area at 1 wpr (Fig. 23.C,D). Due to the frequently observed high unspecific background staining of the BDA, very strict criteria were applied (Steward et al., 2003) to distinguish fragments of regenerated axons to avoid accidental counting of structures such as macrophages, which might be mistaken for short axonal fragments due to internalization of such. BDA-positive structures were only counted as axons if they were found to reveal the morphology of regenerating axons.

Because the analysis was performed using a 10x-objective of a microscope, not all axons which would fall into the category of regenerated axons may have been counted. This magnification, however, was chosen to ensure comparability of the analyzation methods. Comparison of the matrices was drawn on the basis of the two regeneration analyses (PAM and BDA). Quantification of PAM-signal was also achieved using a 10x-objective. In future studies, a more detailed analysis of the regenerated axons in a PEG-based matrix should be considered. The here applied quantification methods provided a good opportunity of screening the implanted matrix materials for their regeneration-promoting features.

Eventually, the two different methods of axon quantification achieved similar results (Fig. 3.12; Fig. 3.15), which reflected the observations made in the course of the study (also see Fig. 3.8B,b; Fig. 3.8.C,c).

4.3.2 Matrigel™ alone is not sufficient to promote spontaneous axonal regeneration when used as a bridging material in chronic SCI

While MG has been found to stimulate axonal elongation and reduce axonal dieback when it is used as a cell carrier substance (Bunge, 2001), after implantation into the chronically injured spinal cord, MG alone did not yield any positive outcome regarding axonal regeneration into an MG bridge in the here presented study. The conducted immunohistochemical analysis revealed no indication of spontaneous regeneration into MG matrix after chronic SCI scar resection at an early time point (shown in Fig. 3.8A,a). These results are in accordance with observations previously made by other research groups (Bunge, 2001;Facchiano et al., 2002). Although MG alone is sometimes described as a regeneration-promoting matrix after nervous system injury (Novikova et al., 2006), occurrence of extensive regeneration into MG has mainly been described for DRG neurons. Such lack of regeneration might in part result from the inhibitory effects of Col4 (a component of MG) on axonal growth (Hermanns et al., 2001b). Furthermore, because of variations in the composition of the gel, MG effects clearly depend on the respectively used batch, in particular, as previously observed by other research groups (Dunn et al., 1991;Serban and Prestwich, 2008;Slobodian et al., 2007). Further controversy about MG is raised by differences in the mixture of its general components such as the growth factor content, which has partially been regarded as a potential contaminant due to varying levels from one manufacturing MG batch to another (Akhyari et al., 2008).

Due to the observed lack of axonal regeneration into a matrix composed of MG after chronic SCI scar removal, MG was not considered as a suitable substance for the desired application and was therefore not included in further analyses.

4.3.3 Alginate hydrogel promotes little spontaneous axonal regeneration and reveals poor integration into host tissue when applied as a matrix into the chronically injured spinal cord

In comparison to MG, ALG led to increased spontaneous axonal regeneration into the area of chronic SCI scar removal at early time points (Fig. 3.8B,b). Yet,

compared with PEG (Fig. 3.8C,c), ALG-matrix only poorly supported the regeneration of axons into the lesion area. Furthermore, the positive effect regarding axon regeneration into ALG at early time points (Fig. 3.8B,b) appeared to be lost at later time points after chronic SCI scar resection (Fig. 3.12B,D, Fig. 3.15B,C,K). Insufficient spontaneous axon regeneration ALG application in chronic SCI was considered to be the result of poor matrix integration and of unfavorable changes in ECM composition at the resection site which will be discussed in more detail later.

The present data suggest that ALG's failure in significantly promoting axonal regeneration partly results from its poor integration into the host tissue (Fig. 3.7, left row). It should be noted that ALG poses similar problems regarding its clinical use as have already been described for MG: As is the case for most biomaterials, ALG, being a naturally occurring polymer, can also induce negative outcomes due to problems in purity, biocompatibility, and batch-to-batch-reproducibility (Orive et al., 2005). ALG was possibly degraded too quickly to allow substantial tissue regeneration (as indicated by the frequently made observation of holes in ALG matrix), and the gel itself did not present sufficient regenerative properties. The development of cystic cavities after acute spinal cord segment excision and filling of the gap with ALG has also been described by Suzuki *et al.* (Suzuki et al., 2002). It was not attributed to tissue preparation procedures but rather to either spontaneous cavity formation after ALG application or to degradation of ALG.

Regarding axonal regeneration into untreated ALG hydrogel, Novikova *et al.* came to similar conclusion as the ones described for the here presented study: After *in vitro* analysis of growth-promoting effects and biocompatibility of ALG hydrogel and its combination with various cell types (Novikova et al., 2006). However, application of ALG gels in the course of *in vitro*-analyses of neurite outgrowth and elongation (Dhoot et al., 2004;Novikova et al., 2006), as well as in investigations of experimental SCI models *in vivo* (Kataoka et al., 2004;Novikov et al., 2002;Prang et al., 2006;Tobias et al., 2005) has previously been demonstrated to achieve good results regarding axonal regeneration into the matrix area. These results may however in part be attributed to other important factors, such as young age of the animals (Kataoka et al., 2004) (changes in maturing neurons are a limiting factor for their regeneration (Blackmore and Letourneau, 2006)) or lyophilization of the gel prior to its implantation.

In comparison to ALG alone, the addition of BPY-DCA to ALG promoted a slight increase in axonal regeneration into the matrix at the analyzed time point of 5 wpr (Fig. 3.15D,K). Animals of the respective group received a filling of the resection cavity with ALG into which the iron chelator (BPY-DCA) was mixed. In several studies from other research groups, ALG was either used as a carrier substance for the delivery of cells, or it was further treated by addition of various factors resulting in a more stable material, or the ALG hydrogel was freeze-dried prior to its application. The effects which lyophilization could have on a combination of the hydrogel material with an aqueous therapeutic solution are not known. In the here presented study, for its application after chronic SCI scar resection, ALG hydrogel was not freeze-dried after its preparation. The fact that beneficial effects of ALG were not obtained in the present chronic SCI studies may result from the use of ALG in its hydrogel form, rather than freeze-dried ALG. However, the use of an injectable matrix was intended, and the process of freeze-drying would not allow injection of the material. More importantly, the matrix materials were tested with regard to their axon growth promoting capacities as a basis for future studies, in which matrices with growth-promoting features can be used in combination with other substances, e.g., iron chelators or growth promoting factors. Freeze-drying might result in the loss of the chelator's effect on fibrous scar formation. Therefore, other ways of inserting the desired therapeutics into an ALG matrix would be required. For this reason, the lyophilization process was dispensed with. However, freeze-drying might change material properties substantially in such a way that axonal in-growth may be increased. The promotion of axonal regenerative capability by ALG did in the here-presented study however by far never come close to that which could be achieved in PEG-treated animals.

The results which were obtained in the here presented study regarding axonal regeneration were not satisfying. Therefore ALG was considered a less attractive material for the intended use as an implant after chronic SCI scar removal.

4.3.4 Significantly increased axon regeneration into the stable matrix which forms in the PEG-treated resection area

Application of PEG 600 into the chronic SCI scar removal cavity was found to lead to the formation of a stable tissue bridge, and extensively promote spontaneous axonal regeneration. The formation of a stable tissue bridge in PEG-treated animals indicates a beneficial effect of PEG-treatment on connective tissue infiltration. Only few fibroblasts were detected to be present in the PEG-treated lesion area (Fig. 3.20D-F). However, the number of fibroblasts (high numbers of fibroblasts were found to be present in the dorsal region of the lesion area also in PEG-treated animals) appears to be sufficient for the formation of connective tissue in the resection area, while at the same time deleterious extracellular Col4-accumulation in the lesion center was decreased.

Mixture of the viscous PEG-fluid with body fluids, e.g., cerebrospinal fluid or plasma, at the site of scar removal might be accountable for the formation of a physically stable, growth-promoting matrix at the site of PEG application, or might at least have provided the necessary favorable environment. This hypothesis is supported by the fact that despite PEG itself being known as a material to which cells or proteins do not generally attach (Gunn et al., 2005;Hern and Hubbell, 1998), the present results are evidence of beneficial cell growth and regeneration into a PEG-treated lesion area, as will later be discussed in further detail.

Comparison of the two matrix materials ALG and PEG was drawn on the basis of two regeneration analyses (PAM and BDA). Quantitative analysis of PAM-IR in the lesion area reflected the positive outcome after insertion of a PEG-matrix into a chronic SCI cavity regarding spontaneous axonal regeneration which was initially indicated by increased PAM-IR at 1 wpr (Fig. 3.8C,c) and could be further confirmed at 5 wpr (Fig. 3.12C,D). The results of the quantification of BDA-labeled axons after tracer injection into the spinal cord further confirmed the positive outcome after insertion of PEG into a chronic SCI cavity regarding spontaneous axonal regeneration (Fig. 3.12).

The generally good outcome after PEG- compared to ALG- or no treatment, respectively, regarding axon regeneration may further be explained by PEG's ability to produce a rapid repair of membrane breaches in severely damaged and dying cells and tissues via molecular sealing (Borgens, 2001), resulting in decreased

apoptosis and necrosis (Luo and Shi, 2007). The ability of PEG to reconnect axons has previously been well described (Baptiste et al., 2009; Borgens and Shi, 2000; Duerstock and Borgens, 2002; Luo et al., 2002; Nehrt et al., 2010). Due to such observations, PEG has been described to be effective only in acute SCI. Furthermore, reduction of oxidative stress, which presents one of the central mechanisms of secondary injury in spinal cord trauma, at the site of injury and adjacent to it, can also be achieved by PEG treatment in acute SCI (Luo and Shi, 2004). In an *in vitro* investigation of neuroprotection mediated by PEG, Liu-Snyder *et al.* demonstrated that PEG's ability to reduce secondary injury and oxidative stress of membranes requires its entry into the cytosol, thereby suggesting physical interaction with membrane organelles as the initial event leading to neuroprotection and repair (Liu-Snyder et al., 2007). These findings are supported by a recent study which demonstrated the ability of PEG 1500 and PEG 2000 to protect injured neuronal mitochondria (Chen et al., 2009).

The assumption that connecting injured axons is the only positive effect elicited by PEG in experimental SCI would require the distal segments of the axons to be still there. In chronic SCI, however, the distal axonal part has undergone Wallerian degeneration (Hagg and Oudega, 2006), therefore resealing of the two axon stumps must be excluded as a possible mechanism of action leading to the observed axonal regeneration in PEG-treated animals. However, mimicking the situation after acute SCI via chronic SCI scar resection – which comprises the re-injury of already injured axons – allows PEG to elicit its beneficial effects resulting in increased axon regeneration.

4.4 Characterization of Acute and Chronic Lesion Area

As has already been suggested, it is rather supposable that the insertion of a matrix material into the spinal cord results in a change of the surrounding tissue, and in the modification of occurring events at the site of application, e.g., tissue regeneration or scar formation. On-going events, e.g., invasion of host cells or in-bleeding, will presumably alter a matrix material's properties and vice versa.

4.4.1 Increased amounts of collagen type IV in ALG matrix

Col4 is one of the main components of BM structures, such as the SCI lesion scar. Our group in the Molecular Neurobiology Laboratory of the University of Düsseldorf has previously developed a treatment to transiently inhibit the collagenous scar formation. The inhibition further resulted in axonal regeneration of CST-axons across the lesion scar into the distal intact spinal cord, and neuroprotection of projecting pyramidal neurons, accompanied by functional recovery in different motor tasks (Klapka et al., 2005). Thus, differences in the composition of the collagenous fibrous scar might be an indication of improved or declined axonal in-growth into a respective matrix.

While IR to Col4 was reduced after PEG-insertion into the resection cavity (Fig. 3.16D, also see chapter 4.4.1), it was prominent in the lesion area of control animals (Fig. 3.16A,B) and in the spinal cord/matrix interface region in animals of the ALG-group (Fig. 3.16C). The majority of BDA-positive axon fragments were counted in the lesion area of animals of the ALG+BPY-DCA group in corresponding regions. This observation argues for the transient inhibition of basal membrane formation in the respective areas after chelator addition. Inhibitory molecules are associated with the fibrous scar (Davies et al., 2004;De Winter et al., 2002;Jones et al., 2003;Niclou et al., 2006). Transient inhibition of scar formation leads to a delay in the accumulation of such growth inhibitors, permitting regenerating axons to grow further into and eventually beyond the lesion scar (Klapka et al., 2005;Schiwy et al., 2009) resulting in the observed increased axon regeneration into PEG-matrix. However, despite the noted increase in axonal regeneration after BPY-DCA addition to ALG, the highly significant increase in spontaneous axonal regeneration resulting from PEG-application (Fig. 3.12;Fig. 3.15) was not achieved, indicating that addition of BPY-DCA alone to ALG does not suffice to achieve mentionable promotion of spontaneous axonal regeneration. The lack of beneficial events, which will be discussed in more detail later, at the site of ALG-matrix insertion is attributed to the observed regenerative failure.

It should be noted, however, that for reasons of comparability, the chelator was solved in water. Although a positive trend regarding axonal regeneration in animals treated with ALG+BPY-DCA was observed, the solution of BPY-DCA in water may have influenced the outcome of the respective experiment. Other studies

from our group in the Molecular Neurobiology Laboratory have reported the solution in TRIS buffer. The buffer should ensure pH-stability of the chelator and thus prevent its possible degradation *in vivo*. However, since TRIS buffer is known to change the release behavior of sodium ALG (Yao et al., 2009), it was therefore not included in the present study for reasons of comparability. The pH of the chelator-containing solution was measured prior to application to ensure physiological conditions. However, it is not known, how the conditions *in vivo* affected the pH of the gel.

Furthermore, it is possible that addition of BPY-DCA to the ALG solution somehow changed the gel's properties. BPY-DCA is a chelating substance with high affinity for divalent iron ions. A chelating agent generally does not exclusively show affinity for a certain type of ions, but is able to chelate other ions to varying degrees (Shumaker et al., 1998). If chelation of Ca^{2+} ions by BPY-DCA occurred, the strength and stability of the gel may have been influenced. Material properties thus may have been altered in such a way that the resulting gel presented a more favorable substrate for axonal growth.

4.4.2 Decreased extracellular matrix deposition in PEG matrix

While IR to Col4 was detected to be reduced after PEG-insertion into the resection cavity (Fig. 3.16D), it was prominent in the lesion area of control animals (Fig. 3.16A,B) and in the spinal cord/matrix interface region in animals of the ALG-group (Fig. 3.16C).

Col4 staining revealed a decrease of extracellular Col4 in the matrix area of PEG-treated animals, but at the same time more defined Col4-positive structures were apparent in comparison to the remaining analyzed groups (Fig. 3.16). PEG has previously been explored to block protein adsorption, cell adhesion, and clearance of macromolecular drugs from circulation (Elbert and Hubbell, 1998). A tissue bridge formed at the site of PEG application, however, may be able to bind to cells and tissues, and may be able to alter cellular and protein interactions. The generally non-adhesive nature of PEG (Cong et al., 2009) possibly decreased the attachment of extracellular Col4, while at the same time it promoted the growth of beneficial Col4-containing structures, such as BV. The effect of the matrix materials on other ECM components, e.g., collagen type I, fibronectin or laminin, was not investigated in this study, but might further contribute to the formation of a stable growth-promoting tissue bridge.

4.4.3 Regenerating axons are attracted to grow into well-revascularized PEG-treated chronic SCI scar resection site

Although occurrence of vWF-positive BV in peri-lesion areas of ALG-treated animals (Fig. 3.17C,G,H) was noted in some (although few) cases, only few small BV had entered the ALG-area at the analyzed time point of 1 wpr (Fig. 3.17C,G,H). This observation may either contribute to, or result from the poor integration of ALG into the surrounding spinal cord tissue.

The appearance of many large and small BV inside of as well as surrounding the PEG matrix (Fig. 3.17D,I,J), however, suggests a good integration of the material into the host tissue, which was assumed also due to the formation of a physically stable tissue bridge after implantation into the injured spinal cord.

Direct experimental trauma induces a decrease in gray and white matter blood flow at the site of injury, and the severity of blood flow reduction correlates with the functional deficits (The Spinal Cord, 2009). The role of angiogenesis after SCI is, however, not clear: While there are studies suggesting a beneficial neuroprotective effect of angiogenesis inhibition (Blight, 1991;Wamil et al., 1998), others report the contribution of angiogenesis in the promotion of neural regeneration (Bakshi et al., 2004;Han et al., 2010;Rauch et al., 2009). Angiogenesis precedes recovery from SCI, where its extent positively correlates with neural regeneration (Glaser et al., 2006;Kaneko et al., 2006). Spinal cord vessels can provide tremendous trophic support (Raab and Plate, 2007;Rauch et al., 2009), they are important in the mediation of tissue survival (Peters et al., 2002), and they present support for regenerating axons growing along them (Bearden and Segal, 2005). The disruption of blood vessels as a consequence of primary injury further influences secondary injury events, e.g., disruption of the blood-spinal cord barrier and induction of inflammatory response mechanisms (Mauter et al., 2000).

Several studies have demonstrated that following injury of blood vessels in the course of SCI, occurrence of revascularization events at the primary site of injury is evident at 1 wpl (Loy et al., 2002;Whetstone et al., 2003;Zhang and Guth, 1997). Such observations have been proposed to be indicative of significant initial attempts to repair the injured vasculature (Imperato-Kalmar et al., 1997;Zhang and Guth, 1997), and they are furthermore concordant with the ones made in the course of this study. While revascularization was frequently detected at the time point of 1 week

post injury in untreated control animals, at the later time point of 5 wpl, blood vessel occurrence in and around the lesion are was markedly decreased (Fig. 3.17A,B,E,F). Petter-Puchner *et al.* observed no vWF-positive endothelial cells inside the scar tissue, and only a few at the lesion site of lesion control animals in transection SCI animals at 28 days post injury, a time point and lesion paradigm resembling the of the presented study (Petter-Puchner *et al.*, 2007). Using the lesion model of compression SCI, Zhang *et al.* also report revascularization events detectable at 1 wpl, yet a dramatic decline in the number of blood vessels thereafter, as tissue necrosis developed. A decrease in the number of blood vessels at later 5 wpr is in the present study most likely attributed to necrotic events at the injury site: The harmed spinal cord tissue in the respective animals was frequently found to be very fragile and in some cases cyst development was noted to have occurred in the lesion center of chronic SCI animals. The cascade of progressive tissue necrosis observed after SCI may be ameliorated by angiogenesis. Such beneficial effects of procedures which induce revascularization or angiogenesis have previously been proposed by Zhang and Guth (Zhang and Guth, 1997). The observed beneficial effects regarding (re-)vascularization of the PEG-treated lesion area may therefore be indicative of not only increased promotion of angiogenesis at the site of chronic SCI scar resection, but they might further be a sign of a reduced loss of BV in surrounding spinal cord tissue due to a PEG-mediated decreased occurrence of secondary damage. A correlation between angiogenesis and white matter sparing was recently suggested by Han *et al.* (Han *et al.*, 2010). PEG-uptake by intact spinal cord tissue surrounding the lesion area is presumable due to the low viscosity of PEG 600 which resembles the viscosity of blood (37 °C). In the respective area PEG may mediate not only the sealing of neuronal membranes, but further the decreased occurrence of secondary injury mechanisms.

4.4.4 Cellular invasion of the lesion area

4.4.4.1 Astrocytes frequently invade PEG-, but not ALG matrix

Although GFAP-IR was found to be slightly diminished in the bordering spinal cord areas of ALG-treated animals (Fig. 3.18C) in comparison to control animals at 1 and 5 wpl (Fig. 3.18A,B), only few astrocytic processes or cells had entered the ALG-matrix at 1 wpr. Such supportive structures might be important for the integration of a

matrix into the host tissue and their lack in the ALG-matrix may further be accountable for the noted lack in regenerative events.

By contrast, frequent occurrence of BV and astrocytes detected in the matrix area of PEG-treated animals in the present study (Fig. 3.17D,I,J;Fig. 3.18D) was considered a sign of successful regenerative events, as association of regenerating BV with astrocytes at the site of injury has been frequently reported (Imperato-Kalmar *et al.*, 1997;Zhang and Guth, 1997).

All BV in the intact adult CNS are surrounded by a continuous sheath of astrocyte processes (Mahoney *et al.*, 2009). In the here presented study, GFAP-IR revealed increased elongation and invasion of astrocytes into the lesion area of PEG-treated animals compared to the other groups (Fig. 3.18A-D). In a recent study, Hejcl *et al.* described the application of a hydrogel alone or in combination with mesenchymal stem cells in a chronic SCI compression model at 5 wpl (Hejcl *et al.*, 2010). The behavioral recovery of the injured rats was analyzed over a period of six months and the spinal cord lesions were analyzed histologically. The authors, too, could demonstrate the occurrence of BV, astrocytes and axons myelinated with SC in the implants, supporting the observations described here.

Astrocyte invasion has been associated with beneficial effects on axonal regeneration. Astrocytes can provide the regenerating neurites with longitudinal orientation as has previously been proposed by Zhang *et al.* (Zhang and Guth, 1997). Davies *et al.* have previously shown that implantation of astrocytes derived from glial-restricted precursor cells into the injured spinal cord can promote axon regeneration and functional recovery (Davies *et al.*, 2006). In addition to serving as regeneration-promoting structures, reactive astrocytes which were found to have invaded the PEG-matrix (both, at early (Fig. 3.18) and at later (Fig. 3.19) time points after injury) could further release neurotrophic factors which boost axonal regeneration. The possibility of such desirable events has previously been reported in a recent study by Yara *et al.* regarding the application of collagen filament grafts after acute spinal cord transection (Yara *et al.*, 2009). The authors suggested a possible association of axonal regeneration and presence of astrocytes and proposed that reactive astrocytes invade into the collagen matrix from the amputation stump where they release neurotrophic factors such as BDNF and NT-3. Yara *et al.* detected astrocyte elongation into the scaffold with an invasion rate similar to that of the neurotrophic factors BDNF and NT-3.

This hypothesis possibly also holds for the observations made in the present study regarding the invasion of astrocytes into the lesion area and axonal regeneration: In the lesion area of ALG-treated animals both, axons and astrocytes were almost exclusively found in the margin areas of the matrix. (Fig.3.8B;Fig. 3.18C). The applied ALG may not have presented an attractive environment for the invasion of astrocytes, and thus these cells could not elicit their positive effects on possibly regenerating axons in the matrix. However, Kataoka *et al.* reported invasion of astrocytes as well as SC into freeze-dried ALG sponges after acute segmental resection SCI in young rats (Kataoka *et al.*, 2001;Kataoka *et al.*, 2004). The authors further observed myelination of regenerated axons in the implant area. In the present study, invasion of ALG matrix with these cell types was a rare event compared to PEG-matrix. As has already been stated above, the differing results are possibly attributable to the different properties of freeze-dried ALG and ALG hydrogel.

4.4.4.2 Increased Col4-immunoreactivity is accompanied by the presence of many fibroblasts in ALG matrix

In previous studies on acute SCI conducted by our group in the Molecular Neurobiology Laboratory, animals further received local injections of cAMP in addition to local chelator application. cAMP inhibits the proliferation and ECM production of meningeal fibroblast invading the lesion area (Duncan *et al.*, 1999). In the present study, immunohistological characterization of the matrix area at 1 wpr revealed an increase in rPH-positive fibroblasts in the lesion area of ALG-treated animals (Fig. 3.20A-C), indicating extensive invasion with the respective cells. In comparison, a strongly decreased fibroblast invasion was noted in the lesion area of PEG-treated animals (Fig. 3.20D-F). rPH is expressed by many cell types (Annunen *et al.*, 1998). It is, however a well-known fibroblast marker frequently used in both, *in vitro* (Kawaguchi *et al.*, 1992) and *in vivo* (Gibbons *et al.*, 2007;Okada *et al.*, 2007) studies. Fibroblasts can be easily identified by their morphology (see Fig. 3.20). The extensive invasion of Col4-producing fibroblasts – cells, which play an important part in the production and secretion of ECM – into the matrix after ALG-treatment (Fig. 3.20A-C) in the here presented study corresponds with the detected deposition of Col4 in the lesion area of ALG-treated animals (Fig. 3.16C), whereas PEG-treated animals revealed a decreased rPH-IR, and Col4 in the lesion area of PEG-treated animals was to a large part exhibited by defined structures, indicating a diminished

accumulation of extracellular Col4 in PEG matrix (Fig. 3.16D). Frequent appearance of fibroblasts in ALG is therefore accounted for the increased ECM-accumulation in the matrix.

In experimental animal studies which included the use of ALG capsules, impurities in the ALG favored the overgrowth of fibroblasts and macrophages over the capsules which eventually led to graft failure (de Vos et al., 1997; de Vos et al., 2002; van Hoogmoed et al., 2003; van Schilfgaarde and de Vos, 1999). Although the ALG-matrix in the present study did not promote extensive invasion of the gel with ED1-positive macrophages and microglia (Fig. 3.23C), a high amount of rPH-positive fibroblasts was found in the matrix area. Therefore, overgrowth of fibroblasts over the ALG matrix may eventually have led to the observed graft failure.

4.4.4.3 No invasion, but accumulation of mature oligodendrocytes in lesion border regions of matrix-treated animals

Immunological staining of sections from both, ALG- or PEG-treated animals, with an antibody against APC revealed an accumulation of mature oligodendrocytes in the GFAP-positive spinal cord lesion margins but not inside the matrix (Fig. 3.21).

Studies from other groups have reported similar observations regarding oligodendrocyte occurrence after SCI. After application of self-assembling nanofibers into the acutely injured mouse spinal cord, Tysseling-Mattiace *et al.* also detected increased numbers of APC-positive oligodendroglia, compared to control-treated animals, in spinal cord areas adjacent to the lesion site (Tysseling-Mattiace et al., 2008). The authors suggested a resulting positive effect on the experimental outcome. Further, in spinal cord areas adjacent to contusion injury sites, Baptiste *et al.* noted an increased neuronal survival, but no increase in survival of APC-positive oligodendrocytes after systemic treatment with PEG after cervical SCI compared to control-treated animals at 1 wpi (Baptiste et al., 2009). In a study on oligodendrocyte genesis after spinal contusion lesion (Tripathi and McTigue, 2007), Tripathi *et al.* described that oligogenesis is protracted after SCI and leads to increased oligodendrocyte numbers. Since most of the new oligodendrocytes were found to be formed in regions of greatest NG2 cell proliferation, and since increased occurrence of oligodendrocytes was observed in the first 2 weeks after injury, the authors concluded the spontaneous development of a dynamic gliogenic zone along lesion borders in the adult spinal cord.

Evidence of oligodendrocyte apoptosis at the time point of 1 week after insult to the spinal cord has previously been provided by several research groups (Beattie et al., 2000; Beattie et al., 2002a; Liu et al., 1997). It has been proposed by Beattie *et al.* that since oligodendrocytes seem to require axons for survival, axon loss after SCI might deprive oligodendrocytes of needed trophic factors (Beattie et al., 2002b). The observation of oligodendrocyte accumulation in the glial scar of PEG- and ALG-treated animals is concordant with this hypothesis because oligodendrocytes were apparent in the (axon-containing) bordering spinal cord regions of both matrices. Yet, there was only rare evidence of oligodendrocytes entering the lesion area of the respective animals. TUNEL or caspase-3 analysis was not performed; therefore the possibility that the APC-positive cells may have been oligodendrocytes undergoing apoptosis at the time of analysis cannot be excluded. It should further be kept in mind that negative influences of oligodendrocytes on regenerating spinal cord axons have been reported (Rabchevsky and Smith, 2001). These effects can be explained by the expression of inhibitory factors in the injured spinal cord. Increased appearance of oligodendrocytes might therefore contribute to an increase of the inhibitory milieu for regenerating axons.

In the present study, the presented data regarding the immunohistological characterization of the lesion area at 1 wpi are not quantitative. Furthermore, in the case of APC-positive oligodendrocytes, only ALG and PEG were compared, without further regarding control animals. This comparison revealed the accumulation of oligodendrocytes in the GFAP-positive area of the lesion border without displaying any differences between the two analyzed groups (Fig. 3.21). Although an increase in oligodendroglia in such respective areas was also noted in the ALG-matrix (Fig. 3.21A,B), the material's properties abolished other positive effects, e.g., extensive Schwann cell and astrocyte invasion or vascularization, respectively, thereby preventing the promotion of axonal regeneration.

Data presented here suggest that oligodendrocytes do not contribute to the observed increase in regenerated axons in the lesion area of PEG-treated animals after chronic SCI scar removal compared with ALG-treated animals, as there were no differences detected between the two groups. However, a generally beneficial effect elicited by oligodendrocytes at the lesion border of matrix-treated animals is further possible but was not subject of further investigations. Such beneficial effects have however previously been attributed to the observed "reactive" response of surviving

oligodendrocytes adjacent SCI lesion sites, as it might represent an important component of local repair mechanisms (Bartholdi and Schwab, 1998). In the respective study conducted by Bartholdi and Schwab in 1998, a peak of such a response (indicated by increased levels of MBP mRNA) was noted around 8 days post acute SCI. At this time, oligodendrocytes displaying strong MBP *in situ*-signal were oriented radially toward the lesion center and arranged parallel to neurofilament-positive axons.

In the present study, only the presence of mature oligodendrocytes was investigated. It is, however, possible that oligodendrocyte precursor cells (OPCs), which may be present in the lesion area at the observed time points, elicit beneficial effects on axonal regeneration into the matrix area. This should be further investigated in future studies via respective immunohistochemical staining with a marker for OPCs (e.g., NG2).

Since in the presented study differences in mature oligodendrocyte occurrence could not explain the noted results regarding axon regeneration after implantation of ALG or PEG into the chronically injured spinal cord, it was assumed that invading endogenous SC, which were found to be numerous present in PEG- but not ALG-matrix (Fig. 3.22), might further aid in mediating the promotion of axonal regeneration into PEG matrix.

4.4.4.4 Many invading Schwann cells are present in PEG, but not ALG matrix

Beneficial effects have been attributed to SC in the course of SCI recovery. Transplanted exogenous SC have been reported to promote axonal regeneration and remyelination, restore conduction properties and improve functional recovery in various models of SCI (Bunge, 2002; Hill et al., 2006; Honmou et al., 1996; Ramer et al., 2004; Xu et al., 1995; Xu et al., 1997; Xu et al., 1999). However, despite significant axon in-growth into SC grafts, functional improvement after implantation of SC alone could only rarely be reported (Rabchevsky and Smith, 2001).

Invasion of endogenous SC into the injured spinal cord can also spontaneously occur and mediate beneficial events after SCI (Black et al., 2006; Hagg and Oudega, 2006; von Euler et al., 2002).

To assess the occurrence of SC from the periphery into the site of chronic SCI scar resection in the here presented study, immunohistochemical staining with an antibody against S100 was performed. S100 is not exclusively expressed by SC, but

can further be found in subpopulations of astrocytes (Garavito et al., 2000) and also oligodendrocytes (Aguirre et al., 2007). Since the lesion area of ALG- as well as PEG-treated animals was detected to be devoid of APC-positive oligodendrocytes (Fig. 3.21), S100-IR in the lesion area was not attributed to these cells. S100 has further been suggested to be preferentially distributed in myelin-forming SC (Mata et al., 1990), whereas GFAP-IR, which is also not restricted to astrocytes, can further label non-myelinating SC. Jessen *et al.* could also demonstrate that while GFAP is suppressed in myelin-forming cells, it is retained in non-myelin-forming SC (Jessen et al., 1990). Mature myelin-forming cells indeed maintained the potential to also express GFAP but will only do so if removed from contact with myelinated axons (Jessen et al., 1990). However, not only double-staining of the lesion area of PEG-treated animals with S100 and PAM (with nuclear DAPI staining) was performed (Fig. 3.22F; Fig. 3.26A,B), but additionally also triple staining of PAM, S100 and GFAP in order to clearly identify SC in the lesion area (Fig. 3.26C).

Only little SC invasion was detected in control animals at both analyzed time points (Fig. 3.22A,D). Although there was an increase in S100-IR at 5 wpl observed (Fig. 3.22D), it was only rarely found to be present in cellular structures which revealed SC-like morphologies and nuclear DAPI-staining. However, SC were numerous present in the lesion area of PEG-treated animals (Fig. 3.22C,F), while their occurrence in the lesion area of ALG-treated animals was found to be rather limited (Fig. 3.22B,E). These results regarding SC invasion into the lesion area are concordant with the observations and axonal quantifications made in the course of the present study: In contrast to ALG-treated (Fig. 3.22B,E) and to control animals (Fig. 3.22A,D), PEG-treated animals revealed not only the highest amount of axons in the lesion area (see Fig. 3.8, Fig. 3.12, Fig. 3.15), but further a highly increased occurrence of S100-positive SC in the same regions.

It can therefore be concluded that although ALG seems to be an attractive substrate for migrating fibroblasts (Fig. 3.20A,B), it is obviously not a favorable substrate for the migration of growth-supporting structures [e.g., BV (Fig. 3.17C,G,H), regeneration-promoting cells, e.g., SC (Fig. 3.22B,E), or axons per se (Fig. 3.12; Fig. 3.15)].

Confocal analysis of the matrix area in sections of PEG-treated animals revealed a frequent association of Schwann cells with axons (Fig. 3.26A-D), indicating the possibility of myelination of these axons by Schwann cells. MBP-IR

revealed that some of the axon fragments present in the lesion center of PEG-treated animals were indeed directly associated with myelinating SC at the analyzed time point (Fig. 3.26E,F), indicating the possibility of myelination of these axons by SC. Myelin is essential for the proper functioning of the nervous system as it allows efficient conduction of axons potentials down the axon.

4.4.5 Decreased invasion of inflammatory cells after matrix implantation

In accordance with reports on a general non-toxicity of the two materials ALG and PEG, no increased but rather a decreased IR to ED1, a marker of rat microglia and macrophages, was found in the lesion area of matrix-treated animals, compared to control animals (Fig. 3.23). The area of positive IR in treated animals was found to be mainly restricted to the margin areas of the lesion. Kigerl *et al.* have recently reported the identification of subpopulations of macrophages with divergent effects which can lead to either neurotoxicity or regeneration after SCI (Kigerl *et al.*, 2009). A similar balance of beneficial and detrimental action of macrophages and microglia had first been suggested by Schwartz (Schwartz, 2003). Because ED1 is a general marker of phagocytic macrophages and microglia, IR to CD3, CD4, CD8 and a general rat B-cell marker to further assess inflammatory responses was additionally investigated. Cells originating from the respective lymphocyte populations were only rarely found in the lesion area of animals from all analyzed groups (Fig. 3.24; Fig. 3.25). Although at times structures appeared to reveal IR to the respective antibodies, DAPI staining was mostly not apparent in these structures, which were therefore not assumed to be inflammatory cells. The lesion area of control animals at the time point of 5 wpl (the only control group analyzed for this specific investigation of invasion of T- and B-lymphocytes) also revealed few, yet apparently slightly more inflammatory cells than the lesion area of treated animals at the time point of 1 wpr (Fig. 3.24).

The reason that only few immunoreactive T-cells were apparent in the lesion area of animals from all groups analyzed, and especially the control animals, where a more manifest inflammatory response would be expected, may lie in the time point analyzed (1 wpr or 5 wpl, respectively): B-lymphocytes are present in the vicinity of

the lesion within hours after SCI up to one week after injury, whereas T-lymphocytes have an estimated life span of 1-2 months (Trivedi et al., 2006). The reason for choosing a time point of 1 week post resection for analysis was to assess beneficial or negative changes in the lesion area at a time, at which the inhibitory fibrous scar is fully established. Therefore, if a further analysis of the invasion of lymphocytes implicated with inflammatory response was desired, a shorter survival time point of 1 wpl should also be analyzed in the case of control-lesioned animals.

As aforementioned, Han *et al.* recently suggested a protective effect of the rescuing of vasculature after SCI (Han et al., 2010). SCI is accompanied by processes of secondary degeneration, such as loss of BV and inflammation. In their paper, the authors found that the promotion of endothelial cell survival might further lead to reduced inflammation. Such observations once again confirm the importance of angiogenesis after SCI (which extensively occurred after insertion of PEG into the chronic scar resection cavity). The differences regarding regeneration into the matrix after ALG- or PEG-application, however, cannot be explained by occurrence of inflammatory processes, as the analyses did not reveal any notable differences in the degree of invasion of inflammatory cells into the matrix at the analyzed time point (Fig. 3.23, Fig. 3.24., Fig. 3.25).

4.5 Regeneration of Axons from Different Neuronal Populations into PEG Matrix after Chronic Scar Resection

Our group in the Molecular Neurobiology Laboratory at the University of Düsseldorf could previously show that different axonal populations reveal differences in their regeneration potential at varying time points after SCI alone, and after acute SCI with subsequent local treatment with the iron chelator BPY-DCA and cAMP, respectively (Schiwy et al., 2009). The present data reveal the possibility of the growth of regenerated axons into and even beyond a chronic SCI scar removal site after insertion of PEG. Fibroblast invasion was found to be limited in PEG-treated animals, resulting in a decrease in collagenous scar formation. Regenerating axons appeared to readily grow into a matrix provided via PEG-application. After application of PEG, damaged membranes of BV and axons may have been repaired, allowing the growth of the respective structures into the matrix area. Growth supporting cells

which are normally associated with these structures, i.e., astrocytes and SC, were stimulated to invade the lesion area, thereby paving the way for in-growth of regenerating axons.

Axon populations maintain a considerable capacity for regeneration or sprouting, respectively, both, spontaneously and as a response to treatment (Camand et al., 2004; de Castro R. et al., 2005; Hill et al., 2004; Schiwy et al., 2009). However, varying selective demands have previously been described for different axon populations (Inman and Steward, 2003; Li and Raisman, 1995).

The here presented data show that axons from different neuronal populations could regenerate into a PEG-matrix after chronic SCI scar removal (Fig. 3.27). Axons from descending tracts involved in motor function, as well as ascending sensory DRG-axons were found in the matrix. The occurrence of regenerated chronically injured BDA-labeled corticospinal tract (CST) fiber fragments, of dopaminergic (TH) and of serotonergic (5-HT) fibers indicates a central origin (Fig. 3.27). Ascending sensory axons identified via CGRP-antibody staining were also found to enter the lesion area. Inman *et al.* previously proposed that after murine contusion SCI, the connective tissue matrix which forms at the site of SCI is permissive for regeneration of some classes of ascending sensory axons, but not for other axonal systems (Inman and Steward, 2003). Schiwy *et al.* also found increased axon regeneration of different neuronal populations after rat transection SCI in AST-treated compared to control-treated rats (Schiwy et al., 2009). The here described data regarding axonal regeneration into PEG matrix after chronic SCI scar removal therefore indicate that beneficial effects mediated by PEG may not be restricted to individual neuronal populations. The observed in-growth of axons from different axonal populations (Fig. 3.8, Fig. 3.12, Fig. 3.15, Fig. 3.27) is likely to be mediated by PEG through contributing to the formation of a permissive tissue bridge and through PEG's ability to enter the spinal cord, where it can preserve cytoskeletal proteins and axonal integrity (Baptiste et al., 2009).

4.6 Chronic Scar Resection does not Notably Impair Open Field Locomotive Behavior

In the aforementioned study by Hejcl *et al.*, the authors could demonstrate that functional recovery in chronic SCI is still possible (Hejcl et al., 2010). Slight

functional recovery after treatment of chronic spinal cord injury has further recently been reported by Tom *et al.* In the respective study, the authors used peripheral nerve bridges to treat chronic cervical contusion SCI (Tom *et al.*, 2009).

The locomotor behavior of all animals was in the here presented study assessed using open field observation and rating of the general locomotion according to Basso *et al.* (Basso *et al.*, 1995).

After exclusion of some animals with strikingly lower BBB scores prior to scar resection than the ones revealed by the majority of the animals, the average score achieved by animals of all analyzed groups at 5 wpr or 10 wpl (“lesion only” controls), respectively, was rated to be 11 (Fig. 3.28). Although there was a slight decrease observed in the first 2-3 weeks after the scar removal procedure, animals with matrix implants were able to soon recover to reach values comparable to “lesion only” controls. The slight reduction of BBB scores observed subsequent to the scar removal procedure could be related to the damage to the intact spinal tissue. After photochemical scar ablation in chronic contusion rat SCI to provide a permissive environment for regenerating axons, Zhang *et al.* also noted a reduction of BBB scale scores, but this reduction was not statistically significant from stabilized behavioral scoring prior to the scar ablation treatment (Zhang *et al.*, 2007). In the present study, regardless of the observed regenerative events after chronic SCI scar resection and subsequent filling of the resection cavity with PEG, notable differences regarding the general locomotor behavior after chronic SCI scar resection, assessed by open-field locomotor analysis were at the time point of sacrifice only detected between “RX only” controls and the remaining analyzed groups (Fig. 3.28B). A score of 11 implies that the animals show a weight-supported walking pattern with consistent plantar stepping but without any forelimb/hindlimb-coordination. Only animals of the “RX only” group generally revealed slightly lower BBB scores in the range of 8-10 during the time period of 5 wpr (Fig. 3.28B). These animals were found to show “sweeping” or non-weight-supported stepping of both hindlimbs (BBB score 8) or weight-supported stepping of only one hindlimb, while the other was only found to make sweeping or non-weight-supported movements. Baptiste *et al.*, who applied PEG-treatment after acute compression SCI, observed a significant neurobehavioral recovery in treated animals. However, the recovery was only a modest one, indicating that PEG may not confer sufficient neuroprotection after acute SCI to be used clinically as a single treatment (Baptiste *et al.*, 2009). In the here presented

study, open field analysis of locomotion was used simply to find out whether the procedures of scar removal and matrix implantation resulted in any negative outcome in comparison to the control situation. This was not observed to be the case.

In previous studies from our group in the Molecular Neurobiology Laboratory, locomotor score recovery was reported to occur between 7 and 10 weeks after acute SCI (Klapka et al., 2005). Generally speaking, a time period of 5 wpr must be considered as too short to reveal signs of neuronal re-connectivity and behavioral functional recovery (Salehi et al., 2009) especially in an injury model which comprises the generation of a 4 mm gap in the dorsal spinal cord.

Therefore, while the behavioral observations made in the course of the here presented study might be seen as an indication for stabilizing effects of matrix implantation after tissue removal in the spinal cord, conclusive behavioral effects need to be assessed in future studies.

In the here presented behavioral analysis, only few animals per group ($n = 5-9$, see Fig. 3.28) were tested. However, significant behavioral analysis requires higher animal numbers (i.e., 10 animals minimum per group). Furthermore, as already mentioned, the extent of the initial SCI transection lesion presents an important factor for the behavioral outcome also after chronic scar resection. Therefore, in an on-going study, a group of 10 animals received a total transection of the thoracic spinal cord. After 5 weeks, an area of 4 mm containing the lesion scar was resected and the resulting cavity was filled with PEG 600. The animals will survive for a longer period of time to allow possible regeneration across the bridged area. Although the total transection of the spinal cord leads to dramatic behavioral deficits in the injured animals, this lesion model is very suitable for the investigation of axonal regeneration and functional recovery. Such recovery may only be weak, but the obtained results will be very clear and unambiguous.

However, the present data reveal the possibility of axonal regeneration of regenerated axons into (Fig. 3.8, Fig. 3.12, Fig. 3.15, Fig. 3.27) and even beyond (Fig. 3.15H-J) a chronic SCI scar removal site after insertion of PEG. Although the number of regenerated axons crossing the lesion area might be too small to achieve significant functional recovery, a further enhancement of the spontaneous regenerative capacity of injured axons via addition of growth (and guidance) promoting agents, in addition to a longer survival time period of the animals after the

operation (as is subject of the current investigation) could lead to a recovery in function, which is the over-all aim of SCI research.

4.7 Additional Considerations

4.7.1 Chemical/Physical Aspects

4.7.1.1 Possible influence of matrix viscosity on regenerative events

ALG's poor ability to promote the spontaneous regeneration capacity of axons, as well as the fact that in ALG or ALG+BPY-treated animals, growth of regenerated axons was observed to primarily occur in the margin areas of the spinal cord/matrix interface but not in the center of the ALG-matrix, could further result from ALG's general material properties. Because of its significant thickening effect, ALG is generally used at lower concentrations to avoid the problem of viscosity. Viscosity is one of the functional properties of ALG. The viscosity of an ALG solution can be manipulated by changing the concentration of the ALG or by using materials with varying chain length (i.e., molecular weight). Typically, the molecular weight for the ALG used in the course of the here described experiments is in the 75,000 – 220,000 g/mol range (manufacturer information). High molecular weight suspensions are not readily pourable or injectable, respectively. The ALG solution used for hydrogel formation in the present study is described to have a viscosity of 20-200 [mPa*s]⁻¹ at 20 °C (manufacturer information). ALG solution loses its viscosity when heated above 60-70 °C. This is due to depolymerization effects. The viscosity gradually decreases and acquires constant value after 24 h, whereas fresh ALG solution has the highest viscosity. The ratio of M to G determines the raft-forming properties. ALG with a high G-content develop stiffer, more porous gels which maintain their integrity for longer periods of time. High ratio (e.g., 70 %) G forms the strongest raft revealing high viscosity. During cationic cross-linking, G-rich ALG do not undergo excessive swelling and subsequent shrinking, thus they better maintain their form. ALG rich in M-residues, on the other hand, develop softer, less porous gels that tend to disintegrate with time and exhibit a high degree of swelling and shrinking during cationic cross-linking (Simpson et al., 2004). ALG with high G-content are used in SCI research mainly for microcapsule formation for cell delivery (Purcell et al., 2009) or when ALG with a porous or fiber-containing scaffold (Prang et al., 2006) are desired. In practice, ALG is used at concentrations less than 10 % w/w.

The ALG percentage used in the present study was 2 % w/v. This is a concentration which is frequently used in the treatment of SCI, either for the encapsulation of cells (Tobias et al., 2001) or as a matrix implant (Novikov et al., 2002). For application of ALG as a matrix in acute SCI to promote axonal regeneration and elongation, M-rich ALG are generally the preferred gels (Kataoka et al., 2004; Novikov et al., 2002; Suzuki et al., 2000). The ALG used for the described experiments is made from an ALG where over 50% of the monomer units are mannuronate (manufacturer information). It is a highly purified and well-characterized sodium ALG.

ALG's failure to promote spontaneous axonal regeneration and invasion of growth-promoting cells could lie in its rheological properties. Recent studies suggest that in addition to chemical cues, mechanical stimuli could also influence neuronal growth. Franze *et al.* demonstrated with *in vitro*-experiments how growing neurons may detect and avoid stiff substrates (Franze et al., 2009). Previous investigations regarding the biomechanics of axonal growth already indicated that unlike most other cell types (e.g., astrocytes), neurons prefer soft substrates (Flanagan et al., 2002; Georges et al., 2006). With their experiments Franze *et al.* demonstrated growth cones' ability to deform gels up to a stiffness of ~300 Pa, which corresponds to their compliance. The authors further reported the observation of a transition from neurons with many branches to those with significantly less branches occurring at a substrate stiffness of ~300 Pa. They concluded that active mechanosensitivity may provide positive stimuli for neuronal growth in a soft environment, whereas more rigid contacts deliver a negative feedback. 2 % sodium ALG gel exhibits a stiffness of ~10 Pa (information regarding the dynamic viscosity of the gel was not found, but would be expected to lie in the higher range of the dynamic viscosity of MG, see Tab. 4.1). While PEG 600, a fluid with a much lower viscosity, achieved good results in the here presented study regarding spontaneous axonal regeneration, the reason for PEG's superiority regarding the promotion of spontaneous axonal regeneration after chronic SCI scar removal, as well as ALG's failure for that matter most likely lies elsewhere than simply in its viscosity. However, matrix viscosity may be of some importance for both, tissue reformation and axonal regeneration.

PEGs are nonvolatile substances. The abovementioned rheological effects and their influences on neuronal growth could also hold for as an argument in the case of beneficial effects exerted by PEG 600 on spontaneous axon regeneration. Viscosity coefficients of brain tissue, blood and the applied matrix materials are listed

in Table 4.1. The brain is one of the softest organs with an elastic modulus of 260-490 Pa (Levental et al., 2006) and a viscosity coefficient of 0.05-0.5 Pa*s (Xin et al., 2009). While the viscosity coefficient of the applied ALG-solution comes close to that of fresh human brain tissue, the ALG gel itself is not a fluid, but rather a gel and thus exhibits a stiffer consistency. The applied PEG solution (PEG 600) has a viscosity of 135 mPa*s (Wente et al., 2007), and thus lies in a range of viscosity of that of brain tissue.

Table 4.1: Viscosity coefficients

Material/Tissue	Viscosity [Pa*s]
fresh human brain tissue	0.05-0.5 (Xin et al., 2009)
blood	0.004-0.025 (source: http://de.wikipedia.org/wiki/Viskosität)
PEG 400	0.09 (Wente et al., 2007)
PEG 600	0.135 (Wente et al., 2007)
PEG 1000 (50 % aq. sol.)	0.024-0.028 (source: http://chemicalland21.com)
ALG (2 % solution)	0.02-0.2 (manufacturer information)
MG	10 (Guiot et al.,)

This may be beneficial for the growth of axons into the material. Growth cones may not be constricted by mechanical factors presented by the matrix. On the other hand, this might also lead to axons remaining inside the matrix without entering the more rigid host tissue. It remains an important issue in the research on scaffold and matrix materials used in SCI, to find the right balance regarding the stiffness or softness, respectively, of applied materials. While a material which is too stiff requires a neurite to exert too much tension, thus resulting in a decreased extension, very soft materials which require only small amounts of tension might cause a neurite to pull the material in toward the cell body rather than to extend, due to possible lack of support for further extension, as has been proposed by Gunn *et al.* (Gunn et al., 2005). Although it can presently only be assumed that rheological properties of PEG 600 may in part contribute to the described spontaneous regeneration of axons, the present data might indicate an influence of a materials' stiffness or viscosity, respectively: While hardly any axonal growth was observed to occur into and inside of an MG-filled lesion area, the spontaneous axonal regeneration capacity was increased in an ALG-matrix, and was further found to be significantly increased in a matrix consisting of PEG 600 (Fig. 3.8; Fig. 3.12; Fig. 3.15), whereas PEG 1000 was

found to lead to the encapsulation of the implant. PEG 1000 exhibits a melting point in the temperature range of 37 °C - 40 °C (source: www.sciencelab.com). This may explain the observed encapsulation of the material at body temperature, which was determined to lie between 36 °C – 38 °C in the rat.

PEG have been described to reduce mechanical trauma to erythrocytes (Kameneva et al., 2003), and they further frequently find use as ingredients of hemostatic agents (Elefteriades, 2009). It is likely that, due to generally non-adhesive properties of PEG (Cong et al., 2009), the mixture of PEG with blood inhibits the formation of a blood clot, which would normally form and subsequently be degraded by activated immune cells (as was observed to be the case for control animals). This hypothesis is further supported by the fact that despite PEG itself being known as a material to which cells or proteins do not generally attach (Elbert and Hubbell, 1998;Gunn et al., 2005;Hern and Hubbell, 1998), the results from the present study indicate beneficial cell growth and regeneration in the lesion area.

Finally, hygroscopic PEG may not only effectively seal membranes, but may further result in beneficial hydration of the lesion area. Liquid PEG, such as PEG 600, is hygroscopic. Their ability to absorb water decreases with increasing molecular weight. Solid types are not hygroscopic. The physical and chemical properties of the PEG matrix could further facilitate the diffusion of nutrients in the lesion area, possibly indicated by increased occurrence of blood vessels in PEG matrix compared to the remaining analyzed groups (Fig. 3.17). Other studies have also demonstrated beneficial integration of PEG-containing agents. Mahoney and Anseth have reported the suitability of lactide-containing PEG hydrogels as synthetic cell carriers for neural transplantation (Mahoney and Anseth, 2006). However, such aspects are at present only speculations. Further analyses are required to investigate the mechanisms and contributing factors of PEG matrix effects.

5 Summary and Perspectives

Much progress has been made in the last years regarding the development of improved therapeutic approaches for the treatment of acute spinal cord injury (SCI). However, since the majority of patients suffer from a chronic injury condition, there is an increased need for effective therapies for chronic SCI patients. Treatments which may have proved effective after acute SCI, are generally not applicable in chronic SCI without further adaption. Due to a changed lesion environment, e.g., a fully developed lesion scar, different demands must be met. The focus of this study was on finding a suitable matrix which could be used to fill the cavity after chronic SCI scar removal. A beneficial matrix should not impede but rather promote general tissue repair and axonal regeneration. In this study characterization of three matrix materials and their influence on axonal regeneration after application in an experimental chronic hemisection SCI model in rat was presented. The three materials – MatrigelTM (MG), alginate hydrogel (ALG), and polyethylene glycol 600 (PEG) - have not previously been used as sole matrix substances in chronic SCI. In the present study, immunohistological analysis revealed the following ranking of matrices with respect to axon profile density and profile numbers after insertion into a chronic SCI scar resection cavity: PEG > ALG > MG. Application of PEG into a chronic SCI scar resection site was found to exert beneficial effects via promotion of the formation of a tissue bridge at the site of application in the spinal cord. This growth-promotional effect is attributed to an extensive invasion of PEG-matrix with growth-supporting Schwann cells and astrocytes, to a beneficial re-vascularization, and to a diminished occurrence of deleterious events after PEG-filling of the resection cavity. The formation of a stable tissue bridge was not possible in control-lesioned and in ALG-treated animals, which resulted in a very fragile structure of the lesion area. Deleterious events at the site of injury as well as lack of growth-supporting cells (Schwann cells) and structures (blood vessels) are accounted for the lack of regeneration into the ALG-matrix. The results further indicate the potential of chronically injured spinal cord axons to spontaneously regenerate into a suitable matrix implanted into a cavity resulting from removal of the inhibitory lesion scar. PEG proved to be an effective material, which, although it does generally not exhibit the features of a biomatrix, is able to promote biomatrix formation at the site of implantation. In future studies, such a beneficial matrix can be used as a basis for further combinations, e.g., with chelators or growth factors, to further improve axonal

regeneration. Although a viscous fluid, such as PEG 600, has never been considered as a basis for bridging a spinal cord injury, the present data show promising results after its application in chronic SCI. Due to lack of guiding structures within the matrix, addition of growth-promoting factors may be required to eventually further achieve directed growth of the numerous axons in the lesion area of PEG-treated animals into the distal spinal cord, where they could make functional reconnections resulting in locomotor recovery. These aspects will be taken into consideration for future studies.

Zusammenfassung

Bei der Entwicklung von Therapieansätzen zur Behandlung akuter Rückenmarkverletzung wurden in den letzten Jahren große Fortschritte erzielt. Jedoch ist die große Mehrheit der Patienten von den Folgen chronischer Verletzungszustände und ihren Folgen betroffen. Daraus resultiert die dringende Notwendigkeit der Entwicklung wirksamer Therapien zur Behandlung von chronischen Rückenmarkverletzungen. Behandlungsstrategien, die sich im Tierexperiment als wirksam nach akuter Verletzung erwiesen haben, sind für die Behandlung chronischer Verletzungen im Allgemeinen nicht ohne weitere Anpassungen übertragbar. Aufgrund von Veränderungen im chronischen Läsionsgebiet, wie z.B. der vollausgebildeten Läsionsnarbe, müssen unterschiedliche Anforderungen erfüllt werden. Ziel der vorliegenden Arbeit war es, eine geeignete Matrixsubstanz zu finden, um die Kavität nach Resektion der chronischen Rückenmarkverletzungsnarbe zu überbrücken. Das Matrixmaterial sollte sich dabei sowohl auf Gewebeneubildung als auch auf axonale Regeneration förderlich auswirken. In der vorliegenden Arbeit werden drei Matrixsubstanzen charakterisiert und ihr Einfluss auf axonale Regeneration nach Anwendung in einem chronischen Hemisektionsmodell in der Ratte dargestellt. Die drei Substanzen – Matrigel™ (MG), Alginat-Hydrogel (ALG), und Polyethylenglykol 600 (PEG) – wurden bislang nie in reiner Form als Matrixsubstanzen im Zuge der Behandlung chronischer Rückenmarkverletzung eingesetzt. Im Rahmen der vorliegenden Arbeit durchgeführte immunhistologische Untersuchungen ergaben folgende Rangfolge der Matrices bezüglich des Einwachsens von Axonen: PEG > ALG > MG. Das Einbringen von PEG in die Narbenresektionskavität bewirkte die Ausbildung einer wachstumsfördernden Gewebebrücke an der Läsionsstelle. Diese Wirkung lässt sich auf das Einwandern wachstumsunterstützender Schwannzellen und Astrozyten, auf eine vorteilhafte Revaskularisierung des Areals, sowie auf eine Verminderung schädlicher Ereignisse nach PEG-Applikation zurückführen. Die Ausbildung einer stabilen Gewebebrücke wurde weder durch Nichtbehandlung in Kontrolltieren, noch durch eine ALG-Matrix begünstigt. ALG-Behandlung führte zu einer fragilen Gewebestruktur an der Verletzungsstelle. Mangelnde Regeneration in die ALG-befüllte Resektionskavität im Zuge der vorliegenden Studie lässt sich mit dem Auftreten schädlicher Ereignisse an der Läsionsstelle, sowie einem Mangel an wachstumsunterstützenden Zellen (Schwannzellen) und Strukturen (Blutgefäße)

erklären. Die Ergebnisse der vorliegenden Studie deuten zudem die Fähigkeit chronisch verletzter Rückenmarkaxone an, nach Entfernung der inhibitorischen Läsionsnarbe in eine geeignete Matrix zu regenerieren. Als eine wirksame Substanz hat sich PEG herausgestellt, das, obwohl es selbst nicht die Eigenschaften einer Biomatrix besitzt, die Ausbildung einer solchen an der Implantationsstelle bewirken kann. Eine solche Matrix kann in zukünftigen Studien als Grundlage für weitere Kombinationen, z.B. mit Eisenchelatoren oder Wachstumsfaktoren, dienen, um die axonale Regeneration noch weiter zu verstärken. Obwohl eine viskose Flüssigkeit wie PEG 600 bislang nicht als Matrix für die Überbrückung einer Rückenmarkverletzung in Betracht gezogen wurde, zeigen die hier präsentierten Daten vielversprechende Ergebnisse nach PEG-Behandlung chronischer Rückenmarkverletzung. Aufgrund fehlender Leitstrukturen in dieser Matrix könnte die Notwendigkeit der Zugabe wachstumsfördernder Faktoren notwendig sein, um die zahlreichen Axone, die in der PEG-Matrix – und vereinzelt sogar im distalen Rückenmark - gefunden wurden, dazu anzuregen, in erhöhter Zahl ins kaudale Rückenmark einzuwachsen. Dort könnten funktionelle Verbindungen neu hergestellt werden, um letztendlich in lokomotorischer Erholung zu resultieren. Diese Aspekte sollen in zukünftigen Studien in Betracht gezogen werden.

6 References

1. (2009) *The Spinal Cord* Academic Press.
2. Afifi,A.K. & Bergman,R.A. (2005) *Functional Neuroanatomy*.
3. Afshari,F.T., Kappagantula,S. & Fawcett,J.W. (2009) Extrinsic and intrinsic factors controlling axonal regeneration after spinal cord injury. *Expert.Rev.Mol.Med.*, **11**, e37.
4. Aguayo,A.J., David,S. & Bray,G.M. (1981) Influences of the glial environment on the elongation of axons after injury: transplantation studies in adult rodents. *J.Exp.Biol.*, **95**, 231-240.
5. Aguirre,A., Dupree,J.L., Mangin,J.M. & Gallo,V. (2007) A functional role for EGFR signaling in myelination and remyelination. *Nat.Neurosci.*, **10**, 990-1002.
6. Ahn,Y.H., Lee,G. & Kang,S.K. (2006) Molecular insights of the injured lesions of rat spinal cords: Inflammation, apoptosis, and cell survival. *Biochem.Biophys.Res.Comm.*, **348**, 560-570.
7. Akesson,E., Holmberg,L., Jonhagen,M.E., Kjaeldgaard,A., Falci,S., Sundstrom,E. & Seiger,A. (2001) Solid human embryonic spinal cord xenografts in acute and chronic spinal cord cavities: a morphological and functional study. *Exp.Neurol*, **170**, 305-316.
8. Akhyari,P., Kamiya,H., Haverich,A., Karck,M. & Lichtenberg,A. (2008) Myocardial tissue engineering: the extracellular matrix. *Eur.J.Cardiothorac.Surg.*, **34**, 229-241.
9. Alberts,B., Johnson,A., Lewis,J., Raff,M., Roberts,K. & Walter,P. (2007) *Molecular Biology of the Cell* Garland Science.
10. Ankeny,D.P., McTigue,D.M. & Jakeman,L.B. (2004) Bone marrow transplants provide tissue protection and directional guidance for axons after contusive spinal cord injury in rats. *Exp.Neurol*, **190**, 17-31.

11. Annunen,P., Autio-Harmainen,H. & Kivirikko,K.I. (1998) The novel type II prolyl 4-hydroxylase is the main enzyme form in chondrocytes and capillary endothelial cells, whereas the type I enzyme predominates in most cells. *J.Biol.Chem.*, **273**, 5989-5992.
12. Aumailley,M. & Gayraud,B. (1998) Structure and biological activity of the extracellular matrix. *J.Mol.Med.*, **76**, 253-265.
13. Bakshi,A., Fisher,O., Dagci,T., Himes,B.T., Fischer,I. & Lowman,A. (2004) Mechanically engineered hydrogel scaffolds for axonal growth and angiogenesis after transplantation in spinal cord injury. *J.Neurosurg.Spine*, **1**, 322-329.
14. Bamber,N.I., Li,H., Lu,X., Oudega,M., Aebischer,P. & Xu,X.M. (2001) Neurotrophins BDNF and NT-3 promote axonal re-entry into the distal host spinal cord through Schwann cell-seeded mini-channels. *Eur.J.Neurosci.*, **13**, 257-268.
15. Ban,D.X., Kong,X.H., Feng,S.Q., Ning,G.Z., Chen,J.T. & Guo,S.F. (2008) Intraspinal cord graft of autologous activated Schwann cells efficiently promotes axonal regeneration and functional recovery after rat's spinal cord injury. *Brain Res.*
16. Baptiste,D.C., Austin,J.W., Zhao,W., Nahirny,A., Sugita,S. & Fehlings,M.G. (2009) Systemic polyethylene glycol promotes neurological recovery and tissue sparing in rats after cervical spinal cord injury. *J.Neuropathol.Exp.Neurol.*, **68**, 661-676.
17. Baptiste,D.C. & Fehlings,M.G. (2006) Pharmacological approaches to repair the injured spinal cord. *J.Neurotrauma*, **23**, 318-334.
18. Barritt,A.W., Davies,M., Marchand,F., Hartley,R., Grist,J., Yip,P., McMahon,S.B. & Bradbury,E.J. (2006) Chondroitinase ABC promotes sprouting of intact and injured spinal systems after spinal cord injury. *J.Neurosci.*, **26**, 10856-10867.

19. Bartholdi,D. & Schwab,M.E. (1998) Oligodendroglial reaction following spinal cord injury in rat: transient upregulation of MBP mRNA. *Glia*, **23**, 278-284.
20. Basso, D. M., Beattie, M. S., and Bresnahan, J. C. A Sensitive and Reliable Locomotor Rating Scale for Open Field Testing in Rats. 1995.
21. Bearden,S.E. & Segal,S.S. (2005) Neurovascular alignment in adult mouse skeletal muscles. *Microcirculation.*, **12**, 161-167.
22. Beattie,M.S., Farooqui,A.A. & Bresnahan,J.C. (2000) Review of current evidence for apoptosis after spinal cord injury. *J.Neurotrauma*, **17**, 915-925.
23. Beattie,M.S., Harrington,A.W., Lee,R., Kim,J.Y., Boyce,S.L., Longo,F.M., Bresnahan,J.C., Hempstead,B.L. & Yoon,S.O. (2002a) ProNGF induces p75-mediated death of oligodendrocytes following spinal cord injury. *Neuron*, **36**, 375-386.
24. Beattie,M.S., Hermann,G.E., Rogers,R.C. & Bresnahan,J.C. (2002b) Cell death in models of spinal cord injury. *Prog.Brain Res.*, **137**, 37-47.
25. Berry,M., Maxwell,W.L., Logan,A., Mathewson,A., McConnell,P., Ashhurst,D.E. & Thomas,G.H. (1983) Deposition of scar tissue in the central nervous system. *Acta Neurochir.Suppl (Wien.)*, **32**, 31-53.
26. Black,J.A., Waxman,S.G. & Smith,K.J. (2006) Remyelination of dorsal column axons by endogenous Schwann cells restores the normal pattern of Nav1.6 and Kv1.2 at nodes of Ranvier. *Brain*, **129**, 1319-1329.
27. Blackmore,M. & Letourneau,P.C. (2006) Changes within maturing neurons limit axonal regeneration in the developing spinal cord. *J.Neurobiol.*, **66**, 348-360.
28. Blakemore,W.F. (2000) Olfactory glia and CNS repair: a step in the road from proof of principle to clinical application. *Brain*, **123**, 1543-1544.
29. Blight,A.R. (1991) Morphometric analysis of blood vessels in chronic experimental spinal cord injury: hypervascularity and recovery of function. *J.Neurol.Sci.*, **106**, 158-174.

30. Borgens,R.B. (2001) Cellular engineering: molecular repair of membranes to rescue cells of the damaged nervous system. *Neurosurgery*, **49**, 370-378.
31. Borgens,R.B. & Shi,R. (2000) Immediate recovery from spinal cord injury through molecular repair of nerve membranes with polyethylene glycol. *FASEB J.*, **14**, 27-35.
32. Borgens,R.B., Shi,R. & Bohnert,D. (2002) Behavioral recovery from spinal cord injury following delayed application of polyethylene glycol. *J.Exp.Biol.*, **205**, 1-12.
33. Boyd,J.G., Doucette,R. & Kawaja,M.D. (2005) Defining the role of olfactory ensheathing cells in facilitating axon remyelination following damage to the spinal cord. *FASEB J.*, **19**, 694-703.
34. Bradbury,E.J. (2002) Chondroitinase ABC promotes functional recovery after spinal cord injury.
35. Brazda,N. & Muller,H.W. (2009) Pharmacological modification of the extracellular matrix to promote regeneration of the injured brain and spinal cord. *Prog.Brain Res.*, **175**, 269-281.
36. Bregman,B.S. (1998) Regeneration in the spinal cord. *Curr.Opin.Neurobiol.*, **8**, 800-807.
37. Buchli,A.D. & Schwab,M.E. (2005) Inhibition of Nogo: a key strategy to increase regeneration, plasticity and functional recovery of the lesioned central nervous system. *Ann.Med.*, **37**, 556-567.
38. Bunge,M.B. (2001) Bridging areas of injury in the spinal cord. *Neuroscientist.*, **7**, 325-339.
39. Bunge,M.B. (2002) Bridging the transected or contused adult rat spinal cord with Schwann cell and olfactory ensheathing glia transplants. *Prog.Brain Res.*, **137**, 275-282.

40. Burdick, J.A., Ward, M., Liang, E., Young, M.J. & Langer, R. (2006) Stimulation of neurite outgrowth by neurotrophins delivered from degradable hydrogels. *Biomaterials*, **27**, 452-459.
41. Busch, S.A., Horn, K.P., Silver, D.J. & Silver, J. (2009) Overcoming macrophage-mediated axonal dieback following CNS injury. *J.Neurosci.*, **29**, 9967-9976.
42. Buss, A., Pech, K., Kakulas, B.A., Martin, D., Schoenen, J., Noth, J. & Brook, G.A. (2007) Growth-modulating molecules are associated with invading Schwann cells and not astrocytes in human traumatic spinal cord injury. *Brain*, **130**, 940-953.
43. Buss, A. & Schwab, M.E. (2003) Sequential loss of myelin proteins during Wallerian degeneration in the rat spinal cord. *Glia*, **42**, 424-432.
44. Cai, J., Ziemba, K.S., Smith, G.M. & Jin, Y. (2007) Evaluation of cellular organization and axonal regeneration through linear PLA foam implants in acute and chronic spinal cord injury. *J.Biomed.Mater.Res.A*.
45. Camand, E., Morel, M.P., Faissner, A., Sotelo, C. & Dusart, I. (2004) Long-term changes in the molecular composition of the glial scar and progressive increase of serotonergic fibre sprouting after hemisection of the mouse spinal cord. *Eur.J.Neurosci.*, **20**, 1161-1176.
46. Cao, Q., Benton, R.L. & Whitemore, S.R. (2002) Stem cell repair of central nervous system injury. *J.Neurosci.Res.*, **68**, 501-510.
47. Cassell, O.C., Morrison, W.A., Messina, A., Penington, A.J., Thompson, E.W., Stevens, G.W., Perera, J.M., Kleinman, H.K., Hurley, J.V., Romeo, R. & Knight, K.R. (2001) The influence of extracellular matrix on the generation of vascularized, engineered, transplantable tissue. *Ann.N.Y.Acad.Sci.*, **944**, 429-442.
48. Chen, H., Quick, E., Leung, G., Hamann, K., Fu, Y., Cheng, J.X. & Shi, R. (2009) Polyethylene glycol protects injured neuronal mitochondria. *Pathobiology*, **76**, 117-128.

49. Christie,S.D. & Mendez,I. (2001) Neural transplantation in spinal cord injury. *Can.J.Neurol.Sci.*, **28**, 6-15.
50. Cole,A. & Shi,R. (2005) Prolonged focal application of polyethylene glycol induces conduction block in guinea pig spinal cord white matter. *Toxicol.In Vitro*, **19**, 215-220.
51. Cong,H., Revzin,A. & Pan,T. (2009) Non-adhesive PEG hydrogel nanostructures for self-assembly of highly ordered colloids. *Nanotechnology.*, **20**, 075307.
52. Coumans,J.V., Lin,T.T., Dai,H.N., MacArthur,L., McAtee,M., Nash,C. & Bregman,B.S. (2001) Axonal regeneration and functional recovery after complete spinal cord transection in rats by delayed treatment with transplants and neurotrophins. *J.Neurosci.*, **21**, 9334-9344.
53. Dasari,V.R., Spomar,D.G., Gondi,C.S., Sloffer,C.A., Saving,K.L., Gujrati,M., Rao,J.S. & Dinh,D.H. (2007) Axonal remyelination by cord blood stem cells after spinal cord injury. *J.Neurotrauma*, **24**, 391-410.
54. David,S. & Aguayo,A.J. (1981) Axonal elongation into peripheral nervous system "bridges" after central nervous system injury in adult rats. *Science*, **214**, 931-933.
55. Davies,J.E., Huang,C., Proschel,C., Noble,M., Mayer-Proschel,M. & Davies,S.J. (2006) Astrocytes derived from glial-restricted precursors promote spinal cord repair. *J.Biol.*, **5**, 7.
56. Davies,J.E., Tang,X., Denning,J.W., Archibald,S.J. & Davies,S.J. (2004) Decorin suppresses neurocan, brevican, phosphacan and NG2 expression and promotes axon growth across adult rat spinal cord injuries. *Eur.J Neurosci*, **19**, 1226-1242.
57. Davies,S.J., Fitch,M.T., Memberg,S.P., Hall,A.K., Raisman,G. & Silver,J. (1997) Regeneration of adult axons in white matter tracts of the central nervous system. *Nature*, **390**, 680-683.

58. Davies,S.J., Goucher,D.R., Doller,C. & Silver,J. (1999) Robust regeneration of adult sensory axons in degenerating white matter of the adult rat spinal cord. *J.Neurosci.*, **19**, 5810-5822.
59. De Biase,A., Knoblach,S.M., Di Giovanni,S., Fan,C., Molon,A., Hoffman,E.P. & Faden,A.I. (2005) Gene expression profiling of experimental traumatic spinal cord injury as a function of distance from impact site and injury severity. *Physiol Genomics*, **22**, 368-381.
60. de Castro R.,Jr., Tajrishi,R., Claros,J. & Stallcup,W.B. (2005) Differential responses of spinal axons to transection: influence of the NG2 proteoglycan. *Exp.Neurol.*, **192**, 299-309.
61. de Vos,P., De Haan,B. & van Schilfgaarde,R. (1997) Effect of the alginate composition on the biocompatibility of alginate-polylysine microcapsules. *Biomaterials*, **18**, 273-278.
62. de Vos,P., van Hoogmoed,C.G., de Haan,B.J. & Busscher,H.J. (2002) Tissue responses against immunisolating alginate-PLL capsules in the immediate posttransplant period. *J.Biomed.Mater.Res.*, **62**, 430-437.
63. De Winter,F., Oudega,M., Lankhorst,A.J., Hamers,F.P., Blits,B., Ruitenbergh,M.J., Pasterkamp,R.J., Gispens,W.H. & Verhaagen,J. (2002) Injury-induced class 3 semaphorin expression in the rat spinal cord. *Exp.Neurol*, **175**, 61-75.
64. Dhoot,N.O., Tobias,C.A., Fischer,I. & Wheatley,M.A. (2004) Peptide-modified alginate surfaces as a growth permissive substrate for neurite outgrowth. *J Biomed.Mater.Res*, **71A**, 191-200.
65. Di Giovanni,S., De Biase,A., Yakovlev,A., Finn,T., Beers,J., Hoffman,E.P. & Faden,A.I. (2004) In vivo and in vitro characterization of novel neuronal plasticity factors identified following spinal cord injury. *J Biol.Chem.*
66. Ditunno,J.F. & Formal,C.S. (1994) Chronic spinal cord injury. *N.Engl.J.Med.*, **330**, 550-556.

67. Dobkin, B.H. & Havton, L.A. (2004) Basic advances and new avenues in therapy of spinal cord injury. *Annu.Rev.Med.*, **55**, 255-282.
68. Dolbeare, D. & Houle, J.D. (2003) Restriction of axonal retraction and promotion of axonal regeneration by chronically injured neurons after intraspinal treatment with glial cell line-derived neurotrophic factor (GDNF). *J.Neurotrauma*, **20**, 1251-1261.
69. Duerstock, B.S. & Borgens, R.B. (2002) Three-dimensional morphometry of spinal cord injury following polyethylene glycol treatment. *J.Exp.Biol.*, **205**, 13-24.
70. Duncan, M.R., Frazier, K.S., Abramson, S., Williams, S., Klapper, H., Huang, X. & Grotendorst, G.R. (1999) Connective tissue growth factor mediates transforming growth factor beta-induced collagen synthesis: down-regulation by cAMP. *FASEB J.*, **13**, 1774-1786.
71. Dunlop, S.A. (2008) Activity-dependent plasticity: implications for recovery after spinal cord injury. *Trends Neurosci.*, **31**, 410-418.
72. Dunn, J.C., Tompkins, R.G. & Yarmush, M.L. (1991) Long-term in vitro function of adult hepatocytes in a collagen sandwich configuration. *Biotechnol.Prog.*, **7**, 237-245.
73. Elbert, D.L. & Hubbell, J.A. (1998) Reduction of fibrous adhesion formation by a copolymer possessing an affinity for anionic surfaces. *J.Biomed.Mater.Res.*, **42**, 55-65.
74. Elefteriades, J.A. (2009) "How I do it: utilization of high-pressure sealants in aortic reconstruction". *J.Cardiothorac.Surg.*, **4**, 27.
75. Ellingson, B.M., Ulmer, J.L., Kurpad, S.N. & Schmit, B.D. (2008) Diffusion tensor MR imaging in chronic spinal cord injury. *AJNR Am.J.Neuroradiol.*, **29**, 1976-1982.

76. Facchiano,F., Fernandez,E., Mancarella,S., Maira,G., Miscusi,M., D'Arcangelo,D., Cimino-Reale,G., Falchetti,M.L., Capogrossi,M.C. & Pallini,R. (2002) Promotion of regeneration of corticospinal tract axons in rats with recombinant vascular endothelial growth factor alone and combined with adenovirus coding for this factor. *J.Neurosurg.*, **97**, 161-168.
77. Fawcett,J.W. (1998) Spinal cord repair: from experimental models to human application. *Spinal Cord.*, **36**, 811-817.
78. Fawcett,J.W. & Asher,R.A. (1999) The glial scar and central nervous system repair. *Brain Res.Bull.*, **49**, 377-391.
79. Fehlings,M.G. & Perrin,R.G. (2006) The timing of surgical intervention in the treatment of spinal cord injury: a systematic review of recent clinical evidence. *Spine*, **31**, S28-S35.
80. Fernandez,E. & Pallini,R. (1985) Connective tissue scarring in experimental spinal cord lesions: significance of dural continuity and role of epidural tissues. *Acta Neurochir.(Wien.)*, **76**, 145-148.
81. Fitch,M.T. & Silver,J. (1999) Beyond the glial scar - Cellular and molecular mechanisms by which glial cells contribute to CNS regenerative failure. In Tuszynski,M. & Kordower,J.H. (eds), *CNS regeneration: Basic science and clinical advances*. Academic Press, pp. 55-88.
82. Flanagan,L.A., Ju,Y.E., Marg,B., Osterfield,M. & Janmey,P.A. (2002) Neurite branching on deformable substrates. *Neuroreport*, **13**, 2411-2415.
83. Fouad,K., Schnell,L., Bunge,M.B., Schwab,M.E., Liebscher,T. & Pearse,D.D. (2005) Combining Schwann cell bridges and olfactory-ensheathing glia grafts with chondroitinase promotes locomotor recovery after complete transection of the spinal cord. *J.Neurosci.*, **25**, 1169-1178.
84. Fridakis,M.J., Spenger,C. & Olson,L. (2004) Partial recovery after treatment of chronic paraplegia in rat. *Exp.Neurol.*, **188**, 33-42.

85. Franze,K., Gerdelmann,J., Weick,M., Betz,T., Pawlizak,S., Lakadamyali,M., Bayer,J., Rillich,K., Gogler,M., Lu,Y.B., Reichenbach,A., Janmey,P. & Kas,J. (2009) Neurite branch retraction is caused by a threshold-dependent mechanical impact. *Biophys.J.*, **97**, 1883-1890.
86. Franzen,R., Schoenen,J., Leprince,P., Joosten,E., Moonen,G. & Martin,D. (1998) Effects of macrophage transplantation in the injured adult rat spinal cord: a combined immunocytochemical and biochemical study. *J.Neurosci.Res.*, **51**, 316-327.
87. Friedman,J.A., Windebank,A.J., Moore,M.J., Spinner,R.J., Currier,B.L. & Yaszemski,M.J. (2002) Biodegradable polymer grafts for surgical repair of the injured spinal cord. *Neurosurgery*, **51**, 742-751.
88. Fu,S.Y. & Gordon,T. (1997) The cellular and molecular basis of peripheral nerve regeneration. *Mol.Neurobiol.*, **14**, 67-116.
89. Gacesa, Peter. Alginates. *Carbohydrate Polymers* 8[8], 161-182. 1988.
90. Garavito,Z.V., Sutachan,J.J., Muneton,V.C. & Hurtado,H. (2000) Is S-100 protein a suitable marker for adult Schwann cells? *In Vitro Cell Dev.Biol.Anim*, **36**, 281-283.
91. Garcia-Alias,G., Lin,R., Akrimi,S.F., Story,D., Bradbury,E.J. & Fawcett,J.W. (2008) Therapeutic time window for the application of chondroitinase ABC after spinal cord injury. *Exp.Neurol.*, **210**, 331-338.
92. George,R. & Griffin,J.W. (1994) Delayed macrophage responses and myelin clearance during Wallerian degeneration in the central nervous system: the dorsal radicotomy model. *Exp.Neurol.*, **129**, 225-236.
93. Georges,P.C., Miller,W.J., Meaney,D.F., Sawyer,E.S. & Janmey,P.A. (2006) Matrices with compliance comparable to that of brain tissue select neuronal over glial growth in mixed cortical cultures. *Biophys.J.*, **90**, 3012-3018.

94. Gibbons,H.M., Hughes,S.M., Roon-Mom,W., Greenwood,J.M., Narayan,P.J., Teoh,H.H., Bergin,P.M., Mee,E.W., Wood,P.C., Faull,R.L. & Dragunow,M. (2007) Cellular composition of human glial cultures from adult biopsy brain tissue. *J.Neurosci.Methods*, **166**, 89-98.
95. Glaser,J., Gonzalez,R., Sadr,E. & Keirstead,H.S. (2006) Neutralization of the chemokine CXCL10 reduces apoptosis and increases axon sprouting after spinal cord injury. *J.Neurosci.Res.*, **84**, 724-734.
96. Goosen,M.F., O'Shea,G.M., Gharapetian,H.M., Chou,S. & Sun,A.M. (1985) Optimization of microencapsulation parameters: Semipermeable microcapsules as a bioartificial pancreas. *Biotechnol.Bioeng.*, **27**, 146-150.
97. Grider,M.H., Chen,Q. & Shine,H.D. (2006) Semi-automated quantification of axonal densities in labeled CNS tissue. *J.Neurosci.Methods*, **155**, 172-179.
98. Grill,R.J., Blesch,A. & Tuszynski,M.H. (1997) Robust growth of chronically injured spinal cord axons induced by grafts of genetically modified NGF-secreting cells. *Exp.Neurol.*, **148**, 444-452.
99. Guiot, C., Pugno, N., Delsanto, P. P., and Deisboeck, T. S. Physical aspects of cancer invasion.
100. Gunn,J.W., Turner,S.D. & Mann,B.K. (2005) Adhesive and mechanical properties of hydrogels influence neurite extension. *J.Biomed.Mater.Res.A*, **72**, 91-97.
101. Guth,L., Albuquerque,E.X., Deshpande,S.S., Barrett,C.P., Donati,E.J. & Warnick,J.E. (1980) Ineffectiveness of enzyme therapy on regeneration in the transected spinal cord of the rat. *J.Neurosurg.*, **52**, 73-86.
102. Hagg,T. & Oudega,M. (2006) Degenerative and spontaneous regenerative processes after spinal cord injury. *J.Neurotrauma*, **23**, 264-280.
103. Han,S., Arnold,S.A., Sithu,S.D., Mahoney,E.T., Geraldts,J.T., Tran,P., Benton,R.L., Maddie,M.A., D'Souza,S.E., Whittemore,S.R. & Hagg,T. (2010) Rescuing vasculature with intravenous angiopoietin-1 and $\alpha\beta_3$ integrin peptide is protective after spinal cord injury. *Brain*, **133**, 1026-1042.

-
104. Hejcl,A., Lesny,P., Pradny,M., Michalek,J., Jendelova,P., Stulik,J. & Sykova,E. (2008) Biocompatible hydrogels in spinal cord injury repair. *Physiol Res.*
105. Hejcl,A., Sedy,J., Kapcalova,M., Arboleda,T.D., Amemori,T., Likavcanova-Masinova,K., Lesny,P., Krumbholcova,E., Pradny,M., Michalek,J., Burian,M., Hajek,M., Jendelova,P. & Sykova,E. (2010) HPMA-RGD hydrogels seeded with mesenchymal stem cells improve functional outcome in chronic spinal cord injury. *Stem Cells Dev.*
106. Hermanns,S., Klapka,N., Gasis,M. & Müller,H.W. (2005) The collagenous wound healing scar in the injured central nervous system and its role in impeding axonal regeneration. In Bähr,M. (ed), *Brain Repair (Advances in Experimental Medicine and Biology)*. Springer.
107. Hermanns,S., Klapka,N. & Muller,H.W. (2001a) The collagenous lesion scar--an obstacle for axonal regeneration in brain and spinal cord injury. *Restor.Neurol.Neurosci.*, **19**, 139-148.
108. Hermanns,S., Reiprich,P. & Muller,H.W. (2001b) A reliable method to reduce collagen scar formation in the lesioned rat spinal cord. *J.Neurosci.Methods*, **110**, 141-146.
109. Hern,D.L. & Hubbell,J.A. (1998) Incorporation of adhesion peptides into nonadhesive hydrogels useful for tissue resurfacing. *J.Biomed.Mater.Res.*, **39**, 266-276.
110. Hill,C.E., Moon,L.D., Wood,P.M. & Bunge,M.B. (2006) Labeled Schwann cell transplantation: cell loss, host Schwann cell replacement, and strategies to enhance survival. *Glia*, **53**, 338-343.
111. Hill,C.E., Proschel,C., Noble,M., Mayer-Proschel,M., Gensel,J.C., Beattie,M.S. & Bresnahan,J.C. (2004) Acute transplantation of glial-restricted precursor cells into spinal cord contusion injuries: survival, differentiation, and effects on lesion environment and axonal regeneration. *Exp.Neurol*, **190**, 289-310.

112. Honmou,O., Felts,P.A., Waxman,S.G. & Kocsis,J.D. (1996) Restoration of normal conduction properties in demyelinated spinal cord axons in the adult rat by transplantation of exogenous Schwann cells. *J.Neurosci.*, **16**, 3199-3208.
113. Horn,E.M., Beaumont,M., Shu,X.Z., Harvey,A., Prestwich,G.D., Horn,K.M., Gibson,A.R., Preul,M.C. & Panitch,A. (2007) Influence of cross-linked hyaluronic acid hydrogels on neurite outgrowth and recovery from spinal cord injury. *J.Neurosurg.Spine*, **6**, 133-140.
114. Houle,J.D. & Tessler,A. (2003) Repair of chronic spinal cord injury. *Exp.Neurol.*, **182**, 247-260.
115. Houle,J.D. & Ziegler,M.K. (1994) Bridging a complete transection lesion of adult rat spinal cord with growth factor-treated nitrocellulose implants. *J.Neural Transplant.Plant.*, **5**, 115-124.
116. Hsu,J.Y. & Xu,X.M. (2005) Early profiles of axonal growth and astroglial response after spinal cord hemisection and implantation of Schwann cell-seeded guidance channels in adult rats. *J.Neurosci.Res.*, **82**, 472-483.
117. Hulsebosch,C.E. (2002) Recent advances in pathophysiology and treatment of spinal cord injury. *Adv.Physiol Educ.*, **26**, 238-255.
118. Iannotti,C., Li,H., Yan,P., Lu,X., Wirthlin,L. & Xu,X.M. (2003) Glial cell line-derived neurotrophic factor-enriched bridging transplants promote propriospinal axonal regeneration and enhance myelination after spinal cord injury. *Exp.Neurol.*, **183**, 379-393.
119. Ibarra,A., Hauben,E., Butovsky,O. & Schwartz,M. (2004) The therapeutic window after spinal cord injury can accommodate T cell-based vaccination and methylprednisolone in rats. *Eur.J.Neurosci.*, **19**, 2984-2990.
120. Imaizumi,T., Lankford,K.L. & Kocsis,J.D. (2000) Transplantation of olfactory ensheathing cells or Schwann cells restores rapid and secure conduction across the transected spinal cord. *Brain Res.*, **854**, 70-78.

121. Imperato-Kalmar,E.L., McKinney,R.A., Schnell,L., Rubin,B.P. & Schwab,M.E. (1997) Local changes in vascular architecture following partial spinal cord lesion in the rat. *Exp.Neurol.*, **145**, 322-328.
122. Inman,D.M. & Steward,O. (2003) Ascending sensory, but not other long-tract axons, regenerate into the connective tissue matrix that forms at the site of a spinal cord injury in mice. *J Comp Neurol*, **462**, 431-449.
123. Jessen,K.R., Morgan,L., Stewart,H.J. & Mirsky,R. (1990) Three markers of adult non-myelin-forming Schwann cells, 217c(Ran-1), A5E3 and GFAP: development and regulation by neuron-Schwann cell interactions. *Development*, **109**, 91-103.
124. Jin,Y., Fischer,I., Tessler,A. & Houle,J.D. (2002) Transplants of fibroblasts genetically modified to express BDNF promote axonal regeneration from supraspinal neurons following chronic spinal cord injury. *Exp.Neurol.*, **177**, 265-275.
125. Jones,L.L., Oudega,M., Bunge,M.B. & Tuszynski,M.H. (2001) Neurotrophic factors, cellular bridges and gene therapy for spinal cord injury. *J.Physiol*, **533**, 83-89.
126. Jones,L.L., Sajed,D. & Tuszynski,M.H. (2003) Axonal regeneration through regions of chondroitin sulfate proteoglycan deposition after spinal cord injury: a balance of permissiveness and inhibition. *J.Neurosci.*, **23**, 9276-9288.
127. Jones,L.L., Yamaguchi,Y., Stallcup,W.B. & Tuszynski,M.H. (2002) NG2 is a major chondroitin sulfate proteoglycan produced after spinal cord injury and is expressed by macrophages and oligodendrocyte progenitors. *J.Neurosci.*, **22**, 2792-2803.
128. Kadoya,K., Tsukada,S., Lu,P., Coppola,G., Geschwind,D., Filbin,M.T., Blesch,A. & Tuszynski,M.H. (2009) Combined intrinsic and extrinsic neuronal mechanisms facilitate bridging axonal regeneration one year after spinal cord injury. *Neuron*, **64**, 165-172.

129. Kalderon,N., Muruganandham,M., Koutcher,J.A. & Potuzak,M. (2007) Therapeutic strategy for acute spinal cord contusion injury: cell elimination combined with microsurgical intervention. *PLoS.ONE.*, **2**, e565.
130. Kameneva,M.V., Repko,B.M., Krasik,E.F., Perricelli,B.C. & Borovetz,H.S. (2003) Polyethylene glycol additives reduce hemolysis in red blood cell suspensions exposed to mechanical stress. *ASAIO J.*, **49**, 537-542.
131. Kaneko,S., Iwanami,A., Nakamura,M., Kishino,A., Kikuchi,K., Shibata,S., Okano,H.J., Ikegami,T., Moriya,A., Konishi,O., Nakayama,C., Kumagai,K., Kimura,T., Sato,Y., Goshima,Y., Taniguchi,M., Ito,M., He,Z., Toyama,Y. & Okano,H. (2006) A selective Sema3A inhibitor enhances regenerative responses and functional recovery of the injured spinal cord. *Nat.Med.*.
132. Kastin,A.J. & Pan,W. (2005) Targeting neurite growth inhibitors to induce CNS regeneration. *Curr.Pharm.Des*, **11**, 1247-1253.
133. Kataoka,K., Suzuki,Y., Kitada,M., Hashimoto,T., Chou,H., Bai,H., Ohta,M., Wu,S., Suzuki,K. & Ide,C. (2004) Alginate enhances elongation of early regenerating axons in spinal cord of young rats. *Tissue Eng*, **10**, 493-504.
134. Kataoka,K., Suzuki,Y., Kitada,M., Ohnishi,K., Suzuki,K., Tanihara,M., Ide,C., Endo,K. & Nishimura,Y. (2001) Alginate, a bioresorbable material derived from brown seaweed, enhances elongation of amputated axons of spinal cord in infant rats. *J.Biomed.Mater.Res.*, **54**, 373-384.
135. Kawaguchi,Y., Harigai,M., Kitani,A., Suzuki,K., Kawakami,M., Ishizuka,T., Hidaka,T., Hara,M., Kawagoe,M. & Nakamura,H. (1992) Effect of prolyl 4-hydroxylase inhibitor on fibroblast collagen production in vitro: an approach to the treatment of systemic sclerosis. *J.Rheumatol.*, **19**, 1710-1715.
136. Kawano,H., Li,H.P., Sango,K., Kawamura,K. & Raisman,G. (2005) Inhibition of collagen synthesis overrides the age-related failure of regeneration of nigrostriatal dopaminergic axons. *J.Neurosci.Res.*, **80**, 191-202.

137. Kerschensteiner,M., Schwab,M.E., Lichtman,J.W. & Misgeld,T. (2005) In vivo imaging of axonal degeneration and regeneration in the injured spinal cord. *Nat.Med.*, **11**, 572-577.
138. Kigerl,K.A., Gensel,J.C., Ankeny,D.P., Alexander,J.K., Donnelly,D.J. & Popovich,P.G. (2009) Identification of two distinct macrophage subsets with divergent effects causing either neurotoxicity or regeneration in the injured mouse spinal cord. *J.Neurosci.*, **29**, 13435-13444.
139. Klapka,N., Hermanns,S. & Muller,H.W. (2002) Interactions between glia and extracellular matrix and their role for axonal growth. In ALDSKOGIUS,H. & FRAHER,J. (eds), *Glial interfaces in the nervous system*. Amsterdam.
140. Klapka,N., Hermanns,S., Straten,G., Masanneck,C., Duis,S., Hamers,F.P., Muller,D., Zuschratter,W. & Muller,H.W. (2005) Suppression of fibrous scarring in spinal cord injury of rat promotes long-distance regeneration of corticospinal tract axons, rescue of primary motoneurons in somatosensory cortex and significant functional recovery. *Eur.J.Neurosci.*, **22**, 3047-3058.
141. Klapka,N. & Muller,H.W. (2006) Collagen matrix in spinal cord injury. *J.Neurotrauma*, **23**, 422-435.
142. Klock,G., Pfeffermann,A., Ryser,C., Grohn,P., Kuttler,B., Hahn,H.J. & Zimmermann,U. (1997) Biocompatibility of mannuronic acid-rich alginates. *Biomaterials*, **18**, 707-713.
143. Koob,A.O., Colby,J.M. & Borgens,R.B. (2008) Behavioral recovery from traumatic brain injury after membrane reconstruction using polyethylene glycol. *J.Biol.Eng*, **2**, 9.
144. Kruse,F., Brazda,N., Küry,P., Bosse,F. & Müller,H.W. (2008) Analyzing Complex Gene Expression Profiles in Sensorimotor Cortex Following Spinal Cord Injury and Regeneration Promoting Treatment. In Müller,H.W. (ed), *Neural Degeneration and Repair : Gene Expression Profiling, Proteomics, and Systems Biology*. Johnn Wiley & Sons.

145. Kwon,B.K., Borisoff,J.F. & Tetzlaff,W. (2002a) Molecular targets for therapeutic intervention after spinal cord injury. *Mol.Interv.*, **2**, 244-258.
146. Kwon,B.K., Liu,J., Messerer,C., Kobayashi,N.R., McGraw,J., Oschipok,L. & Tetzlaff,W. (2002b) Survival and regeneration of rubrospinal neurons 1 year after spinal cord injury. *Proc.Natl.Acad.Sci U.S A*, **99**, 3246-3251.
147. Kwon,B.K., Oxland,T.R. & Tetzlaff,W. (2002c) Animal models used in spinal cord regeneration research. *Spine*, **27**, 1504-1510.
148. Lakatos,A., Smith,P.M., Barnett,S.C. & Franklin,R.J. (2003) Meningeal cells enhance limited CNS remyelination by transplanted olfactory ensheathing cells. *Brain*, **126**, 598-609.
149. Lee,S.K. & Wolfe,S.W. (2000) Peripheral nerve injury and repair. *J.Am.Acad.Orthop.Surg.*, **8**, 243-252.
150. Levental, I., Georges, P. C., and Janmey, P. A. Soft biological materials and their impact on cell function. *Soft Matter* 3, 299-306. 2006.
151. Li,Y. & Raisman,G. (1995) Sprouts from cut corticospinal axons persist in the presence of astrocytic scarring in long-term lesions of the adult rat spinal cord. *Exp.Neurol.*, **134**, 102-111.
152. Liesi,P. & Kauppila,T. (2002) Induction of type IV collagen and other basement-membrane-associated proteins after spinal cord injury of the adult rat may participate in formation of the glial scar. *Exp.Neurol*, **173**, 31-45.
153. Liu,S., Said,G. & Tadie,M. (2001) Regrowth of the rostral spinal axons into the caudal ventral roots through a collagen tube implanted into hemisected adult rat spinal cord. *Neurosurgery*, **49**, 143-150.
154. Liu,X.Z., Xu,X.M., Hu,R., Du,C., Zhang,S.X., McDonald,J.W., Dong,H.X., Wu,Y.J., Fan,G.S., Jacquin,M.F., Hsu,C.Y. & Choi,D.W. (1997) Neuronal and glial apoptosis after traumatic spinal cord injury. *J.Neurosci.*, **17**, 5395-5406.

155. Liu-Snyder,P., Logan,M.P., Shi,R., Smith,D.T. & Borgens,R.B. (2007) Neuroprotection from secondary injury by polyethylene glycol requires its internalization. *J.Exp.Biol.*, **210**, 1455-1462.
156. Loy,D.N., Crawford,C.H., Darnall,J.B., Burke,D.A., Onifer,S.M. & Whittemore,S.R. (2002) Temporal progression of angiogenesis and basal lamina deposition after contusive spinal cord injury in the adult rat. *J.Comp Neurol.*, **445**, 308-324.
157. Lu,J., Ashwell,K.W., Hayek,R. & Waite,P. (2001) Fluororuby as a marker for detection of acute axonal injury in rat spinal cord. *Brain Res.*, **915**, 118-123.
158. Lu,P. & Tuszynski,M.H. (2008) Growth factors and combinatorial therapies for CNS regeneration. *Exp.Neurol.*, **209**, 313-320.
159. Luo,J., Borgens,R. & Shi,R. (2002) Polyethylene glycol immediately repairs neuronal membranes and inhibits free radical production after acute spinal cord injury. *J.Neurochem.*, **83**, 471-480.
160. Luo,J. & Shi,R. (2004) Diffusive oxidative stress following acute spinal cord injury in guinea pigs and its inhibition by polyethylene glycol. *Neurosci.Lett.*, **359**, 167-170.
161. Luo,J. & Shi,R. (2007) Polyethylene glycol inhibits apoptotic cell death following traumatic spinal cord injury. *Brain Res.*, **1155**, 10-16.
162. Luo,J., Zhang,H.T., Jiang,X.D., Xue,S. & Ke,Y.Q. (2009) Combination of bone marrow stromal cell transplantation with mobilization by granulocyte-colony stimulating factor promotes functional recovery after spinal cord transection. *Acta Neurochir.(Wien.)*.
163. Mahoney,E.T., Benton,R.L., Maddie,M.A., Whittemore,S.R. & Hagg,T. (2009) ADAM8 is selectively up-regulated in endothelial cells and is associated with angiogenesis after spinal cord injury in adult mice. *J.Comp Neurol.*, **512**, 243-255.

164. Mahoney, M.J. & Anseth, K.S. (2006) Three-dimensional growth and function of neural tissue in degradable polyethylene glycol hydrogels. *Biomaterials*, **27**, 2265-2274.
165. Markakis, E.A. & Redmond, D.E., Jr. (2005) Know thyself: autologous cell transplantation strategies for brain repair. *Exp. Neurol.*, **196**, 6-8.
166. Marks, J.D., Pan, C.Y., Bushell, T., Cromie, W. & Lee, R.C. (2001) Amphiphilic, tri-block copolymers provide potent membrane-targeted neuroprotection. *FASEB J.*, **15**, 1107-1109.
167. Mata, M., Alessi, D. & Fink, D.J. (1990) S100 is preferentially distributed in myelin-forming Schwann cells. *J. Neurocytol.*, **19**, 432-442.
168. Mauter, A.E., Weinzierl, M.R., Donovan, F. & Noble, L.J. (2000) Vascular events after spinal cord injury: contribution to secondary pathogenesis. *Phys. Ther.*, **80**, 673-687.
169. McKerracher, L. (2001) Spinal cord repair: strategies to promote axon regeneration. *Neurobiol. Dis.*, **8**, 11-18.
170. Meijering, E., Jacob, M., Sarria, J.C., Steiner, P., Hirling, H. & Unser, M. (2004) Design and validation of a tool for neurite tracing and analysis in fluorescence microscopy images. *Cytometry A*, **58**, 167-176.
171. Miranda, J.D., White, L.A., Marcillo, A.E., Willson, C.A., Jagid, J. & Whittemore, S.R. (1999) Induction of Eph B3 after spinal cord injury. *Exp. Neurol.*, **156**, 218-222.
172. Murray, M. (2004) Cellular transplants: steps toward restoration of function in spinal injured animals. *Prog. Brain Res.*, **143**, 133-146.
173. Murray, M., Kim, D., Liu, Y., Tobias, C., Tessler, A. & Fischer, I. (2002) Transplantation of genetically modified cells contributes to repair and recovery from spinal injury. *Brain Res. Brain Res. Rev.*, **40**, 292-300.

174. Nehrt,A., Hamann,K., Ouyang,H. & Shi,R. (2010) Polyethylene glycol enhances axolemmal resealing following transection in cultured cells and in ex vivo spinal cord. *J.Neurotrauma*, **27**, 151-161.
175. Niclou,S.P., Ehlert,E.M. & Verhaagen,J. (2006) Chemorepellent axon guidance molecules in spinal cord injury. *J.Neurotrauma*, **23**, 409-421.
176. Nomura,H., Tator,C.H. & Shoichet,M.S. (2006) Bioengineered strategies for spinal cord repair. *J.Neurotrauma*, **23**, 496-507.
177. NovaMatrix Product Information Bulletin. PRONOVA™ UP - Ultrapure Sodium Alginates .
178. Novikov,L.N., Novikova,L.N., Mosahebi,A., Wiberg,M., Terenghi,G. & Kellerth,J.O. (2002) A novel biodegradable implant for neuronal rescue and regeneration after spinal cord injury. *Biomaterials*, **23**, 3369-3376.
179. Novikova,L.N., Mosahebi,A., Wiberg,M., Terenghi,G., Kellerth,J.O. & Novikov,L.N. (2006) Alginate hydrogel and matrigel as potential cell carriers for neurotransplantation. *J.Biomed.Mater.Res.A*.
180. Novikova,L.N., Novikov,L.N. & Kellerth,J.O. (2003) Biopolymers and biodegradable smart implants for tissue regeneration after spinal cord injury. *Curr.Opin.Neurol*, **16**, 711-715.
181. Nunamaker,E.A., Purcell,E.K. & Kipke,D.R. (2007) In vivo stability and biocompatibility of implanted calcium alginate disks. *J.Biomed.Mater.Res.A*, **83**, 1128-1137.
182. Okada,M., Miyamoto,O., Shibuya,S., Zhang,X., Yamamoto,T. & Itano,T. (2007) Expression and role of type I collagen in a rat spinal cord contusion injury model. *Neurosci.Res.*, **58**, 371-377.
183. Opatz,J., Kury,P., Schiwy,N., Jarve,A., Estrada,V., Brazda,N., Bosse,F. & Muller,H.W. (2009) SDF-1 stimulates neurite growth on inhibitory CNS myelin. *Mol.Cell Neurosci.*, **40**, 293-300.

184. Orive,G., Carcaboso,A.M., Hernandez,R.M., Gascon,A.R. & Pedraz,J.L. (2005) Biocompatibility evaluation of different alginates and alginate-based microcapsules. *Biomacromolecules.*, **6**, 927-931.
185. Oudega,M. (2007) Schwann cell and olfactory ensheathing cell implantation for repair of the contused spinal cord. *Acta Physiol (Oxf)*, **189**, 181-189.
186. Oudega,M. & Xu,X.M. (2006) Schwann cell transplantation for repair of the adult spinal cord. *J.Neurotrauma*, **23**, 453-467.
187. Pasterkamp,R.J. & Verhaagen,J. (2006) Semaphorins in axon regeneration: developmental guidance molecules gone wrong? *Philos.Trans.R.Soc.Lond B Biol.Sci.*, **361**, 1499-1511.
188. Paxinos,G. & Watson,C. (2005) *The Rat Brain in Stereotaxic Coordinates* Academic Press, New York.
189. Pearse,D.D. & Bunge,M.B. (2006) Designing cell- and gene-based regeneration strategies to repair the injured spinal cord. *J.Neurotrauma*, **23**, 438-452.
190. Pekny,M. & Nilsson,M. (2005) Astrocyte activation and reactive gliosis. *Glia*, **50**, 427-434.
191. Peters,M.C., Polverini,P.J. & Mooney,D.J. (2002) Engineering vascular networks in porous polymer matrices. *J.Biomed.Mater.Res.*, **60**, 668-678.
192. Petter-Puchner,A.H., Froetscher,W., Krametter-Froetscher,R., Lorinson,D., Redl,H. & van Griensven,M. (2007) The long-term neurocompatibility of human fibrin sealant and equine collagen as biomatrices in experimental spinal cord injury. *Exp.Toxicol.Pathol.*, **58**, 237-245.
193. Plunet,W., Kwon,B.K. & Tetzlaff,W. (2002) Promoting axonal regeneration in the central nervous system by enhancing the cell body response to axotomy. *J.Neurosci.Res.*, **68**, 1-6.
194. Popovich,P.G. & Longbrake,E.E. (2008) Can the immune system be harnessed to repair the CNS? *Nat.Rev.Neurosci.*, **9**, 481-493.

195. Prang,P., Muller,R., Eljaouhari,A., Heckmann,K., Kunz,W., Weber,T., Faber,C., Vroemen,M., Bogdahn,U. & Weidner,N. (2006) The promotion of oriented axonal regrowth in the injured spinal cord by alginate-based anisotropic capillary hydrogels. *Biomaterials*, **27**, 3560-3569.
196. Purcell,E.K., Singh,A. & Kipke,D.R. (2009) Alginate composition effects on a neural stem cell-seeded scaffold. *Tissue Eng Part C.Methods*, **15**, 541-550.
197. Raab,S. & Plate,K.H. (2007) Different networks, common growth factors: shared growth factors and receptors of the vascular and the nervous system. *Acta Neuropathol.*, **113**, 607-626.
198. Rabchevsky,A.G. & Smith,G.M. (2001) Therapeutic interventions following mammalian spinal cord injury. *Arch.Neurol.*, **58**, 721-726.
199. Ramer,L.M., Au,E., Richter,M.W., Liu,J., Tetzlaff,W. & Roskams,A.J. (2004) Peripheral olfactory ensheathing cells reduce scar and cavity formation and promote regeneration after spinal cord injury. *J.Comp Neurol*, **473**, 1-15.
200. Ramer,L.M., Ramer,M.S. & Steeves,J.D. (2005) Setting the stage for functional repair of spinal cord injuries: a cast of thousands. *Spinal Cord.*, **43**, 134-161.
201. Ramer,M.S., Harper,G.P. & Bradbury,E.J. (2000) Progress in spinal cord research - a refined strategy for the International Spinal Research Trust. *Spinal Cord.*, **38**, 449-472.
202. Ramon-Cueto,A., Plant,G.W., Avila,J. & Bunge,M.B. (1998) Long-distance axonal regeneration in the transected adult rat spinal cord is promoted by olfactory ensheathing glia transplants. *J.Neurosci.*, **18**, 3803-3815.
203. Rasouli,A., Bhatia,N., Dinh,P., Cahill,K., Suryadevara,S. & Gupta,R. (2009) Resection of glial scar following spinal cord injury. *J.Orthop.Res.*, **27**, 931-936.

-
204. Rauch,M.F., Hynes,S.R., Bertram,J., Redmond,A., Robinson,R., Williams,C., Xu,H., Madri,J.A. & Lavik,E.B. (2009) Engineering angiogenesis following spinal cord injury: a coculture of neural progenitor and endothelial cells in a degradable polymer implant leads to an increase in vessel density and formation of the blood-spinal cord barrier. *Eur.J.Neurosci.*, **29**, 132-145.
205. Reier,P.J. (2004) Cellular transplantation strategies for spinal cord injury and translational neurobiology. *NeuroRx.*, **1**, 424-451.
206. Reier,P.J., Stensaas,L.J. & Guth,L. (1983) The astrocytic scar as an impediment to regeneration in the central nervous system. In Kao,C.C., Bunge,R.P. & Reier,P.J. (eds), *Spinal Cord Reconstruction*. Raven Press, New York, pp. 163-195.
207. Reiner,A., Veenman,C.L., Medina,L., Jiao,Y., Del Mar,N. & Honig,M.G. (2000) Pathway tracing using biotinylated dextran amines. *J Neurosci Methods*, **103**, 23-37.
208. Remminghorst,U. & Rehm,B.H. (2006) Bacterial alginates: from biosynthesis to applications. *Biotechnol.Lett.*, **28**, 1701-1712.
209. Ribotta,M., Gaviria,M., Menet,V. & Privat,A. (2002) Strategies for regeneration and repair in spinal cord traumatic injury. *Prog.Brain Res.*, **137**, 191-212.
210. Rodriguez,F.J., Verdu,E., Ceballos,D. & Navarro,X. (2000) Nerve guides seeded with autologous schwann cells improve nerve regeneration. *Exp.Neurol.*, **161**, 571-584.
211. Rosenberg,L.J. & Wrathall,J.R. (2001) Time course studies on the effectiveness of tetrodotoxin in reducing consequences of spinal cord contusion. *J.Neurosci.Res.*, **66**, 191-202.
212. Rosenzweig,E.S. & McDonald,J.W. (2004) Rodent models for treatment of spinal cord injury: research trends and progress toward useful repair. *Curr.Opin.Neurol.*, **17**, 121-131.

213. Rowland,J.W., Hawryluk,G.W., Kwon,B. & Fehlings,M.G. (2008) Current status of acute spinal cord injury pathophysiology and emerging therapies: promise on the horizon. *Neurosurg.Focus.*, **25**, E2.
214. Ruff,R.L., McKerracher,L. & Selzer,M.E. (2008) Repair and neurorehabilitation strategies for spinal cord injury. *Ann.N.Y.Acad.Sci.*, **1142**, 1-20.
215. Salehi,M., Pasbakhsh,P., Soleimani,M., Abbasi,M., Hasanzadeh,G., Modaresi,M.H. & Sobhani,A. (2009) Repair of spinal cord injury by co-transplantation of embryonic stem cell-derived motor neuron and olfactory ensheathing cell. *Iran Biomed.J.*, **13**, 125-135.
216. Samadikuchaksaraei,A. (2007) An overview of tissue engineering approaches for management of spinal cord injuries. *J.Neuroeng.Rehabil.*, **4**, 15.
217. Sandvig,A., Berry,M., Barrett,L.B., Butt,A. & Logan,A. (2004) Myelin-, reactive glia-, and scar-derived CNS axon growth inhibitors: expression, receptor signaling, and correlation with axon regeneration. *Glia*, **46**, 225-251.
218. Schiwy,N., Brazda,N. & Muller,H.W. (2009) Enhanced regenerative axon growth of multiple fibre populations in traumatic spinal cord injury following scar-suppressing treatment. *Eur.J.Neurosci.*, **30**, 1544-1553.
219. Schwab,J.M., Beschorner,R., Nguyen,T.D., Meyermann,R. & Schluesener,H.J. (2001) Differential cellular accumulation of connective tissue growth factor defines a subset of reactive astrocytes, invading fibroblasts, and endothelial cells following central nervous system injury in rats and humans. *J Neurotrauma*, **18**, 377-388.
220. Schwartz,E.D., Chin,C.L., Shumsky,J.S., Jawad,A.F., Brown,B.K., Wehrli,S., Tessler,A., Murray,M. & Hackney,D.B. (2005a) Apparent diffusion coefficients in spinal cord transplants and surrounding white matter correlate with degree of axonal dieback after injury in rats. *AJNR Am.J.Neuroradiol.*, **26**, 7-18.
221. Schwartz,E.D., Cooper,E.T., Chin,C.L., Wehrli,S., Tessler,A. & Hackney,D.B. (2005b) Ex vivo evaluation of ADC values within spinal cord white matter tracts. *AJNR Am.J.Neuroradiol.*, **26**, 390-397.

-
222. Schwartz,M. (2003) Macrophages and microglia in central nervous system injury: are they helpful or harmful? *J.Cereb.Blood Flow Metab*, **23**, 385-394.
223. Schwartz,M. & Hauben,E. (2002) T cell-based therapeutic vaccination for spinal cord injury. *Prog.Brain Res.*, **137**, 401-406.
224. Schweigreiter,R. & Bandtlow,C.E. (2006) Nogo in the injured spinal cord. *J.Neurotrauma*, **23**, 384-396.
225. Serban,M.A. & Prestwich,G.D. (2008) Modular extracellular matrices: solutions for the puzzle. *Methods*, **45**, 93-98.
226. Shi,R. & Borgens,R.B. (1999) Acute repair of crushed guinea pig spinal cord by polyethylene glycol. *J Neurophysiol*, **81**, 2406-2414.
227. Shi,R. & Borgens,R.B. (2000) Anatomical repair of nerve membranes in crushed mammalian spinal cord with polyethylene glycol. *J.Neurocytol.*, **29**, 633-643.
228. Shumaker,D.K., Vann,L.R., Goldberg,M.W., Allen,T.D. & Wilson,K.L. (1998) TPEN, a Zn²⁺/Fe²⁺ chelator with low affinity for Ca²⁺, inhibits lamin assembly, destabilizes nuclear architecture and may independently protect nuclei from apoptosis in vitro. *Cell Calcium*, **23**, 151-164.
229. Silver,J. & Miller,J.H. (2004) Regeneration beyond the glial scar. *Nat.Rev.Neurosci.*, **5**, 146-156.
230. Simpson,N.E., Stabler,C.L., Simpson,C.P., Sambanis,A. & Constantinidis,I. (2004) The role of the CaCl₂-guluronic acid interaction on alginate encapsulated betaTC3 cells. *Biomaterials*, **25**, 2603-2610.
231. Slobodian,I., Krassioukov-Enns,D. & Del Bigio,M.R. (2007) Protein and synthetic polymer injection for induction of obstructive hydrocephalus in rats. *Cerebrospinal.Fluid Res.*, **4**, 9.

232. Someya,Y., Koda,M., Dezawa,M., Kadota,T., Hashimoto,M., Kamada,T., Nishio,Y., Kadota,R., Mannoji,C., Miyashita,T., Okawa,A., Yoshinaga,K. & Yamazaki,M. (2008) Reduction of cystic cavity, promotion of axonal regeneration and sparing, and functional recovery with transplanted bone marrow stromal cell-derived Schwann cells after contusion injury to the adult rat spinal cord. *J.Neurosurg.Spine*, **9**, 600-610.
233. Steward, O., Zheng, B., and Tessier-Lavigne, M. False Resurrections: Distinguishing Regenerated from Spared Axons in the Injured Central Nervous System. *J.Comp Neurol.* 459, 1-8. 2003.
234. Stichel,C.C., Hermanns,S., Luhmann,H.J., Lausberg,F., Niermann,H., D'Urso,D., Servos,G., Hartwig,H.G. & Muller,H.W. (1999a) Inhibition of collagen IV deposition promotes regeneration of injured CNS axons. *Eur.J.Neurosci.*, **11**, 632-646.
235. Stichel,C.C. & Muller,H.W. (1998) Experimental strategies to promote axonal regeneration after traumatic central nervous system injury. *Prog.Neurobiol.*, **56**, 119-148.
236. Stichel,C.C. & Müller,H.W. (1998) The CNS lesion scar: new vistas on an old regeneration barrier. *Cell Tissue Res.*, **294**, 1-9.
237. Stichel,C.C., Niermann,H., D'Urso,D., Lausberg,F., Hermanns,S. & Müller,H.W. (1999b) Basal membrane-depleted scar in lesioned CNS: characteristics and relationships with regenerating axons. *Neuroscience*, **93**, 321-333.
238. Stoll,G. & Muller,H.W. (1999) Nerve injury, axonal degeneration and neural regeneration: basic insights. *Brain Pathol.*, **9**, 313-325.
239. Stroncek,J.D. & Reichert,W.M. (2007) Overview of Wound Healing in Different Tissue Types. In Reichert,W.M. (ed), *Indwelling Neural Implants: Strategies for Contending with the In Vivo Environment*. CRC Press.

240. Suzuki,K., Suzuki,Y., Ohnishi,K., Endo,K., Tanihara,M. & Nishimura,Y. (1999) Regeneration of transected spinal cord in young adult rats using freeze-dried alginate gel. *Neuroreport*, **10**, 2891-2894.
241. Suzuki,K., Suzuki,Y., Tanihara,M., Ohnishi,K., Hashimoto,T., Endo,K. & Nishimura,Y. (2000) Reconstruction of rat peripheral nerve gap without sutures using freeze-dried alginate gel. *J.Biomed.Mater.Res.*, **49**, 528-533.
242. Suzuki,Y., Kitaura,M., Wu,S., Kataoka,K., Suzuki,K., Endo,K., Nishimura,Y. & Ide,C. (2002) Electrophysiological and horseradish peroxidase-tracing studies of nerve regeneration through alginate-filled gap in adult rat spinal cord. *Neurosci.Lett.*, **318**, 121-124.
243. Talac,R., Friedman,J.A., Moore,M.J., Lu,L., Jabbari,E., Windebank,A.J., Currier,B.L. & Yaszemski,M.J. (2004) Animal models of spinal cord injury for evaluation of tissue engineering treatment strategies. *Biomaterials*, **25**, 1505-1510.
244. Tang,X., Davies,J.E. & Davies,S.J. (2003) Changes in distribution, cell associations, and protein expression levels of NG2, neurocan, phosphacan, brevican, versican V2, and tenascin-C during acute to chronic maturation of spinal cord scar tissue. *J Neurosci.Res.*, **71**, 427-444.
245. Tester,N.J. & Howland,D.R. (2008) Chondroitinase ABC improves basic and skilled locomotion in spinal cord injured cats. *Exp.Neurol.*, **209**, 483-496.
246. Tobias,C.A., Dhoot,N.O., Wheatley,M.A., Tessler,A., Murray,M. & Fischer,I. (2001) Grafting of encapsulated BDNF-producing fibroblasts into the injured spinal cord without immune suppression in adult rats. *J.Neurotrauma*, **18**, 287-301.
247. Tobias,C.A., Han,S.S., Shumsky,J.S., Kim,D., Tumolo,M., Dhoot,N.O., Wheatley,M.A., Fischer,I., Tessler,A. & Murray,M. (2005) Alginate encapsulated BDNF-producing fibroblast grafts permit recovery of function after spinal cord injury in the absence of immune suppression. *J.Neurotrauma*, **22**, 138-156.

-
248. Tom, V.J. & Houle, J.D. (2008) Intraspinal microinjection of chondroitinase ABC following injury promotes axonal regeneration out of a peripheral nerve graft bridge. *Exp. Neurol.*, **211**, 315-319.
249. Tom, V.J., Sandrow-Feinberg, H.R., Miller, K., Santi, L., Connors, T., Lemay, M.A. & Houle, J.D. (2009) Combining peripheral nerve grafts and chondroitinase promotes functional axonal regeneration in the chronically injured spinal cord. *J. Neurosci.*, **29**, 14881-14890.
250. Tripathi, R. & McTigue, D.M. (2007) Prominent oligodendrocyte genesis along the border of spinal contusion lesions. *Glia*, **55**, 698-711.
251. Trivedi, A., Olivas, A.D. & Noble-Haeusslein, L.J. (2006) Inflammation and Spinal Cord Injury: Infiltrating Leukocytes as Determinants of Injury and Repair Processes. *Clin. Neurosci. Res.*, **6**, 283-292.
252. Tuszynski, M.H., Grill, R., Jones, L.L., Brant, A., Blesch, A., Low, K., Lacroix, S. & Lu, P. (2003) NT-3 gene delivery elicits growth of chronically injured corticospinal axons and modestly improves functional deficits after chronic scar resection. *Exp. Neurol.*, **181**, 47-56.
253. Tysseling-Mattiace, V.M., Sahni, V., Niece, K.L., Birch, D., Czeisler, C., Fehlings, M.G., Stupp, S.I. & Kessler, J.A. (2008) Self-assembling nanofibers inhibit glial scar formation and promote axon elongation after spinal cord injury. *J. Neurosci.*, **28**, 3814-3823.
254. Ung, R.V., Lapointe, N.P., Tremblay, C., Larouche, A. & Guertin, P.A. (2007) Spontaneous recovery of hindlimb movement in completely spinal cord transected mice: a comparison of assessment methods and conditions. *Spinal Cord.*, **45**, 367-379.
255. Urso, M.L., Chen, Y.W., Scrimgeour, A.G., Lee, P.C., Lee, K.F. & Clarkson, P.M. (2007) Alterations in mRNA expression and protein products following spinal cord injury in humans. *J. Physiol.*, **579**, 877-892.

-
256. van Hoogmoed,C.G., Busscher,H.J. & de Vos,P. (2003) Fourier transform infrared spectroscopy studies of alginate-PLL capsules with varying compositions. *J.Biomed.Mater.Res.A*, **67**, 172-178.
257. van Schilfgaarde,R. & de Vos,P. (1999) Factors influencing the properties and performance of microcapsules for immunoprotection of pancreatic islets. *J.Mol.Med.*, **77**, 199-205.
258. von Euler,M., Janson,A.M., Larsen,J.O., Seiger,A., Forno,L., Bunge,M.B. & Sundstrom,E. (2002) Spontaneous axonal regeneration in rodent spinal cord after ischemic injury. *J.Neuropathol.Exp.Neurol*, **61**, 64-75.
259. von Meyenburg,J., Brosamle,C., Metz,G.A. & Schwab,M.E. (1998) Regeneration and sprouting of chronically injured corticospinal tract fibers in adult rats promoted by NT-3 and the mAb IN-1, which neutralizes myelin-associated neurite growth inhibitors. *Exp.Neurol.*, **154**, 583-594.
260. Wamil,A.W., Wamil,B.D. & Hellerqvist,C.G. (1998) CM101-mediated recovery of walking ability in adult mice paralyzed by spinal cord injury. *Proc.Natl.Acad.Sci.U.S.A*, **95**, 13188-13193.
261. Wee,S. & Gombotz,W.R. (1998) Protein release from alginate matrices. *Adv.Drug Deliv.Rev.*, **31**, 267-285.
262. Wente, W., Dauch, D., and Borrmann, L. Mixing of highly viscous liquids using Eppendorf MixMate®. 2007. *Eppendorf Applications*.
263. Whetstone,W.D., Hsu,J.Y., Eisenberg,M., Werb,Z. & Noble-Haeusslein,L.J. (2003) Blood-spinal cord barrier after spinal cord injury: relation to revascularization and wound healing. *J.Neurosci.Res.*, **74**, 227-239.
264. Woerly,S., Doan,V.D., Evans-Martin,F., Paramore,C.G. & Peduzzi,J.D. (2001a) Spinal cord reconstruction using NeuroGel implants and functional recovery after chronic injury. *J.Neurosci.Res.*, **66**, 1187-1197.

-
265. Woerly,S., Doan,V.D., Sosa,N., de Vellis,J. & Espinosa,A. (2001b) Reconstruction of the transected cat spinal cord following NeuroGel implantation: axonal tracing, immunohistochemical and ultrastructural studies. *Int.J.Dev.Neurosci.*, **19**, 63-83.
266. Woerly,S., Pinet,E., de Robertis,L., Van Diep,D. & Bousmina,M. (2001c) Spinal cord repair with PHPMA hydrogel containing RGD peptides (NeuroGel). *Biomaterials*, **22**, 1095-1111.
267. Wu,X., Yoo,S. & Wrathall,J.R. (2005) Real-time quantitative PCR analysis of temporal-spatial alterations in gene expression after spinal cord contusion. *J.Neurochem.*, **93**, 943-952.
268. Xie,F. & Zheng,B. (2008) White matter inhibitors in CNS axon regeneration failure. *Exp.Neurol.*, **209**, 302-312.
269. Xin, J., Liu, X.-Z., and Wu, J. R. Ultrasound Attenuation in Biological Tissue Predicted by the Modified Doublet Mechanics Model. *Chinese Physics Letters* 26[7]. 2009.
270. Xu,X.M., Chen,A., Guenard,V., Kleitman,N. & Bunge,M.B. (1997) Bridging Schwann cell transplants promote axonal regeneration from both the rostral and caudal stumps of transected adult rat spinal cord. *J.Neurocytol.*, **26**, 1-16.
271. Xu,X.M., Guenard,V., Kleitman,N. & Bunge,M.B. (1995) Axonal regeneration into Schwann cell-seeded guidance channels grafted into transected adult rat spinal cord. *J.Comp Neurol.*, **351**, 145-160.
272. Xu,X.M., Zhang,S.X., Li,H., Aebischer,P. & Bunge,M.B. (1999) Regrowth of axons into the distal spinal cord through a Schwann-cell- seeded mini-channel implanted into hemisected adult rat spinal cord. *Eur.J.Neurosci.*, **11**, 1723-1740.
273. Yang,Y., De Laporte,L., Rives,C.B., Jang,J.H., Lin,W.C., Shull,K.R. & Shea,L.D. (2005) Neurotrophin releasing single and multiple lumen nerve conduits. *J.Control Release*, **104**, 433-446.

-
274. Yao,B., Ni,C., Xiong,C., Zhu,C. & Huang,B. (2009) Hydrophobic modification of sodium alginate and its application in drug controlled release. *Bioprocess.Biosyst.Eng.*
275. Yara,T., Kato,Y., Kataoka,H., Kanchiku,T., Suzuki,H., Gondo,T., Yoshii,S. & Taguchi,T. (2009) Environmental factors involved in axonal regeneration following spinal cord transection in rats. *Med.Mol.Morphol.*, **42**, 150-154.
276. Ye,J.H. & Houle,J.D. (1997) Treatment of the chronically injured spinal cord with neurotrophic factors can promote axonal regeneration from supraspinal neurons. *Exp.Neurol.*, **143**, 70-81.
277. Yen,C.N., Lin,Y.R., Chang,M.D., Tien,C.W., Wu,Y.C., Liao,C.J. & Hu,Y.C. (2008) Use of porous alginate sponges for substantial chondrocyte expansion and matrix production: effects of seeding density. *Biotechnol.Prog.*, **24**, 452-457.
278. Yurchenco,P.D. & Schittny,J.C. (1990) Molecular architecture of basement membranes. *FASEB J.*, **4**, 1577-1590.
279. Zahm,D.S., Williams,E. & Wohltmann,C. (1996) Ventral striatopallidothalamic projection: IV. Relative involvements of neurochemically distinct subterritories in the ventral pallidum and adjacent parts of the rostroventral forebrain. *J.Comp Neurol.*, **364**, 340-362.
280. Zhang,S., Kluge,B., Huang,F., Nordstrom,T., Doolen,S., Gross,M., Sarmiere,P. & Holmberg,E.G. (2007) Photochemical scar ablation in chronically contused spinal cord of rat. *J.Neurotrauma*, **24**, 411-420.
281. Zhang,Z. & Guth,L. (1997) Experimental spinal cord injury: Wallerian degeneration in the dorsal column is followed by revascularization, glial proliferation, and nerve regeneration. *Exp.Neurol.*, **147**, 159-171.

DANKSAGUNG

Ich möchte Herrn Prof. Dr. Hans Werner Müller herzlich für die Betreuung der Arbeit, für hilfreiche und anregende Diskussionen und vor allem dafür danken, dass er mir die Möglichkeit gegeben hat, in diesem äußerst spannenden Bereich der Wissenschaft zu arbeiten.

Herrn Prof. Dr. Dieter Willbold möchte ich ebenfalls meinen Dank dafür aussprechen, dass er sich zur Betreuung meiner Arbeit bereit erklärt hat.

Ein besonderer Dank gilt Dr. Nicole Brazda, nicht nur für ihre Motivation durch ihre Begeisterung für das wissenschaftliche Arbeiten, ihre kreativen Einfälle sowie hilfreiche Diskussionen und Anregungen, sondern auch dafür, dass sie mir mit ihrer Gelassenheit, wenn es nötig erschien, die notwendige Ruhe zurückgegeben hat.

Auch den übrigen Mitarbeitern des Labors für molekulare Neurobiologie möchte ich herzlich danken: Nora Schiwy für anregende Gespräche und Diskussionen und für unterhaltsame Kongressreisen. Christine Schmitz und Marcia Gasis für ihren Arbeitseinsatz und ihre Hilfe bei den Experimenten. Dr. Christina Vogelaar, Dr. Frank Bosse, Anne Järve und Jessica Schira dafür, dass sie jederzeit bereit waren, mit mir Fragen und Ideen zu erörtern. Euch allen vielen Dank für Eure Bereitschaft, mit Eurem Wissen und Können zur ein oder anderen Problemlösung beizutragen. Nicht zuletzt haben die gute Atmosphäre und die zahlreichen Diskussionen dazu beigetragen, dass mir die Arbeit im Labor immer wieder besonderen Spaß macht.

Dr. Jessica Opatz danke ich für die zahlreichen (immer unterhaltsamen und oft lehrreichen) Konversationen und Diskussionen, für ihre Sorge um mein leibliches Wohl und für die gemeinsamen Unternehmungen. Jede einzelne war ein Erlebnis.

Dr. Michael Gliem aus der Arbeitsgruppe Jander bin ich sehr dankbar für die Bereitstellung einer ruhigen Arbeitsatmosphäre in der Schlussphase dieser Arbeit.

Mein ganz besonderer Dank gilt meiner Familie: Meinen Eltern Manuel und Marlene Estrada, meiner Schwester Ines und meinem Schwager Kirk, die mich während der gesamten Zeit und auch darüber hinaus immer unterstützt haben. Vielen Dank dafür.

Eidesstattliche Erklärung:

Hiermit erkläre ich, dass ich die vorliegende Arbeit selbst verfasst und keine anderen als die angegebenen Quellen und Hilfsmittel verwendet, sowie Zitate kenntlich gemacht habe.

Düsseldorf, im Mai 2010